

Influence of ship-induced currents on the erosion and permeability of sand-mud mixtures in the Twentekanalen

Niels Nijborg



Influence of ship-induced currents on the erosion and permeability of sand-mud mixtures in the Twentekanalen

An explorative research into the interaction between ship-induced currents and erosion of sand-mud mixtures, and the plastering process of such a mixture regarding the permeability in time, related to the conditions in the Twentekanalen (the Netherlands).

Master's thesis

by

N.A. Nijborg

in partial fulfilment of the requirements for the degree of

Master of Science

Civil Engineering and Management

Specialization: Water Engineering and Management

| | |
|---------------------|--|
| Date | 16/11/2016 |
| Version | Final |
| Author | Niels A. Nijborg |
| Contact email/phone | nielsnijborg@gmail.com / +31 624573914 |
| University | University of Twente |
| Faculty | Engineering Technology (CTW) |
| Program | Water Engineering and Management |

Master Thesis committee

| | |
|-----------------------|--|
| Dr.Ir. J.S. Ribberink | University of Twente, Department of Water Engineering and Management |
| Dr. J.J. Warmink | University of Twente, Department of Water Engineering and Management |
| Ing. G. Menting | Rijkswaterstaat, Department of Water, Traffic and Environment |
| A. Talmon PhD MSc | Deltares |

Summary

Over the last decades there is a trend of ever growing ships worldwide in order to increase their transport efficiency. The draught increases and increasingly larger propellers are built on these modern ships. However, the dimensions of numerous inland navigation channels do not meet the requirements for these larger vessels. A direct consequence is the significant increase in ship-induced flow velocities under and around the ships which could cause severe bottom and bank erosion. Scour induced by the propeller wash has become one of the most important issues for the design and maintenance of navigation channels and harbour structures (Hong, Chiew, & Cheng, 2013).

The Twentekanalen in the Netherlands are currently categorized as class IV waterway, however considering the economic development in the hinterland and ongoing deployment of larger vessels Rijkswaterstaat decided to enlarge these waterways to class Va in 2017. On the one hand this research focussed on the increase in ship-induced flow velocities and the consequences regarding bottom erosion in the side channel of the Twentekanalen. On the other hand this research also focussed on seepage which is for a large extent dependent on the resistive bed of the canal. In 2010 (maintenance) dredging activities took place in the side channel of the Twentekanalen where at specific trajectories the resistive sludge layer was removed which resulted in higher groundwater levels in the area behind the dikes causing nuisance for both residents and farmers in terms of flooded basements and reduced crop yield. In 2016 a temporary sludge layer is constructed on the bottom of the side channel to reduce the amount of seepage and consequently lower the groundwater level. Monitoring the groundwater levels revealed that the groundwater levels were lowered, however not sufficient to mitigate problems for farmers and residents. Concluding, Rijkswaterstaat would like to gain more insights in bottom erosion caused by larger ships and the effects of sludge on the bottom of the channel with respect to the hydraulic conductivity.

Therefore, the objective of this research was to *“to visualize the erosion profile and estimate the equilibrium erosion depth of a sand-clay sediment mixture under the influence of shipping in the axis of the side channel of the Twentekanalen, and to test whether clay particles are infiltrated into the sandy subsoil affecting the hydraulic conductivity”*. To achieve this objective two separate laboratory experiments were conducted: (1) a scale model of a ship towed in a flume over a sand-clay mixture in which different parameters are varied and (2) a plastering experiment to determine the effects of clay plastering in a sand filter on the hydraulic conductivity. Findings of the experiments are translated and scaled for the situation of the Twentekanalen.

Erosion experiment - The erosion profile in the sand-clay mixture starts to develop directly after a ship has passed, relatively fast in the beginning and reduces with every ship passage eventually resulting in an equilibrium depth. Underneath the ship the bottom erodes and the eroded sediment is transported to the sides of the channel. At small sailing speeds the propeller wash appeared to be dominant and higher efflux velocity of the propeller results in a wider and deeper scour hole. The return current starts to play a role with increasing sailing speeds while simultaneously the impact time of the propeller on the bottom decreases. Moreover, flow velocities at the bottom caused by the propeller wash are decreasing when sailing speed increases assuming a constant efflux velocity. Erosion certainly takes place when large sailing speeds were applied, however a clear scour hole did not develop. Additionally, the erosion depth is dependent on the slope stability of the erosion hole, hence the strength of the sediment and the sand-clay ratio. Comparison with existing erosion formulas for sand seems to give fairly reasonable results, however these are established for continuously rotating propellers located on the same location contradicting to the conducted experiment in this research. This research focussed on erosion by moving ships and might be an explanation for the different empirical coefficients in these formulas. Therefore, more research into moving propellers and subsequent erosion is needed. Furthermore, quantitative research is advised to determine the effects of cohesive properties on the erosion depth under influence of shipping currents and to incorporate specific cohesive properties in an erosion formula.

Plastering experiment - Clay plastering appeared of great importance regarding the hydraulic conductivity. Pouring a natural sludge or sand-clay mixture on top of a sandy soil directly influences the hydraulic conductivity. Moreover, the amount of clay particles in the mixture is important, more clay particles clogging more pores and results in even lower hydraulic conductivity. Additionally, it was observed that de hydraulic conductivity decreases when the sludge is stirred with the sandy subsoil. Hence, it is concluded that also the distribution of clay particles within the sandy subsoil is affecting the hydraulic conductivity. The invasion depth of clay particles, affecting the hydraulic conductivity and subsequently the amount of seepage, is therefore an interesting issue to examine in more detail.

Translation and recommendation for the Twentekanalen – As a result of larger ships in the future and adjustments to the profile of the channel, the ship-induced flow velocities in the Twentekanalen increase substantially with an increase of 20% regarding the return current and roughly 60% for the propeller wash. Maximum flow velocities on the bottom of 2.9 m/s for moored ships and 1.9 m/s for sailing ships could occur. The occurring ship-induced flow velocities are significantly larger than the critical velocities of natural sludges, thus the application of a stable natural sludge layer on the bottom of the Twentekanalen is very unlikely. Increasing critical erosion velocities e.g. by compacting and or adding more clay are most likely not sufficient. Measures to decrease flow velocities on the bottom by deepening or widening the channel were found not sufficient or expected too costly. Currently, the erosion tracks in the side channel of the Twentekanalen ranges from 0.15 m to 0.5 m found in bathymetry measurements. It is likely that erosion tracks become deeper due to the increasing flow velocities of the larger vessels. The experiments in which reality is best reflected show erosion tracks of 2 - 5 cm corresponding to 0.4 and 1 m in reality (scale 1:20). These results are verified with existing formulas which are validated to similar situations of inland navigation channels in reality. Erosion tracks calculated with these formulas resulted in an erosion range expected in the Twentekanalen of 0.15 - 1 m in accordance with the experiments.

Clay plastering is important for the seepage hindrance in the surroundings. Samples of the inserted sludge layer in 2016 revealed that the requirements for physical characteristics were far from met. In particular the clay content was significantly lower than the minimum requirement. It seems that especially the percentage of clay within the sludge is important while the layer thickness is of less importance also taking into consideration the displacement of sludge over the profile. Lastly, it is known that mixing the sand with the sludge consequently causes a better distribution of clay particles resulting in a lower hydraulic conductivity. Therefore, related to the Twentekanalen this would mean that ship-induced currents do not have directly negative consequences for the amount of seepage because it could mix the clay particles with the sandy subsoil.

Preface

This thesis is made as a completion of the Master's programme Civil Engineering and Management at the University of Twente. This report contains the results of an explorative research initiated by Rijkswaterstaat and related to the ship-induced erosion and hydraulic conductivity of sand-mud mixtures in the Twentekanalen. While writing the research proposal the opportunity arose to perform experiments at Deltares in Delft to acquire better understanding of above processes. I would like to thank Rijkswaterstaat and Deltares for making this all possible. I worked with great pleasure on the research and learned a lot about doing experiments and translating the experimental results to the situation in reality incorporating existing theories. What I liked the most was the combination between academic and practical approaches. I discovered both worlds since I conducted the experiments at Deltares and discussed the practical implications at Rijkswaterstaat.

Despite some issues with the experimental set-up and equipment in the beginning of my research I enjoyed working on this Master's thesis. I am very grateful to the employees of Deltares and Rijkswaterstaat who helped me during these difficult times. In particular I want to thank Marcel Grootenboer and Marcel Busink from Deltares for putting a lot of time and effort in my research that made my experiments successful. The execution of the experiments would not have been possible without them. I also would like to thank Riemer Bouma, Hanneke Pentenga and the entire project team from Rijkswaterstaat for their support and the useful information they provided.

I would like to thank my supervisors in particular. First of all I would like to thank Arno Talmon (supervisor from Deltares) for his ideas and discussions regarding the set-up of the experiments. Thanks for your expertise and time which helped me a lot in interpreting the results and translation to practice. It definitely improved my work. Furthermore, I would like to thank Geert Menting (supervisor Rijkswaterstaat) for his enthusiasm about the topic, endless discussions and help with interpreting results. He was always interested in the results and available to answer my questions. Besides, I also want to thank my supervisors from the University of Twente; Jan Ribberink and Jord Warmink. Jan Ribberink supervised this Master's thesis and always had a critical, however very useful, view towards the results and structure of the report. Especially at the start of the project he helped me with narrowing the research and during early discussions he warned me of possible challenges which could arise while doing experiments. His input helped a lot in the completion of this research. Secondly, I would like to thank Jord Warmink for his support and guidance during the project. He critically reviewed my work and came up with suggestions for improvements. With his detailed feedback I was able to improve my work. The co-operation between me and my supervisors was pleasant and I enjoyed working with all of you.

Finally, I would like to thank my family, friends and fellow students for their support and of course making my time as a student unforgettable.

Niels Nijborg
Enschede, November 2016

Table of Contents

| | | |
|-----------|---|-----------|
| 1 | Introduction..... | 1 |
| 1.1 | <i>Background.....</i> | 1 |
| 1.2 | <i>Problem definition and research gap.....</i> | 2 |
| 1.3 | <i>Research objective and questions.....</i> | 4 |
| 1.4 | <i>Methodology.....</i> | 4 |
| 1.5 | <i>Thesis outline.....</i> | 6 |
| 2 | Literature survey..... | 7 |
| 2.1 | <i>Erosion modes sand-mud mixtures.....</i> | 7 |
| 2.2 | <i>Theory propeller wash.....</i> | 8 |
| 2.3 | <i>Theory ship induced erosion.....</i> | 9 |
| 2.4 | <i>Theory soil plastering.....</i> | 11 |
| 3 | Case Twentekanalen: Starting points..... | 12 |
| 3.1 | <i>Cross section side channel Twentekanalen.....</i> | 12 |
| 3.2 | <i>Ship-induced flow velocities.....</i> | 13 |
| 4 | Experimental set-up..... | 14 |
| 4.1 | <i>Erosion experiment.....</i> | 14 |
| 4.2 | <i>Plastering experiment.....</i> | 20 |
| 5 | Experimental results..... | 22 |
| 5.1 | <i>Results erosion experiment.....</i> | 22 |
| 5.2 | <i>Results plastering experiment.....</i> | 32 |
| 6 | Case Twentekanalen vs Experimental results..... | 38 |
| 6.1 | <i>Erosion profile Twentekanalen.....</i> | 38 |
| 6.2 | <i>Plastering of clay particles in Twentekanalen.....</i> | 44 |
| 7 | Discussion..... | 47 |
| 7.1 | <i>Erosion experiment.....</i> | 47 |
| 7.2 | <i>Plastering experiments.....</i> | 48 |
| 7.3 | <i>Usability experimental results for reality.....</i> | 48 |
| 8 | Conclusions and recommendations..... | 49 |
| 8.1 | <i>Conclusions.....</i> | 49 |
| 8.2 | <i>Recommendations.....</i> | 50 |
| 9 | References..... | 52 |
| 10 | Appendices..... | 55 |

List of symbols

| | | |
|----------------|---|-----------------------------------|
| a_{pr} | Empirical coefficient regarding the decay of axial velocity of the propeller wash | [-] |
| b_{pr} | Empirical coefficient regarding the decay of axial velocity of the propeller wash | [-] |
| A | Area | [m ²] |
| B_f | Width fairway bottom | [m] |
| B_s | Beam width | [m] |
| B_w | Width waterline | [m] |
| B^* | Load coefficient | [-] |
| B_{85}^* | Stability coefficient | [-] |
| C_m | Constant for sailing vessels (=0.3) | [-] |
| C_D | Resistance coefficient ship's impoundment | [-] |
| c_d | Drained strength | [Pa] |
| c_u | Undrained strength | [Pa] |
| c_v | Terzaghi consolidation coefficient | [m ² /s] |
| D_{50} | Median particle diameter | [m] |
| D_{85} | 85-percentile diameter of the sediment sample | [m] |
| D_{pr} | True propeller diameter | [m] |
| D_0 | Effective propeller diameter (= $1 \times D_{pr}$ for propellers in a nozzle and $0.7 \times D_{pr}$ for propellers without a nozzle) | [m] |
| d_{max} | Maximum erosion depth | [m] |
| dt | Impact time | [h] |
| F_0 | Densimetric Froude number = $U_{pr,0}/\sqrt{g\Delta d_{50}}$ | [-] |
| f_t | Correction factor temperature | [-] |
| f_w | Friction factor | [-] |
| g | Gravitational acceleration | [m/s ²] |
| h | Water depth | [m] |
| h_k | Under keel clearance | [m] |
| h_s | Thickness sediment layer | [m] |
| i | Hydraulic gradient | [-] |
| k | Hydraulic conductivity | [m/s] |
| K | Erosion constant | [m ² /s ⁴] |
| L_s | Ship's length | [m] |
| N | Amount of ship passages | [year ⁻¹] |
| n | Amount of propeller rotations | [s ⁻¹] |
| Q | Discharge | [m ³ /s] |
| t | Time | [s] |
| TK | Abbreviation for Twentekanalen | |
| T | Draught | [m] |
| T_{bow} | Draught at the bow | [m] |
| U | Degree of consolidation | [-] |
| U_0 | Ambient flow velocity (natural flow in channel) | [m/s] |
| U_{cr} | Critical flow velocity | [m/s] |
| $U_{pr,0}$ | Efflux velocity propeller | [m/s] |
| $U_{pr,b0}$ | Initial bottom velocity propeller | [m/s] |
| $U_{pr,b1}$ | Velocity in scour hole after erosion (= assumed critical erosion velocity) | [m/s] |
| $U_{r,b}$ | Return current underneath the ship | [m/s] |
| r_u | Turbulence intensity | [-] |
| V_s | Vessel's sailing speed | [m/s] |
| x | Distance in longitudinal direction | [m] |
| y | Distance in transverse direction | [m] |
| z_b | Offset height (distance from propeller axis to the bottom) | [m] |
| α | Empirical coefficient erosion formula or Turbulence coefficient | [-] |
| β | Empirical coefficient erosion formula | [-] |
| η | Impoundment at the bow | [m] |
| ρ_w | Density of water | [kg/m ³] |
| $\hat{\tau}_b$ | Peak stresses larger than the mean bed shear stress | [Pa] |
| $\bar{\tau}_b$ | Mean bed shear stress | [Pa] |
| γ | Shape factor ship | [-] |
| λ | Scale factor | [-] |
| Δ | Relative density | [-] |

1 Introduction

1.1 Background

The Twentekanalen, which are managed by Rijkswaterstaat, are economically important waterways for the province Overijssel and especially region Twente. The Twentekanalen also form a hinterland connection with the harbour of Rotterdam, Amsterdam and Antwerp. The Twentekanalen (total length is 65 km) are connected to the river IJssel at Eefde (north of Zutphen) and the main channel connects Almen, Lochem, Goor, Delden, Hengelo and Enschede. A side channel west of Delden connects the main channel to Almelo (Figure 1). The Ministry of Infrastructure and Environment invests in the improvement of important hinterland connections to ensure the reliability and accessibility of the waterways, to improve the competitiveness of transport over water, and to relieve road transport and environment (Rijkswaterstaat, 2015).



Figure 1: Twentekanalen [phase 1 = purple; phase 2 = red] (Rijkswaterstaat, 2015).

Rijkswaterstaat is responsible for the execution of the plans. Currently the Twentekanalen are categorized as class IV waterway, however considering the economic developments in the hinterland and the ongoing deployment of larger vessels it is concluded that the current classification does not fulfil the requirements anymore. Rijkswaterstaat has decided to enlarge the waterways from class IV to class Va in order to satisfy the requirements of larger vessels, to increase accessibility, to stimulate economy and employment in the region (Rijkswaterstaat, 2015). Rijkswaterstaat has enlarged the channel between Eefde and Delden in 2010 and the other parts of the Twentekanalen will be enlarged in 2020 (respectively phase 1 and phase 2 in Figure 1). With enlarging is meant that the waterway is deepened and/or widened.

The water level in major parts of the Twentekanalen is substantially higher than the surrounding surface level. This difference in height results in 'leakage' of water towards the surrounding area (called seepage) and can cause damage to agriculture, houses etc. The amount of seepage from the canal to the surrounding area is for a large extent dependent on the resistive bed of the canal. In 2003 Rijkswaterstaat conducted tests in the field in order to determine whether dredging activities affect the amount of seepage and came to the conclusion that it significantly affects the seepage (Rijkswaterstaat, 2003). In 2010 (maintenance) dredging activities took place in the side channel of the Twentekanalen where at specific trajectories the resistive sludge layer was removed which resulted in higher groundwater levels and nuisance. Tauw (2014) examined the water problems and concluded that a causal relationship exists between the water nuisance and dredging operations. Tauw (2014) divided the side channel and the main channel Delden – Enschede (phase 2 in Figure 1) based on strong / slight seepage (Appendix A). It turned out that especially in the side channel seepage is large and causing problems in the surrounding area.

Rijkswaterstaat has started the exploration and preparation for enlarging Twentekanalen phase 2. It comprises for example elaboration of canal design, applications for permits and establishment of the contract for the contractor. In particular the contract formation comprises many technical issues which should be covered. One of the technical issues is managing the seepage nuisance related to the canal bed resistance. Typical question of the client (Rijkswaterstaat) is: "How the contractor deals with seepage and how the contractor ensures that the seepage does not increase in time compared to the situation directly after construction, e.g. due to shipping turbulence?" Arcadis (2015) analysed several alternatives to deal with seepage based on costs, aspects of implementation and license issues. The preferred option according to Arcadis based on the criteria is the application of clay (present to a greater or lesser extent, in mud / sludge mixtures) on the bottom of the Twentekanalen. The bed does not have to be impermeable because in case of an impermeable canal bed the problem of drought can occur. The situation should be restored to the situation before dredging activities in 2010.

1.2 Problem definition and research gap

Sludge layers are present on the bottom of shipping channels to prevent seepage. During maintenance dredging in 2010 in the side channel of the Twentekanalen, a portion of the seepage reducing layer in the form of sludge is removed and thereby causing seepage from the channel to the area behind. At this moment new dredging activities are prepared in order to enlarge the shipping canals. To prevent new flooding problems, the seepage reducing sludge layer needs to be reconstructed sufficiently after dredging. However, there is limited knowledge about how the layer develops after reconstruction and how to construct the new layer.

Estimates of the currents below ships and subsequent erosion can be based on rules of thumb, mathematical modelling and scale modelling. These estimates, however, are not sufficiently reliable to predict the stability and erosion of the channel bottom. The impact of shipping on the sludge layer in the Twentekanalen is unknown and therefore, it is not possible to determine if the recommended properties of the new sludge layer in the channels are sufficient.

Bathymetry data of the Twentekanalen reveals that in the axis of the canal (centerline) the water depth is larger than at the sides (see Appendix C). In other words, the bottom in the axis of the canal is lower than at the sides (Figure 2). From visual observations and experiments (e.g. Robijns, 2014) it is known that these tracks in the canal bed are most likely caused by shipping because the ships, most of the time, sail in the axis of the canal. The flow velocities of the ship-induced currents on the bottom are relatively large and turbulent (Brovchenko et al., 2007) thereby eroding and stirring up sediment. The sediment will be deposited in the areas at both sides of the ship because there the (flow) conditions are relatively calm compared to under the ship.

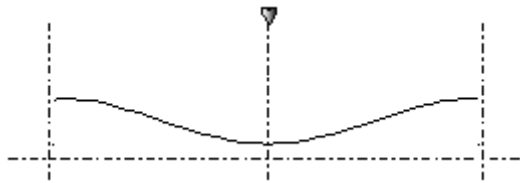


Figure 2: Bed profile due to shipping in the centerline of the Twente Canal (in Dutch this profile is called 'Kattenrug').

As regards to seepage, practical experiments of Rijkswaterstaat (2003) showed that the way in which the sludge layer reduces seepage mainly depends on four aspects:

- 1) Composition of the sludge layer
- 2) Settling velocity of the specific sediment fractions within the sludge layer
- 3) Distribution of the sludge layer over de canal bed (thickness)
- 4) Time (consolidation / compaction)

In the above points the mobility of the sediment plays an important role. This mobility, in turn, may be influenced by the natural flow and by flows caused by shipping, e.g. turbulent jets caused by shipping propellers. In general can be said, as also concluded in the field experiments of Rijkswaterstaat (2003), the finer the sediment fraction in the sludge layer the lower the hydraulic conductivity¹, and therefore the less seepage. The settling (velocity) and distribution of the specific sediment fractions within the sludge layer are highly dependent on flow characteristics such as flow velocity and turbulent eddies in the water column. A negative relation exist between the mobility and the hydraulic conductivity:

- Smaller grain size → more mobile (↑) and lower hydraulic conductivity (↓)
- Larger grain size → less mobile (↓) and higher hydraulic conductivity (↑)

However, cohesive properties (e.g. due to clay particles) affect the mobility of the particles as is described below.

¹ Low values of hydraulic conductivity indicate that the material / layer is less permeable, whereas high values indicate more permeable.

In the past, research and experiments have been carried out in order to study the influences of currents under and around ships on the bottom (Robijns, 2014; WL| Delft Hydraulics, 1987). These experiments are carried out in a flume with non-cohesive sediments, mainly sand. However, cohesive sediments behave differently compared to non-cohesive sediments and by adding clay or mud to sand the erodibility decreases significantly (Mitchener & Torfs, 1996). For example, Torfs (1995) measured a 2-5 times higher critical erosion shear stress than the critical shear stress of pure sand when 10% mud was added to the mixture. In the paper of Mitchener and Torfs (1996) is also mentioned that the maximum critical erosion shear stress of a sand-mud mixture is probably reached with a mixture containing 50 – 70% sand corresponding to 50 – 30 % mud. The latter is because of smoothing of the sand due to the presence of mud, the cohesive bonding between particles and compaction of the cohesive bed due to the presence of sand. However, to confirm this hypothesis more experiments need to be done because of a lack of data in this region of sand-mud fractions with respect to erodibility. In addition, most of the experiments are carried out with uniform flow where the magnitude of turbulence is minimal. In this research water flows due to shipping are important which are commonly characterized by highly turbulent flows (Brovchenko et al., 2007).

Rijkswaterstaat stated that erosion of the seepage reducing sludge layer is allowed, however the level of seepage should remain at the same level as before the maintenance dredging in 2010. Already mentioned above is that the thickness of the remaining sludge layer is important. After construction of the new seepage reducing layer in the form of a sand-mud mixture, ships in all probability cause erosion of this layer. It is likely that after a certain period of time an equilibrium is reached in terms of erosion depth in the axis of the canal². Hence, a residual layer with a specific thickness remains in the centerline of the canal highly influencing the amount of seepage. Furthermore, it is known that clay affects the hydraulic conductivity, however the effects of shipping on the hydraulic conductivity in time is unknown.

Summarizing, the research gap can be divided into five aspects. Two from a literature point of view and three from the point of view of Rijkswaterstaat.

From a literature point of view:

- 1) A lack of data exists of sand-mud mixtures containing 50 – 70% sand corresponding to 50 – 30% mud regarding the erodibility under uniform flow.
- 2) It is unknown how sand-mud mixtures erode under highly turbulent flow conditions (e.g. due to shipping).

From Rijkswaterstaat point of view:

- 3) It is unknown how the erosion profile and erosion depth develops in the side channel of the Twentekanalen owing to ship-induced currents.
- 4) It is unknown what the remaining thickness of the seepage reducing layer (sand-mud) is after erosion and if this layer is sufficient to prevent seepage problems.
- 5) It is unknown how the hydraulic conductivity changes over time after constructing a new seepage reducing layer under the influence of shipping.

With respect to the research gap and the defined problem a summarized problem definition for Rijkswaterstaat is formulated:

The knowledge within Rijkswaterstaat regarding the erodibility of sand-mud mixtures as seepage reducing layer due to shipping is insufficient. Rijkswaterstaat would like to gain more insights in the erosion behaviour of a sand-mud layer on the bottom of the canal (e.g. due to shipping turbulence) and the hydraulic conductivity of such a layer to be able to test or to judge whether the proposed method by the contractor does fulfil the requirements.

² Note: the profile of the bed remains dynamic because ships do not all the time sail exactly in the centerline of the canal and sometimes ships have to pass each other resulting in manoeuvring towards the banks.

1.3 Research objective and questions

In this paragraph the objective of the research is formulated and in order to structure the research corresponding research questions are established. The discussed research gap in paragraph 1.2 forms the basis of the research questions in accordance with the demands of Rijkswaterstaat. The scope of this research is related to bottom erosion and hydraulic conductivity under influence of shipping within the side channel of the Twentekanalen.

1.3.1 Research objective

The objective of this research is to visualize the erosion profile and estimate the equilibrium erosion depth of a sand-clay sediment mixture under the influence of shipping in the axis of the side channel of the Twentekanalen, and to test whether clay particles are infiltrated into the sandy subsoil affecting the hydraulic conductivity. Rijkswaterstaat can gather information from this research to judge whether a contractor is able to fulfil the requirements in order to construct the necessary long lasting protection against seepage flooding.

1.3.2 Research questions

The subject comprises several processes such as hydraulic loadings, sediment transport and seepage which makes it an extensive research. To cover the relevant processes within the scope of this research four sub questions are established in order to answer the main question. The main question and sub questions are formulated below.

Main question

What will be the effect of ship-induced hydraulic loadings on the erosion profile, equilibrium erosion depth and hydraulic conductivity of the sand-mud mixture in the Twentekanalen after enlarging and construction of the new layer?

Sub questions

- 1 What are the ship-induced flow velocities in the side channel of the Twentekanalen assuming stagnant water in current and future situation?
- 2 How does the erosion profile and equilibrium depth in a sand-clay mixture develop under influence of ship-induced currents during the experiment in the flume?
 - 2.1. What are the time-averaged flow velocities induced by the propeller wash?
 - 2.2. How large is the equilibrium erosion depth?
 - 2.3. What is the relationship between the maximum erosion depth and the propeller wash?
 - 2.4. How are the particle sizes distributed over the erosion profile?
- 3 How does clay plastering affect the hydraulic conductivity over time?
 - 3.1. What are the effects of an artificial sand-clay mixture poured on top of a sandy subsoil on the hydraulic conductivity over time?
 - 3.2. What are the effects of a natural sand-mud layer retrieved from the Twentekanalen poured on top of a sandy subsoil on the hydraulic conductivity over time?
- 4 How will the seepage reducing natural sand-mud mixture which is used in the Twentekanalen develop over time regarding erosion and hydraulic conductivity?

1.4 Methodology

To structure this research and to answer the research questions the following methodology is used which is illustrated in Figure 3. The methodology connects the specific issues with each other and ensures the fulfilment of the objective. Erosion and clay plastering are investigated in two separate experiments described in sequence below. In the end of the report results of both experiments are applied to the situation of the Twentekanalen.

Ship-induced erosion

The starting point of this research is to determine the occurring flow velocities on the bottom of the Twentekanalen in current and future situation (RQ. 1). These flow velocities will serve as input for the erosion experiment in which the relevant parameters will be scaled. Additionally, the obtained flow velocities also serve as input to estimate the erosion depth in the Twentekanalen according to existing erosion depth formulas. The purpose of the erosion experiment is to visualize the erosion profile caused by sailing vessels and to determine the equilibrium erosion depth in the flume experiment (RQ 2). In order to represent the reality as much as possible the relevant parameters are scaled, hence it is necessary to know the flow velocities in the propeller wash (RQ 2.1). Secondly, the profile is measured after every ship passage to be able to visualize the development and equilibrium erosion depth (RQ 2.2). Thirdly, attempts are made to find a relationship between the maximum erosion depth and the propeller wash also based on existing formulas in literature (RQ 2.3). Last aspect in the erosion experiment is related to the particle size distribution over the erosion profile which is of interest as regards to the permeability (RQ 2.4).

Clay plastering

It is known that clay plastering affects the permeability significantly. In the plastering experiment is studied how the hydraulic conductivity changes over time owing to clay plastering (RQ. 3). The plastering experiment is carried out with an artificial sand-clay mixture used in the erosion experiment as well as the natural sludge layer currently present in the side channel of the Twentekanalen (RQ 3.1 and RQ 3.2 respectively). Based on the differences between these mixtures the effect of composition is studied.

Translation to Twentekanalen

This research ends with the translation from the experimental results to the situation of the Twentekanalen (RQ 4). The obtained information in the sub questions will answer the main research question and does fulfil the predefined objective.

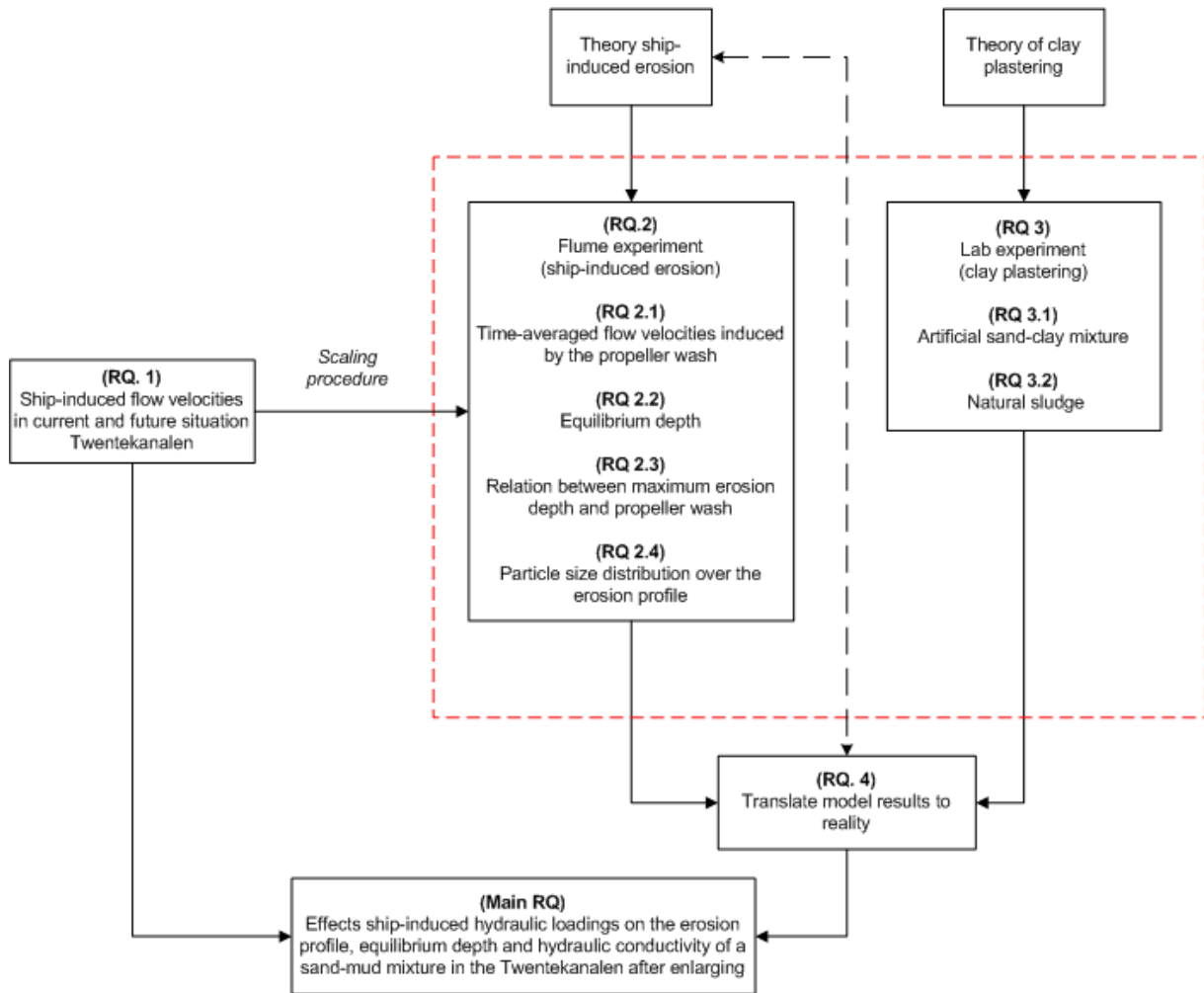


Figure 3: Methodology in order to answer the main research question and to fulfil the objective of this research. The dashed red line signifies the conducted experiments; the dashed black line indicates the comparison with existing literature.

Terminology

In literature (and in practical sense) the terminology regarding sand-mud mixtures does not always match. The most found terms to define these mixtures are briefly explained below and are also used in the context of this report: (1) sand-mud mixtures, (2) sludge, and (3) sand-clay mixtures.

1. Sand ranges from $63 \mu\text{m}$ to 2mm whereas mud is the fraction of sediment $< 63 \mu\text{m}$ which is the sum of the silt and clay particles mixed with water.
2. In natural sand-mud mixtures also organic materials might be present affecting the properties of the mixture. In practical sense natural sand-mud mixtures are often named 'sludge'.
3. Sand-clay mixtures do not contain silt and/or organic material but only sand and clay which fraction is $< 2 \mu\text{m}$.

1.5 Thesis outline

Section 2 describes the existing literature regarding the propeller wash, ship-induced erosion and clay plastering. The current and future situation of the Twentekanalen case is discussed in section 3 where relevant parameters are obtained which serve as starting points for the experiments (RQ 1). Section 4 describes the experimental set-up for both the erosion and clay plastering experiment and deployed measuring instruments. The experimental results are discussed in section 5 in which a distinction is made between the results of the erosion experiment in paragraph 5.1 (RQ. 2) and the results of the plastering experiment in paragraph 5.2 (RQ. 3). Section 6 discusses the translation of the model results to the Twentekanalen case study regarding the development of erosion and hydraulic conductivity in time (RQ. 4). Also possible measures are mentioned to mitigate negative consequences with regard to seepage and examined for feasibility. The discussion of the experimental results and the discussion with respect to the usability of the results for the Twentekanalen is provided in section 7. The conclusions of this research are presented in section 8. Finally, the appendices show background information on the side channel of the Twentekanalen, applied methods and formulas to determine flow velocities, specifics on the preparation of the experiments, sludge parameters, and original total measurement series of the plastering experiments.

2 Literature survey

From literature it appears that the knowledge on the erodibility of sand-mud mixtures under influence of shipping currents is limited. Erosion formulas are developed for sand, however erosion formulas for sand-mud mixtures to predict the erosion depth in channels due to shipping currents were not found. This section provides information with respect to the erosion modes of sand-mud mixtures in paragraph 2.1. Characteristics of the propeller wash and important parameters to determine erosion depths are discussed in paragraph 2.2 and 2.3 respectively. Paragraph 2.4 describes the plastering theory from which information regarding hydraulic conductivity can be retrieved.

2.1 Erosion modes sand-mud mixtures

Winterwerp and Van Kesteren (2004) formulated four erosion modes based on the geotechnical approach of Schofield and Wroth (1968): entrainment, floc erosion, surface erosion and mass erosion. The paper of Jacobs et al. (2011) describe these modes as follows. Entrainment occurs when fluid mud is entrained by a turbulent flow. Floc erosion is the disruption of individual flocs from the surface of the bed by flow-induced peak bed shear stresses. Surface erosion is a drained failure process (no pore water pressure gradients), which occurs when the mean bed shear stress is larger than the mean erosion threshold. As a result, sand and mud simultaneously and continuously erode from the whole surface layer of the sediment bed, which is in contrast with the random (in both space and time) character of floc erosion. Finally, mass erosion is an undrained process during which lumps of material are eroded due to external fluid stresses, which largely exceed the cohesive bed strength as well as the strength resulting from pore water pressure gradients. Table 1 and Figure 4 proposes a classification for erosion modes based on erosion thresholds. It is noted that different erosion modes may occur simultaneously. The erosion rates for floc and mass erosion are expected to strongly relate to the stochastic character of the flow.

Table 1: Erosion modes based on erosion thresholds; after Winterwerp and Van Kesteren (2004). $\hat{\tau}_b$ reflects the bed peak shear stresses larger than the mean bed shear stress [Pa]; c_d reflects the drained strength [Pa]; $\bar{\tau}_b$ reflects the mean bed shear stress [Pa]; c_u reflects the undrained shear strength [Pa].

| | |
|-----------------|----------------------------|
| Stable bed | $\hat{\tau}_b < c_d$ |
| Floc erosion | $\hat{\tau}_b > c_d$ |
| Surface erosion | $c_d < \bar{\tau}_b < c_u$ |
| Mass erosion | $\hat{\tau}_b > c_u$ |

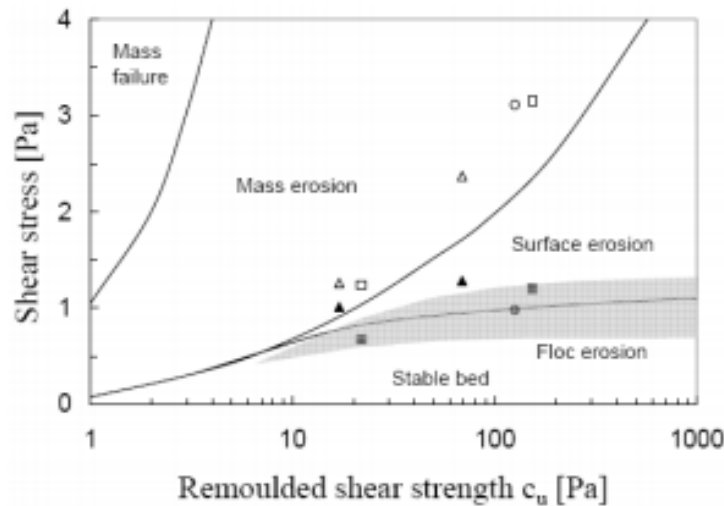


Figure 4: Classification of erosion modes for cohesive soils with the bed shear stress as a function of the bed strength after Winterwerp and Van Kesteren (2004). The grey area indicates that under the same conditions both floc erosion and surface erosion could be observed.

Winterwerp and Van Kesteren (2004) give a criterion for the threshold of mass erosion:

$$\tau_{e,m} = \frac{1}{2} f_w \rho_w u_b^2 > f_w (2 - 5) c_u \quad (2.1)$$

Where, $\tau_{e,m}$ = erosion threshold for mass erosion (= $\bar{\tau}_b$ or $\hat{\tau}_b$, depending on the occurring flow velocity) [Pa]; f_w = friction factor [-]; ρ_w = density of water [kg/m³]; u_b = bottom velocity [m/s]; c_u = undrained shear strength [Pa]

The undrained shear strength gives an indication of the resistance of the sediment bed to erosion and can be measured using a vane test (see Appendix E). Eq. 2.1 is used in the scaling procedure discussed in paragraph 4.1.7.

2.2 Theory propeller wash

Most inland navigation ships are equipped with propulsion systems: propeller(s) responsible for forward thrust and bow and/or stern thruster(s), mainly for the manoeuvrability of the ship. The velocity distribution and important parameters of a propeller are shown in Figure 5. Flow velocity data presented by Arcadis (2015) and reproduced in paragraph 3.2 shows that besides primary and secondary water movements, especially the propeller wash will influence the erosion of the canal bed and is therefore of major interest in this research.

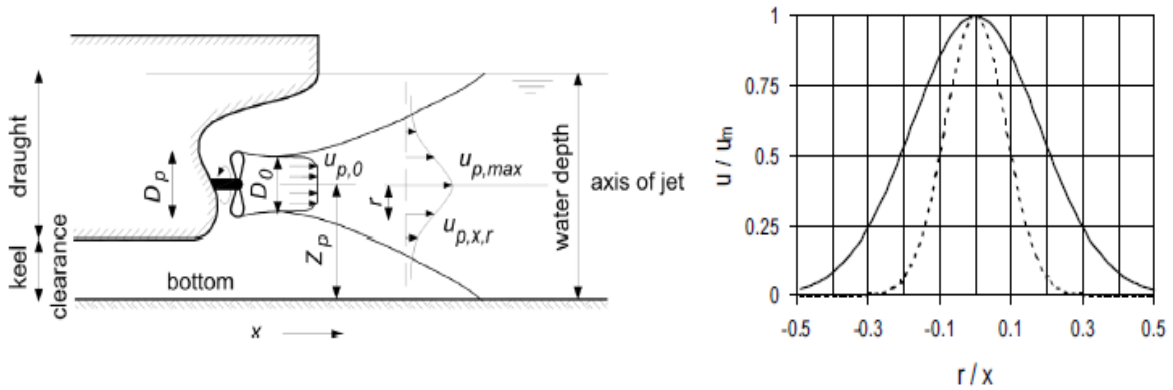


Figure 5: (Left) Water movements due to main propeller; after The Rock Manual (CIRIA, 2007) | (Right) Velocity distribution in propeller wash (solid line) and free jet (dashed line); after Schiereck (2004).

The velocity distribution can be described as a Gaussian curve, see Figure 5. In other words, the maximum flow velocity of the propeller wash occurs at the centre nearby the propeller while closer to the bottom or to the water surface the flow velocities will decrease.

Previous research have shown that the velocity within the ship's propeller is the initial step to investigate scouring induced by the propeller. Blaauw and Van der Kaa (1978), Verheij (1983), Hamill (1987, 1988) have experimentally studied the propeller wash and also focussed on the prediction of the maximum scour depth in free water. Through dimensional analysis they found out that the densimetric Froude number (Eq. 2.2) plays the most important role in affecting the scour depth:

$$F_0 = U_{pr,0} / \sqrt{g \Delta d_{50}} \quad (2.2)$$

with $U_{pr,0}$ = efflux velocity [m/s]; g = gravitational constant [m/s^2]; Δ = relative density [-]; d_{50} = median particle diameter [m]

One of the parameters within the densimetric Froude number is the velocity within the ship's propeller which is called efflux or outflow velocity. In fact, the propeller jet is composed of three velocity components, (1) the axial component, (2) the tangential component and (3) the radial component. Since the axial velocity field is largely contributing to bed scouring, only this velocity component is studied in this research. The efflux velocity in other words is the maximum axial velocity at the centerline of the propeller axis. The axial momentum theory has been widely accepted to predict the efflux velocity, however some researchers have refined the theoretical equation through experimental investigations. Furthermore as can be seen in Figure 6 the axial velocity field behind the propeller can be distinguished into a zone close to the propeller which is called the 'zone of flow establishment' and a zone at larger distance from the propeller which is called the 'zone of established flow'. Many researchers propose (Albertson et al., 1950; Fuehrer & Römisch, 1977; Blaauw & Van der Kaa, 1978) that the maximum axial velocity is constant within the entire zone of flow establishment up to a certain distance from the propeller as can be seen in Figure 6. However, other researchers (Hamill, 1987; Stewart, 1992; Lam et al., 2011) in turn propose that the maximum axial velocity is not constant within the zone of flow establishment. Evidently, the scientific community does not agree with each other on the axial velocity distribution of a ship's propeller. The paper of Lam et al. (2011) provides a complete overview of previous research and existing formulas to predict efflux velocities and decaying maximum axial velocity functions supported by experimental data.

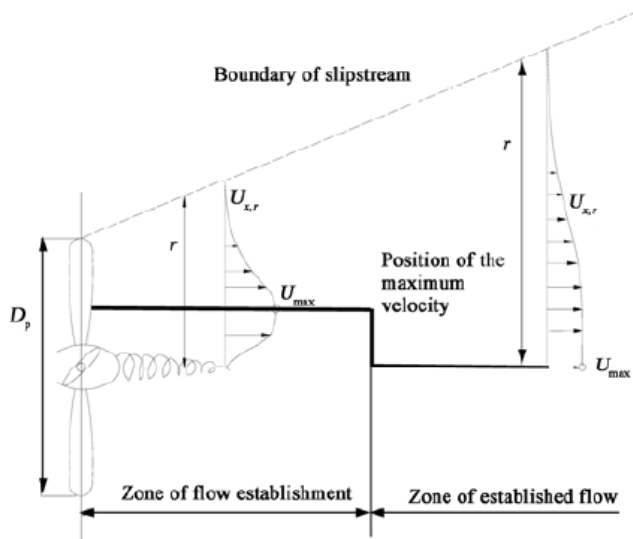


Figure 6: Schematic representation of the position of the zone of flow establishment and the zone of established flow; from Lam et al. (2011).

In this research it is assumed that the axial velocity measured at one propeller diameter behind the actual location of the propeller ($x/D_{pr} = 1$) is equal to the efflux velocity which seems a valid assumption based on the paper of Lam et al. (2011) because the measuring location is very close to the propeller. Due to the absence of essential data such as the thrust coefficient it cannot be compared with existing formulas to predict efflux velocities.

2.3 Theory ship induced erosion

At present, quantitative research regarding erosion due to ships is scarce. Proper physically-based formulas to determine bottom and/or bank erosion caused by ship currents are not available yet. Empirical formulas exist but lack sufficient experimental data, and data from reality for validation. As ships become larger over the last decades, their propulsion engines need to become more powerful. Scour induced by propeller wash has become one of the most important parameters for the design and maintenance of navigation channels with limited depth (Hong et al., 2013). Figure 7 depicts the erosion profile caused by the propeller on the bottom due to sailing vessels.

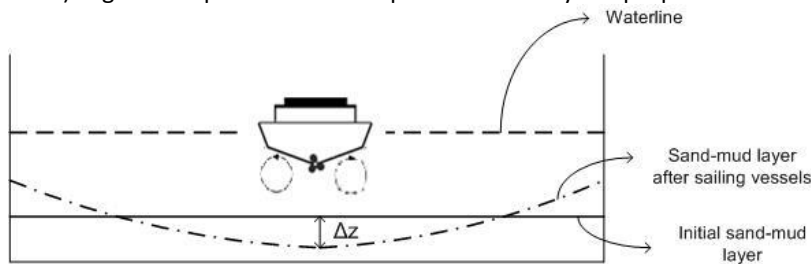


Figure 7: Bottom erosion caused by sailing vessels in the axis of the channel.

Besides bottom erosion also bank erosion can be caused by the propeller wash or other ship-induced currents, however bank erosion is beyond the scope of this research. Figure 7 tends to show that bottom erosion is only due to the propeller wash which is certainly not true. As stated in Appendix D the return current generates flow velocities beneath the ship's hull which is able to erode the bottom if channel dimensions are relatively small, underkeel clearance is small and sailing speed is high.

Existing formulas to predict bottom erosion due to shipping currents can be distinguished in formulas regarding the return current erosion and formulas regarding the propeller wash. An important remark for these formulas is that almost all are experimentally determined in a laboratory using a non-cohesive sediment bed. No erosion formulas on sand-clay mixtures were found in literature and are assumed to be non-existent yet. However, in canals evidence of erosion tracks in natural sand-mud mixtures is visible (see Appendix C) which probably is caused by shipping movements. An overview of existing formulas to estimate the maximum scour depth is given in Table 2 based on cohesionless sediments.

Table 2: Existing formulas to estimate scour depth.

| | | |
|----------------------------|---|--|
| Hoffmans & Verheij (1997) | Return current | $z_m = (\alpha U_r - U_c)^2 \sqrt{\frac{Ndt}{K\Delta^{1.7}}}$ <p>With: z_m = erosion depth [m]; $\alpha = 1.5 + 5r_0$ [-]; r_0 = turbulence intensity [-]; U_r = return current below the ship's keel [m/s]; U_c = critical flow velocity [m/s]; N = amount of ship passages [-]; $dt = L/V_s$ [h]; K = erosion constant [m²/s⁴]; Δ = relative density [-]</p> |
| Ducker & Miller (1996) | Propeller wash | $\frac{d_{max}}{d_{85}} = C_m \cdot 4.6 \left(\frac{B^*}{B_{85}^*} \right)^{2.25}$ <p>With: d_{max} = erosion depth [m]; d_{85} = 85th percentile of particle diameter [m]; C_m = constant [-]; $B^* = \frac{U_{pr,b}}{\sqrt{d_{85}g\Delta}}$ [-] with $U_{pr,b}$ = maximum flow velocity on the bottom [m/s]; B_{85}^* = stability coefficient = 1.25 [-] by definition for flat surfaces and free propellers</p> |
| Verheij (1983) | Propeller wash <i>Valid for</i> $5.12 \leq F_0 \leq 5.39$ | $\frac{d_{max}}{z_b} = 4 \cdot 10^{-3} \left(\frac{F_0}{z_b/D_0} \right)^{2.9}$ <p>With: d_{max} = maximum scour depth [m]; z_b = offset height [m]; F_0 = densimetric Froude number = $U_{pr,0}/\sqrt{g\Delta d_{50}}$ with $U_{pr,0}$ = efflux velocity [m/s]; g = gravitational constant [m/s²]; Δ = relative density [-]; d_{50} = median particle diameter [m]; D_0 = effective propeller diameter [m] (= 0.7 times propeller diameter for free propellers without nozzle to 1 times the diameter for propellers in a nozzle)</p> |
| Hamill (1987) | Propeller wash <i>Valid for</i> $5.55 < F_0 < 7.73$ | $\frac{d_{max}}{z_b} = 0.0467 \left(\frac{F_0}{z_b/D_0} \right)^{1.39}$ |
| Hong, Chiew & Cheng (2013) | <i>Propeller wash</i> <i>Valid for</i> $0.5 < \frac{y_0}{D_p} < 1.5$ and $5.55 < F_0 < 11.1$ | $\frac{d_{s,me}}{D_p} = 0.265 \left[F_0 - 4.114 \left(\frac{y_0}{D_p} \right) \right]^{0.955} \left(\frac{y_0}{D_p} \right)^{-0.022}$ <p>With: $d_{s,me}$ = maximum scour depth [m]; D_p = diameter of propeller [m]; F_0 = densimetric Froude number [-]; y_0 = offset height [m];</p> |

Rijkswaterstaat is interested in the bed erosion and in particular the erosion of the seepage reducing sludge layer since this layer will be reconstructed after enlarging the Twentekanalen in order to cope with the seepage inconvenience for local farmers and residents. Besides influencing the geo-hydrological characteristics in the area also instability of sheet piles can be caused by the propeller wash. An estimation of the scour depth can be found with the equations in Table 2, however these are based on sand or gravel. Hence, the scour depth in a sand-clay layer only cannot be predicted accurately according to these formulas due to cohesive properties. Nevertheless, assuming exposure of the sand bottom to ship-induced currents after erosion of the sludge layer gives an indication of the erosion tracks in the Twentekanalen.

A drawback from the equations developed by Verheij (1983), Hamill (1987) and Hong et al. (2013) is that these are derived in a situation with a continuously rotating propeller at one single position. Logically, this is not the situation occurring in reality in which ships are sailing through the channel. However, when ships need to manoeuvre a lot at small sailing speeds (e.g. near locks, bridges, turning basins and docks) the impact time on the bottom will become larger. Additionally, also the propeller wash velocity on the bottom is larger for ships at small sailing speeds because the velocity on the bottom is reduced by a larger sailing speed (BAW, 2005) assuming constant efflux velocity. In accordance with CUR report-201, the propeller wash bottom velocity should be reduced by 0.5 times the sailing speed (CUR, 1999). Concluding, these equations predict a theoretical maximum erosion depth for moored ships while this research focusses on the erosion tracks of a sand-mud layer caused by sailing ships. Furthermore, the validity range of the densimetric Froude number is rather small while in reality much larger densimetric Froude numbers occur. Another important difference is that the suspended sediment can deposit on the bed again after the ship has passed which is not possible by a continuously rotating propeller. The erosion formulas developed specifically for scour induced by the propeller wash show the importance of the densimetric Froude number, and the ratio of the offset height divided by the (effective) propeller diameter. The maximum equilibrium scour depth increases with the increase in densimetric Froude number and decreases with increasing offset height ratio. These parameters are important and varied in this research to study the effects with regards to the erosion of a sand-clay mixture. Nevertheless, the equations developed by Verheij (1983) and Hamill (1987) are used to compare with erosion in a sand-clay mixture of the experiment. For the situation of the Twentekanalen on full-scale the formulas of Hoffmans and Verheij (1997) and Ducker and Miller (1996) are used to compare the magnitude of obtained erosion depths. The first equation is validated in a full-scale experiment with ships in the Julianakanaal comparable with the situation of Twentekanalen.

2.4 Theory soil plastering

In this section the plastering theory is described which can be divided into three processes: (1) intrusion or mud-spurt, (2) blocking and (3) consolidation. Initially the plastering theory is developed in order to gain understanding of the soil plastering mechanism in tunnelling technologies, however it is expected that this theory is also applicable to understand the mechanism of clay intrusion into a sandy subsoil and its effect on the hydraulic conductivity changes over time. The latter is interesting regarding the situation of seepage nuisance in the Twentekanalen.

The paper of Talmon et al. (2013) presents a schematization of a clay suspension that has invaded into a water-saturated granular soil plus the course of the invasion process in time (Figure 8) and describes the plastering process as follows:

“The pressurized clay suspension has quickly invaded the pores (mud spurt). This flow has, however, been slowed down by an increase of contact area between the clay suspension and the pores, and by blocking of the pores by fine solid particles (if present in the clay suspension). The clay suspension commences to consolidate during this process and a (internal and/or external) filter cake will be formed.”

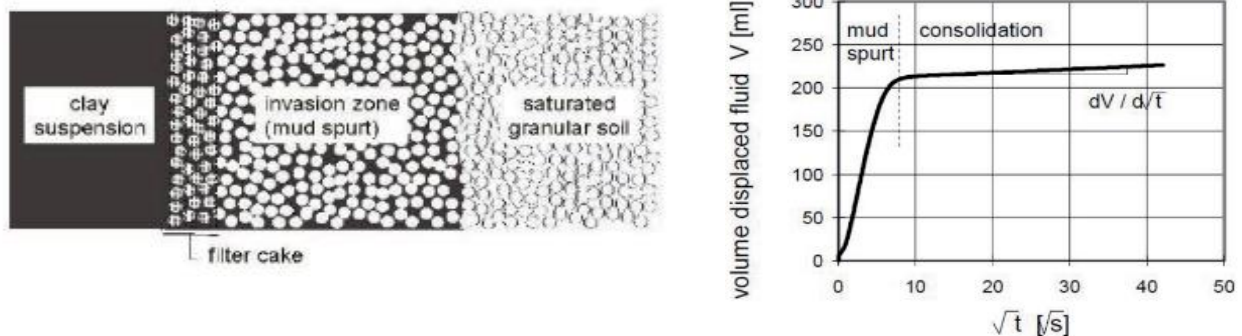


Figure 8: (Left) Invasion of clay suspension into saturated granular soil. (Right) Typical course of displaced fluid in a plastering test; after Talmon et al. (2013).

The right graph in Figure 8 shows that initially in the mud spurt phase the increase in volume of displaced fluid (seepage) is relatively large. At the end of the mud spurt (moment of consolidation), indicating that the pores of the subsoil become clogged, the rate of seepage has decreased significantly. In fact, three permeabilities can be distinguished in the left image of Figure 8:

1. Permeability of the sand skeleton to water relevant for groundwater flow to surroundings;
2. Permeability of the sand skeleton with respect to the clay suspension relevant to the mud spurt;
3. Permeability of the clay fabric to water in the clay relevant to consolidation of the clay and residual seepage of water when mud spurt and consolidation have come to a halt (filter cake).

Moreover, in the paper of Talmon et al. (2013) a framework is developed to model the plastering process in which equations are derived and validated with experiments (mainly with clay suspensions accompanying small yield stresses in the order of 0 – 10 Pa). This report demonstrates that the plastering theory (mud spurt and consolidation process) can also be applied to the seepage problem in which sludge is poured on top of sand filter.

3 Case Twentekanalen: Starting points

In order to translate the results of the flume experiment to field conditions it is necessary to have information on the conditions in the Twentekanalen. Natural flow velocities and flow velocities caused by shipping are dependent on the cross section of the channel. Therefore, in paragraph 3.1 the current profile and profile after enlarging is depicted. Another important parameter in this research is the hydraulic conductivity of the subsoil which is largely responsible for the amount of seepage to the surrounding area described in Appendix B. Moreover, soil samples of the existing sludge layer in the side channel were taken and analysed in the laboratory (Appendix H), and served as input for the plastering experiments (Paragraph 4.2 & 5.2). Paragraph 3.2 calculates the current (normative) flow velocities in the Twentekanalen with shipping class IV and future flow velocities after enlarging with shipping class Va. (RQ. 1).

3.1 Cross section side channel Twentekanalen

A schematized cross section of the current and future profile at 13.5 km in the side channel is shown in Figure 9. At the bifurcation point near Delden the surface level is 11.3 m+ NAP and the surface level at the harbour of Almelo is 9.3 m+ NAP. The Twentekanalen are divided by locks and the maximum discharge to transport an excess of water is rather small. Arcadis (2015) used in their calculations a maximum discharge of the main channel (Delden-Hengelo) of 25 m³/s corresponding to a flow velocity of about 0.17 m/s (depending on the cross section). From these calculations it is concluded that velocities due to natural flow are not of importance regarding the bottom erosion compared to flow velocities originating from ships.

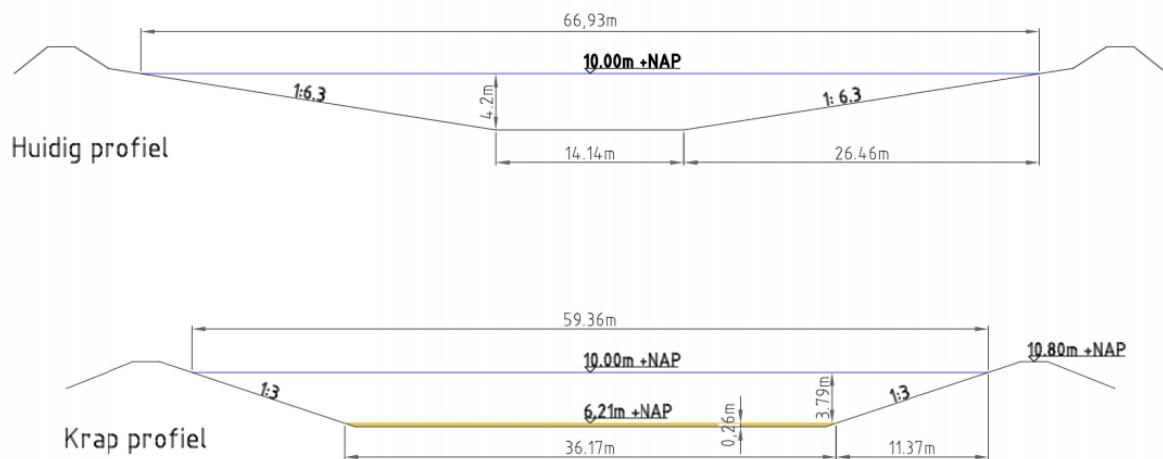


Figure 9: (Top) current profile dimensions at 13.5 km of the side channel. (Bottom) dimensions future profile at 13.5 km of the side channel. The brown colour refers to the sludge layer.

Note that the future profile (Figure 9, bottom) is mainly widened compared to the current situation (Figure 9, top). In fact, at some locations the water depth in the current situation is already larger than the minimum prescribed water depth for shipping class Va according to “Richtlijn Vaarwegen” which is 1.3 times the draught plus a safety margin of 0.15 m (Rijkswaterstaat, 2011). Logically, at locations where the depth is already larger than the minimum prescribed depth, no measures are taken and the larger water depth remains. However, for calculation of flow velocities the minimum dimensions corresponding to a waterway suitable for shipping class Va (Rijkswaterstaat, 2011) are chosen as normative because most likely it produces the maximum flow velocities on the bottom.

3.2 Ship-induced flow velocities

This research focusses on the interaction between the ship-induced currents and the sediment bed. Enlarging the Twentekanalen from class IV to class Va implies also intensified flow velocities on bottom and banks of the canal due to these larger vessels (Arcadis, 2015). Shipping class Va is normative for the side channel of the Twentekanalen in the future situation based on the dimensions of the ship according to "Richtlijn Vaarwegen" (Rijkswaterstaat, 2011). In Table 3 a comparison is made between class IV vessels in the current situation and class Va vessels in the future situation with corresponding properties.

Table 3: Properties vessels Class IV and Class Va related to the Twentekanalen.

| | Class IV vessel | | Class Va vessel | |
|---|-----------------|-----------------|-----------------|-----------------|
| | <i>Loaded</i> | <i>Unloaded</i> | <i>Loaded</i> | <i>Unloaded</i> |
| Width ship [m] | 9.5 | 9.5 | 11.4 | 11.4 |
| Length ship [m] | 85 | 85 | 110 | 110 |
| Draught [m] | 2.5 | 1.8 | 2.8 | 1.8 |
| Diameter propeller [m] | 1.9 | 1.9 | 1.9 | 1.9 |
| Power main propeller [kW] | 1766 | 1766 | 1766 | 1766 |
| Power bow thruster [kW] | 544 | 544 | 544 | 544 |
| Number of propellers [-] | 2 | 2 | 2 | 2 |
| Block coefficient [-] | 1 | 1 | 1 | 1 |
| Yt (distance propeller tip to keel) [m] | 0.15 | 0.15 | 0.15 | 0.15 |
| Coefficient for secondary waves [-] | 1 | 0.35 | 1 | 0.35 |
| Yt bow thruster [m] | 0.2 | 0.2 | 0.2 | 0.2 |
| % of limit speed [-] | 0.75 | 0.9 | 0.75 | 0.9 |

The difference between these ships is only related to the width, length and the draught. The other characteristics are in both situation equal in which a distinction should be made between loaded and unloaded ships. The second issue determining the flow velocities of ships on the banks and the bottom is the profile of the canal (see Figure 9)³.

Until now the calculation of ship-induced flow velocities takes place via empirical formulas because exact physical solutions are not available yet (even with numerical models it is inaccurate). Three types of ship-induced currents are distinguished: (1) primary water movements, (2) secondary water movements and (3) propeller wash. In this study the empirical formulas summarized in the Rock Manual (CIRIA, 2007, pp. 434-442) are used to quantify the occurring flow velocities and are presented in Appendix D.

These equations are implemented in Matlab in which the input comprises the assumed trapezium future profile depicted in Figure 9 and the parameters in Table 3. The results of the calculation are shown in Table 4. It is known that secondary waves play an important role regarding bank erosion, however the influence on bottom erosion is very limited. Bank erosion is beyond the scope of this research, therefore secondary water movements are neglected here.

Table 4: Ship-induced flow velocities in the current and future situation regarding different shipping class and profile.

| | Current situation Class IV | | Future situation Class Va ('Krap' profile) | |
|--|-------------------------------|-----------------|---|-----------------|
| | <i>Loaded</i> | <i>Unloaded</i> | <i>Loaded</i> | <i>Unloaded</i> |
| Actual sailing speed [m/s] | 2.1 | 2.8 | 2.1 | 2.9 |
| Max. Return current canal [m/s] | 0.5 | 0.7 | 0.7 | 0.8 |
| Return current underneath ship (lower limit) [m/s] | 0.8 | 1.0 | 1.0 | 1.2 |
| Return current underneath ship (upper limit) [m/s] | 1.1 | 1.3 | 1.3 | 1.6 |
| Velocity directly behind propeller [m/s] | 7.2 | 7.2 | 7.2 | 7.2 |
| Velocity on the bottom due to the main propeller for ships at rest [m/s] | 2.2 | 1.8 | 2.9 | 2.0 |
| Velocity on the bottom due to the main propeller for sailing ships [m/s] | 1.2 | 0.4 | 1.9 | 0.5 |

Table 4 shows that when changing to shipping class Va the flow velocities on the bottom will increase. The return current increases with roughly 20% to 1.6 m/s and the bottom velocity caused by the propeller wash for sailing ships increases with roughly 60% to 1.9 m/s compared to the current situation with shipping class IV. For moored ships the flow velocities on the bottom are even higher because the bottom velocity for sailing ships should be reduced by 0.5 times the actual sailing speed (CUR, 1999).

³ Remember that the cross section is not similar along the entire length of the side channel. In order to estimate flow velocities in different parts of the canal it is necessary to repeat the calculation with the correct cross section for the part of interest.

4 Experimental set-up

To be able to examine the ship-induced currents and subsequent erosion pattern (RQ. 2) an erosion experiment is set up, which is described in paragraph 4.1. The erosion pattern in a sand-clay mixture is studied by means of a scale model in which a model ship sails through a flume and by measuring the bottom profile after every ship passage. The sailing and propeller wash velocities are determined beforehand and are scaled according to the situation in the Twentekanalen with the aid of velocity measurements executed in the flume in longitudinal direction, transverse direction and in height. Paragraph 4.1 describes the experimental facility, sediment mixture characteristics, measuring equipment and scaling method to scale the occurring flow velocities in the Twentekanalen and it gives an overview of the conducted experiments.

Paragraph 4.2 describes the plastering experiment in which the experiments are carried out with both an artificial sand-clay mixture and a natural sand-mud mixture taken from the Twentekanalen on top of a sand filter according to the plastering theory of Talmon et al. (2013). The outcomes of these experiments give insights in the effects of clay plastering on the hydraulic conductivity (RQ. 3).

4.1 Erosion experiment

4.1.1 Experimental facility

The experiments are carried out in the flume ('Water-Grond Goot') at the experimental facility of Deltares in Delft, the Netherlands. The width and length of the used flume are 3 m and 30 m respectively and the depth is 2 m. The flume is equipped with a (moving) measuring bridge and a towing facility. The flume can be seen in Figure 10.



Figure 10: (Left) Experimental facility (Right) model ship.

Beside the flume also a model ship is provided by Deltares (Figure 10). This ship has a length of 3 m, a width of 0.56 m and a maximum draught of approximately 0.35 m. The diameter of the ship's propeller was 0.13 m. The ship was fixed in a frame which was connected to the moving measuring bridge. A consequence of fixing the ship to the frame is that it could not move vertically while sailing. This experimental situation does not completely reflect reality, since ships will experience squat, which depends on (amongst others) sailing speed (Eloot et al., 2008). In this experiment especially the interaction between the ship-induced currents with respect to the underkeel clearance and the bottom is relevant. A fixed underkeel clearance makes it easier to interpret the results. The underkeel clearance is adjustable by two threaded bolts. In this way the ship can be lowered or raised to obtain the required underkeel clearance.

Due to start-up of the ship (e.g. propeller start rotating) initial waves are created which might lead to more turbulence in the water column and unwanted reflection of waves at the end of the flume. These unwanted water motions might influence the results. To minimize these effects the measurements are performed in the middle of the flume (Figure 11).

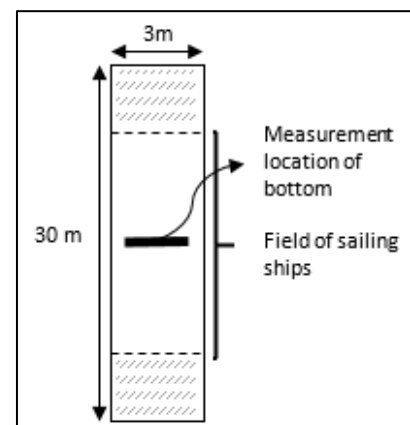


Figure 11: Measurement domain in flume.

4.1.2 Mixture characteristics

The available sediment mixture is an artificially created mixture with sand and kaolinite clay which was stored in a basin besides the flume. An important phase in this research was the preparation of the flume with the available sediment. Appendix D describes how this process took place and highlights interesting facts. The sand-clay mixture was engineered by Van de Ree (2015) guided by Walther van Kesteren of Deltares for another not related research. The sediment mixture is described in Table 5 where the sand-fines ratio (SFR) is 3.3, Water-Clay ratio of 200% and a mixture density of 1740 kg/m³.

Table 5: Composition of the sediment mixture according to Van de Ree (2015).

| Substance | Percentage weight [%] |
|------------------------------------|-----------------------|
| Fine sand (133 μm) | 26 |
| Coarse sand (330 μm) | 26 |
| Clay (15 % kaolinite + 1% Illite) | 16 |
| Tap water | 30 |
| Saline | 2 |

Drawback of this sediment mixture in relation to the Twentekanalen is that this sediment is created with saline water conditions while the water in the Twentekanalen is fresh. Winterwerp and van Kesteren (2004) stated that the flocculation process is for example affected by the pH-value and electrochemical interaction which is different in fresh water compared to saline water. However, it is assumed that it would not have a significant effect on the predicted erosion depth. Rheological parameters and strength being the relevant properties. The strength of the sediment as applied in the flume can be found in Figure 51 of Appendix E.

The sediment bed is prepared and the surface is flattened with a special beam to create a sediment layer of 10 cm. The imperfections of the sediment bed varied around 1 - 1.5 cm over the length and width in the flume. To be able to establish the proper keel clearance the height of the sediment is measured with a ruler at different locations in the flume from which the average is taken. The bed was flattened before every set of measurements which served as the reference situation.

4.1.3 Conditions to be simulated

Rijkswaterstaat requested the experiments to cover relevant vessel – fairway interaction to get insights in future behaviour of the sand-mud mixture in the side channel Twentekanalen after enlarging. Normative conditions occurring in reality in the side channel are shown in Table 6. It is expected that the propeller wash is most severe regarding bottom erosion after enlarging (see Table 4), hence the choice was made to simulate loaded vessels. Furthermore it is assumed that the vessels sail most of the time in the axis of the channel.

Table 6: Normative conditions in the side channel of the Twentekanalen with respect to the magnitude of shipping flow velocities on the bottom.

| Parameter | Value |
|--|----------------------------|
| Length ship (L_s) | 110 m |
| Beam width ship (B_s) | 11.4 m |
| Sailing speed (V_s) | 2.0 m |
| Efflux velocity propeller ($U_{pr,0}$) | 7.2 m/s |
| Maximum natural flow velocity (U_0) | 0.2 m/s (assumed 0 m/s) |
| Draught (T) | 2.8 m |
| Water depth (h) | 3.64 m |
| Under keel clearance (h_k) | 0.84 m |
| Offset height (z_p) (=distance from propeller axis to the bottom) | 2.1 m |
| Width water line (B_w) | 60 m |
| Width fairway (B_f) | 36 m |

4.1.4 Measuring equipment & methods

The data of interest are flow velocities originating from the propeller, the scour depth after a certain amount of ship passages, and the offset height which is determined by a ruler.

The propeller is driven by an electric motor which is controlled by a potentiometer. The flow velocities in the propeller wash are expected to have the largest impact on the erosion profiles based on the calculated flow velocities in paragraph 3.2. Therefore, it is necessary to examine these flow velocities at different locations in the flume both in depth as in width. The purpose is to determine efflux velocities, velocities on the bottom, the critical velocities and to confirm with existing literature to get confidence in the measurements. The flow velocities were measured with an electromagnetic velocity meter (EMS) which measures bi-directional water velocity in two perpendicular directions (Figure 12). The measurement principle is based on conductive fluid moving through a magnetic field⁴. The measuring period was chosen to be five minutes with a frequency of 50Hz because of the known large turbulence. The efflux velocity is determined before execution of the erosion experiment whereas the velocity at the original bottom and at the bottom of the scour hole are measured afterwards.

Based on bathymetry measurements in navigation channels, e.g. the Twentekanalen, it is expected that an erosion track develops below the ship. Likewise, the bathymetry was mapped in the experiment using an echo sounder (or ultrasonic sensor) after every passage of a ship. This echo sounder was fixed on a measuring bridge and placed on exactly the same location after every ship passage. By means of an electric driving mechanism the echo sounder was displaced along a beam of 1 m (Figure 12). The transducer has a frequency is 5 MHz, a measuring frequency of 200 Hz and a range from 20 – 500 mm. The transducer frequency seems high, however this is necessary to detect the top layer of the sediment rather than the concrete bottom of the flume. Lower frequencies penetrate deeper into the soil which is undesirable. A point of attention is the timeframe in which the bathymetry measurements were carried out. These scans were made within 15 to 30 minutes after every ship passage meaning that deposition of (very) fine sediments was certainly not finished. However, these effects can be neglected as is explained and illustrated in Appendix I. The data of both instruments and the position of the echo sounder were gathered by a computer on the measuring bridge.



Figure 12: (Left) movable echo sounder; (Right) EMS measuring propeller wash.

4.1.5 Restrictions experimental conditions

The dimensions of the flume are fixed. However, more factors might restrict the outcomes of the experiment, which are described below.

Maximum sailing speed

The maximum sailing speed is set at 75% of the limit speed based on Schijf (1949). The limit speed is the theoretical maximum sailing speed of the ship based on the ship's characteristics and the channel profile. However, sailing at the maximum speed is not cost-efficient and in practise loaded ships will reach 75% of the limit speed. This value is based on data of the ships in which a distinction is made between loaded (75% of limit speed) and unloaded ships (90% of limit speed). The choice is made to simulate loaded vessels and the applied sailing speed is 75% of the limit speed despite the fact that a speed restriction is imposed in the side channel of the Twentekanalen (Jol, 2014): loaded vessels 7 km/h and unloaded vessels 9 km/h. The calculated maximum sailing speed (see Table 4) is generally higher than the imposed speed restriction which means that relatively extreme conditions are chosen. The effects of the sailing speed is studied by varying the scaled sailing speed in the experiment (see Table 7).

⁴ More information can be found at <https://www.deltares.nl/app/uploads/2016/04/Programmable-electromagnetic-liquid-velocity-meter.pdf>

Maximum draught model ship

The maximum draught of the model ship is limited by the dimensions of the ship (see Figure 13). In this case the maximum draught is 0.35 m otherwise water will flow into the model ship. However, at the bow of the sailing ship water is 'pushed' upwards (= impoundment) resulting in a larger draught at the bow which is in fact larger than the imposed maximum draught ($h - h_k$). To prevent water flowing into the model ship it is necessary to limit the maximum draught at the bow even further.

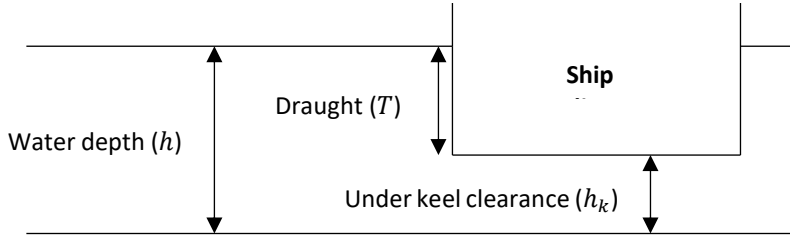


Figure 13: Schematized draught of a ship.

The draught at the bow is calculated with the aid of the method of Bouwmeester (1977):

$$T_{bow} = T + \eta \quad (4.1)$$

T_{bow} = draught at the bow [m]; T = draught [m]; η = the impoundment or at the bow [m]

$$\eta = C_D \cdot \frac{(V_s - U_0)^2}{2 \cdot g} \quad (4.2)$$

C_D = resistance coefficient [-]; V_s = sailing speed [m/s]; U_0 = ambient velocity [m/s]; g = gravity constant [m/s²]

$$C_D = \gamma \cdot \left(\frac{T}{h}\right)^2 \quad (4.3)$$

γ = shape coefficient (= set at 1 based on available ship data) [-]; T = draught [m]; h = water depth [m]

The parameters chosen in this research (Table 7) all remain below the maximum draught of the model ship.

Minimum keel clearance

As regards to keel clearance there is not a specific minimum limit, however it appears that taking measurements will be very difficult when keel clearance is too small. Talmon and Verheij (2014) mention in a more or less similar experiment that the minimum keel clearance is set at 0.01 m (10 mm).

4.1.6 Scaling

In order to simulate the reality as much as possible (i.e. geometric similarity, kinematic similarity and dynamic similarity) all relevant parameters need to be scaled. The scale factor is the ratio of the value in reality and the value in the model:

$$\lambda_x = \frac{X_{reality}}{X_{model}}$$

The scale factor is indicated by λ and a scale factor of 10 means that the physical dimensions in the model are 10 times smaller than in reality. For a few parameters the value in reality is equal to the parameter value in the model. This applies for example to the gravitational acceleration which means: $\lambda_g = 1$.

Generally, in most experiments this also applies to the viscosity and the density, however in the situation of the Twentekanal in reality is dealt with fresh water while in the model the water could be brackish due to salt left behind in the sediment (from earlier experiments). Therefore, it is not completely true to apply a scale factor of 1 for these parameters. However, it seems valid to apply viscosity of fresh water because in the experiment fresh water is used and only a small amount of sand-clay is extracted from the basin, hence $\lambda_\nu = 1$.

Scaling water motions

In scaling procedures often dimensionless quantities are used because these must be equal for both the scaled model as for the situation in reality according to similitude theory. In fluid dynamics the Froude number and the

Reynolds number are often used as dimensionless numbers and will form the starting point for the scaling procedure (Eq. 4.4 and 4.5):

Froude scaling (ratio inertia – gravity)

$$Fr = \frac{u^2}{g \cdot h} \rightarrow \lambda_{Fr} = \frac{\lambda_u}{\sqrt{(\lambda_g \cdot \lambda_h)}} = \frac{\lambda_u}{\sqrt{\lambda_h}} = 1 \rightarrow \lambda_u = \lambda_h^{0.5} \quad (4.4)$$

Reynolds scaling (ratio inertia – viscosity)

$$Re = \frac{u \cdot L}{\nu} \rightarrow \lambda_{Re} = \frac{\lambda_u \cdot \lambda_L}{\sqrt{\lambda_\nu}} = \lambda_u \cdot \lambda_L = 1 \rightarrow \lambda_u = \lambda_L^{-1} \quad (4.5)$$

It can be seen that these criteria do not match with each other. Delefortie (2007) mentions that scaling according to Froude's law is a better option than scaling according to the Reynolds number because in ship hydrodynamics the presence of free surface increases the importance of gravity forces and the scaled speed results in some cases in disproportionately large values according to Reynolds scaling. Also Blaauw and Van der Kaa (1978) and Verheij (1983) proposed that scale effects by differences in Reynolds number due to flow in a propeller are insignificant as long as the flow in the model is turbulent which will be the case in this research ($Re > 4000$, meaning that inertial forces will be dominant while viscous effects play a minor role). Therefore, the scaling procedure related to ships sailing in canals or at open water is often applied according to the Froude law and is also applied in this research.

4.1.7 Scaling choices

In similar earlier research Talmon and Verheij (2014) provided information about the scaling choices and discussed the pros and cons. These choices are also adopted in this research because the used flume and ship are the same. For the horizontal and vertical length scale the choice is made to adopt the non-distorted scale because of geometric similarity between model and reality. By doing this the translation from model results to reality is easier compared to a distorted scale. It is decided to use a scale of 1:20 because of the dimensions of ship and the flume. Larger scales (up to 1:10) were possible but gave problems with model ship availability. Smaller scales were also possible, but in principal larger scales results in better approximations of the situation in reality. Therefore it is decided to make use of a 1:20 length scale which is also representative for the actual keel clearance and offset height. It should be noted that the propeller diameter is scaled with factor 15 which is a larger scale than factor 20. However the efflux velocity is measured beforehand which is the most important parameter regarding bottom erosion (see paragraph 2.2) and scaled properly. Bottom velocities are measured afterwards (Table 9) and these velocities showed correspondence with occurring scaled bottom velocities in reality (Table 4).

Eq. 2.1 shows that the squared of the velocity scales with the strength of the sediment assuming mass erosion. Scaling according to Froude's law results in a velocity scale of the square root of the length scale. Hence, the sediment strength scales with the length scale. Appendix H demonstrates that the sediment strength also scales to a factor 20. Thus:

- Horizontal length scale: $\lambda_L = \frac{1}{20}$
- Vertical length scale: $\lambda_h = \frac{1}{20}$
- Velocity scale: $\lambda_u = \lambda_h^{0.5} = \frac{1}{\sqrt{20}}$
- Sediment strength scale: $\lambda_s = \frac{1}{20}$

4.1.8 Experimental choices & procedure

In this research is chosen to simulate situations with varying keel clearance, sailing speed and efflux velocity. The undisturbed water depth in reality is approximately 3.8 m. However along the channel, depths of 3.64 m might occur (= minimum prescribed water depth). To take this into account the draught of the ship is raised until the under keel clearance of 0.84 m is reached which is the minimum keel clearance because the maximum draught of shipping class Va in the side channel of the Twentekanaal is 2.8 m. In other words, the only parameter that is varied is the keel clearance and consequently the draught whereas the water depth is constant and stagnant water is applied. The required water depth in the flume could not be set at the scaled water depth because the position of the propeller would be partly above the waterline. The water depth in the experiment is raised to approximately 36 cm while the other parameters are scaled properly. It is assumed that this choice would not have an impact on the results for propeller induced erosion because as is already known, the offset height, propeller diameter and efflux velocities are significant for scour induced by the propeller wash. Furthermore, to assess the effects of the return current and propeller wash on the erosion profile the sailing speed and efflux velocity were varied.

Experimental procedure

The sediment bed in the experiments is flattened one day in advance, except for Exp. 5 which is flattened one hour in advance due to time constraints. The experiments consist of two sessions performed at the same day in which one parameter is varied between the sessions while the other parameters are kept the same. Note that the sediment bed is not flattened between the sessions.

A reference situation of the profile is created with the echo sounder before execution of the different experiments. The output of the echo sounder occasionally showed measurement errors and could for example be caused by interference. With measurement errors is meant that the output showed a value of 999 mm which is an error value because the space underneath the echo sounder was 36 cm at maximum. Linear interpolation have been applied in order to create realistic values at these locations. In particular Exp. 4 and 5 showed more measurement errors than the other experiments and are also executed at the same day. Presumably this is caused by an increase in interference with the echo sounder.

Exp. 1

The first session of six ship passages is carried out with sailing speed of 0.1 m/s and an efflux velocity of 1.47 m/s. The bottom profile is measured with the echo sounder after every ship passage. The second session on the same day of four ship passages is performed with a larger efflux velocity (1.89 m/s) while the other parameters are kept the same. This experiment shows the effects of the efflux velocity on the dimensions of the scour hole.

Exp. 2

This experiment corresponds to the situation in reality with minimum keel clearance (0.84 m) and efflux velocity of 8.0 m/s. Note that the efflux velocity is slightly larger than the situation in reality (see Table 3 vs Table 7) caused by a failure of the propeller propulsion which was detected after the performed experiments. The consequence is that the velocities in the propeller wash are larger and the predicted erosion depth in reality is likely to be somewhat overestimated. The first session of nine ship passages is carried out with a sailing speed of 0.45 m/s and again the bottom profile is measured after every passage. The second session of five ship passages is carried out with a smaller sailing speed (0.1 m/s) to assess the effects of the sailing speed on the erosion depth.

Exp. 3

The first session of nine ship passages is carried out with sailing speed of 0.45 m/s while the second session of six ship passages is carried out with sailing speed of 0.1 m/s. The difference with Exp. 2 is the keel clearance which is lowered to 2.0 cm. The last shipping passage (Ship 016) is carried out with sailing speed of 0.015 m/s. This experiment shows the effects of both the sailing speed and keel clearance.

Exp. 4

The first session of eight ship passages is carried out with a sailing speed of 0.45 m/s and an efflux velocity of 1.79 m/s. The keel clearance is raised to 5.5 cm and reflects a possible situation in reality. The second session of five ship passages is performed with a sailing speed of 0.1 m/s. This experiment shows the effects of both the sailing speed and keel clearance.

Exp. 5

To assess the effects of the propeller wash, the efflux velocity is decreased to 1.26 m/s in this experiment. This experiment contains one session of five ship passages, keel clearance of 2.0 cm and a sailing speed of 0.1 m/s.

Overview conducted experiments

In Table 7 the (scaled) values of parameters used in the experiment are presented together with parameter values in reality.

Table 7: Scaled parameter values applied in experiment vs parameter values in reality (see Table 6 for symbols). Exp. 2 and 4 reflect reality the most.

| No. | Experiment | | | | | | Reality | | | | |
|--------|------------|------------|------------|-------------|------------------|-----|---------|-----------|-------------|-------------|------------------|
| | h (cm) | h_k (cm) | z_p (cm) | V_s (m/s) | $U_{pr,0}$ (m/s) | | h (m) | h_k (m) | z_p (m) | V_s (m/s) | $U_{pr,0}$ (m/s) |
| Exp. 1 | 36 | 2.0 | 8.5 | 0.1 | 1.47 – 1.89 | 7.2 | 0.4 | 1.7 | 0.45 | 6.57 – 8.45 | |
| Exp. 2 | 36 | 4.2 | 10.7 | 0.45 – 0.1 | 1.79 | 7.2 | 0.84 | 2.1 | 2.02 – 0.45 | 8.0 | |
| Exp. 3 | 36 | 2.0 | 8.5 | 0.45 – 0.1 | 1.79 | 7.2 | 0.4 | 1.7 | 2.02 – 0.45 | 8.0 | |
| Exp. 4 | 36 | 5.5 | 12 | 0.45 – 0.1 | 1.79 | 7.2 | 1.1 | 2.4 | 2.02 – 0.45 | 8.0 | |
| Exp. 5 | 36 | 2.0 | 8.5 | 0.1 | 1.26 | 7.2 | 0.4 | 1.7 | 0.45 | 5.63 | |

4.2 Plastering experiment

This section describes the experimental set-up for the plastering experiment based on the plastering theory (Talmon et al., 2013) discussed in paragraph 2.4 and its effects on the hydraulic conductivity (RQ.3).

The plastering tests were conducted in a perspex cylindrical test cell with an inner diameter of 6 cm and a length of 30 cm. The pore pressures were measured via pressure sensors equipped with ceramic porous filters at different heights in the soil (Figure 14). The sand is inserted in different layers which are subsequently compacted. The sand-clay mixture or natural sludge is poured gently on top of the sandy subsoil before closing the lid. Then a pressure of approximately 1.5 m water column (=150 mbar) is applied which is more or less similar to the maximum water level differences between the side channel of the Twentekanalen and the surrounding groundwater level at the section of interest, assuming pressure loss of groundwater flow to be negligible. The water barrel is connected to the plastering cell via a tube. The plastering process starts when the bottom valve is opened. At this moment the water can flow through the sediment and the mud-spurt is expected to start directly. The pressure is maintained during the experiment by continuously adding water to the system whereby the excess of water is drained by means of an overflow. The invaded fluid volume is measured by monitoring the weight of water collected in a container underneath the apparatus by an electronic balance which records the weight every second.

The pressure sensors are calibrated beforehand and were verified by applying a certain water pressure in the perspex tube and convert the output to millibar. Additionally, a sponge is used in the perspex tube as well as in the container underneath the apparatus. This is done because otherwise a scour hole arises in the sludge layer due to the inflow of water. The sponge is applied to the collection container to minimize the fluctuation in weight due to vibrations of water drops falling into the container. The data of both the pressure sensors and weight of collected water in time were gathered by a computer.

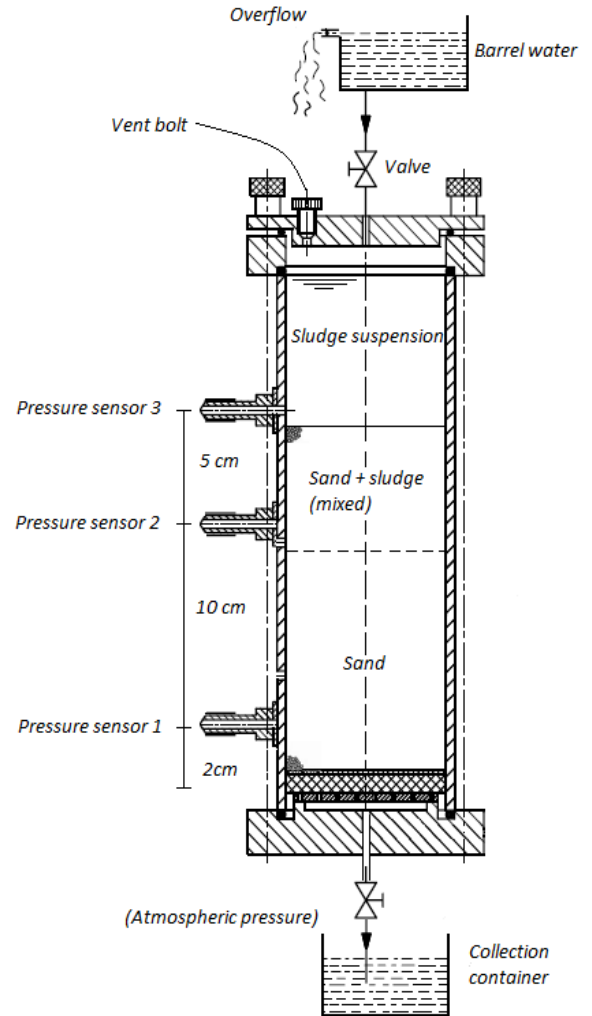


Figure 14: Schematic overview of the plastering experiment; modified after NEN 5123.

Soil samples of the side channel of the Twentekanalen are obtained and analysed in the laboratory (Appendix H). The samples were taken from the top layer of the bottom indicating that sludge and sand was partly mixed. Clean Itterbeck sand is used to verify that the plastering theory of Talmon et al. (2013) is also applicable to the seepage problem studied in this research. The properties of the Itterbeck sand can be found in Appendix I and it appears that the properties fairly corresponds to the sand in the Twentekanalen (Figure 40). In total seven experiments are performed. Exp. 1-4 are carried out with Itterbeck sand in which the clay mixture on top differs. Exp. 5-7 are carried out with sand of the bottom samples of the Twentekanalen in which the natural sludge of the bottom sample is poured on top. Exact grain size distributions were not retrieved, however sediment characteristics of either the sludge or sand can be found in the studies of Tauw (2016) and Arcadis (2015). An example of a sand and sludge sample is shown in Appendix B. To be able to assess the effects of the clay mixture on the hydraulic conductivity the conditions were varied. The calculated hydraulic conductivity values following the NEN 5123 are based on Darcy's law (Eq. 4.6), however these values only serve as a comparison between the tests and should not be interpreted as the true value.

$$k = \frac{Q}{i \cdot A} \cdot f_t \quad (4.6)$$

Where,

k = hydraulic conductivity [m/s]

Q = flow rate [m^3/s] = V_w/t with V_w = volume of water [m^3] and t = time [s]

i = hydraulic gradient [-] = $\Delta H/x$ with ΔH = difference in hydraulic head between pressure sensors (subtracted hydrostatic pressure) [m] and x = distance between pressure sensors [m]

A = area [m²]

f_t = correction factor temperature [-] (0.771 at 20°C in this research)

Another remark is the use of pressure sensors in these experiments instead of stand pipes filled with water applied in a standard constant head method (NEN 5123), which means that is dealt with absolute pressures. The hydrostatic water pressure is subtracted from the hydraulic head between the pressure sensors.

▪ Exp. 1-4

In Exp. 1 no clay mixture is applied and serves as the reference case. In Exp. 2 the artificial sand-clay mixture used in the erosion experiments is poured on top of the sand filter to explore the plastering processes. After Exp. 1 and 2 the plastering cell is cleaned and clean Itterbeck sand is again inserted. Exp. 3 and 4 uses the natural sludge mixture of the Twentekanalen on top of the sand filter and these experiments assess the effects the hydraulic conductivity change compared to the Exp. 1 and 2 but also the effects of stirring the sediment.

▪ Exp. 5-7

In these experiments the soil samples obtained from the Twentekanalen are used. The sandy part of the sample (Figure 56) is used as the sand filter whereas the sludge is used as clay mixture on top of the sand filter. Exp. 5, 6 and 7 respectively applies no sludge, stable sludge layer and sludge stirred with sand filter. The plastering processes are assessed, however also the changes in hydraulic conductivity are evaluated.

Overview conducted experiments

Table 8 presents an overview of the conducted experiments.

Table 8: Overview plastering experiments.

| | Sand filter | Clay mixture on top |
|---------------|-------------------------|---|
| Exp. 1 | Itterbeck sand | None |
| Exp. 2 | Itterbeck sand | Artificial sand-clay mixture (see Table 5) |
| Exp. 3 | Itterbeck sand | Natural sludge TK |
| Exp. 4 | Itterbeck sand | Natural sludge TK stirred with the Itterbeck sand (\approx 4 cm) |
| Exp. 5 | Sand TK (bottom sample) | None |
| Exp. 6 | Sand TK (bottom sample) | Natural sludge TK |
| Exp. 7 | Sand TK (bottom sample) | Natural sludge TK stirred with the TK sand (\approx 4 cm) |

5 Experimental results

5.1 Results erosion experiment

The results of the erosion experiments are divided into four distinct parts in which RQ. 2.1 – 2.4 are answered in paragraph 5.1.1 - 5.1.4 respectively. An overview of experimental conditions is listed in Table 7.

5.1.1 Axial propeller flow velocities

Figure 15 projects the time-averaged flow velocities at one propeller diameter behind the actual propeller ($x/D_{pr} = 1$) which is interpreted as the efflux velocity related to the number of propeller rotations per second⁵. The plot shows a linear relation between the imposed rotations and the efflux velocity and is used to establish the scaled efflux velocity in the experiment.

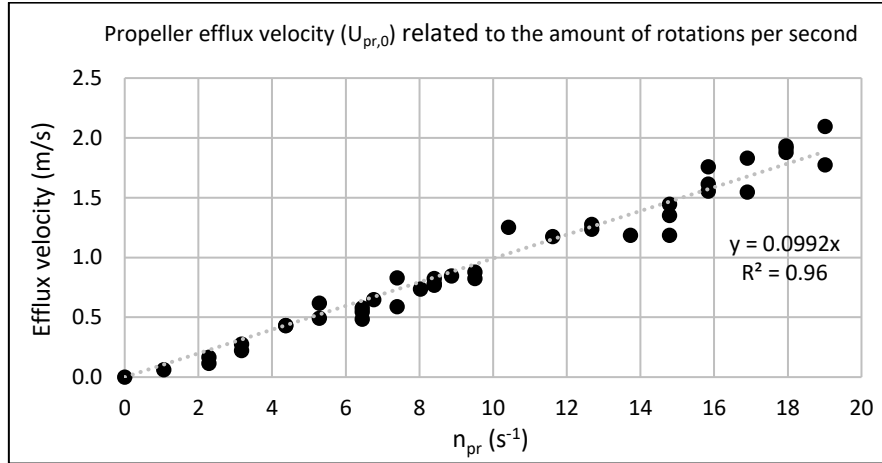


Figure 15: Time-averaged propeller efflux velocities at one propeller diameter behind the propeller ($x/D_{pr} = 1$).

Once the efflux velocity is known, certain decay in maximum velocity occurs as distance from the propeller increases. The decay in maximum velocity is assumed taking place in the zone of established flow rather than the zone of flow establishment close to the propeller. The centre line velocity behind a propeller can be written as (Lam et al., 2011):

$$\frac{U_{pr,centerline}}{U_{pr,0}} = a_{pr} \left(\frac{x}{D_{pr}} \right)^{-b_{pr}} \quad \text{for } \frac{x}{D_{pr}} > a_{pr} \quad (5.1)$$

Lam et al. (2011) shows an overview of different velocity decay functions found in literature; values found for a_{pr} globally range from 1-2.8 and values for b_{pr} between 0.6-1. However, no agreement has been reached among researchers regarding the maximum axial velocity decay functions.

Figure 16 shows the measured maximum time-averaged flow velocities behind the propeller's tip on the centerline at different distances converted to the number of propeller diameters (x/D_{pr}). As expected the largest flow velocities are obtained at a short distance behind the propeller and are decreasing at larger distances according to a power distribution equal to Eq. 5.1. In order to be certain that the zone of established flow has been reached, the power distribution is fitted at $x/D_{pr} \geq 3$. Additionally, within the zone of flow establishment ($0 \leq x/D_{pr} \leq 3$) the maximum axial velocity seems to decrease linearly with distance on the centerline in accordance with the research of Lam et al. (2011) and Stewart (1992). Hence, certainly not constant as proposed by Blaauw and Van der Kaa (1978). Nevertheless, it is still assumed that very close to the propeller i.e. $0 \leq x/D_{pr} \leq 1$ or closer, the velocity is constant. However, this assumed linear relationship is based only on three, four and five data points (see Figure 16) which is limited. Smaller resolution of data within the zone of flow establishment might support this proposed relationship.

⁵ The rotations per second are measured using a Hall Effect sensor which in fact counts the number of times a magnet, mounted on the propeller axis, is passing by the sensor each second.

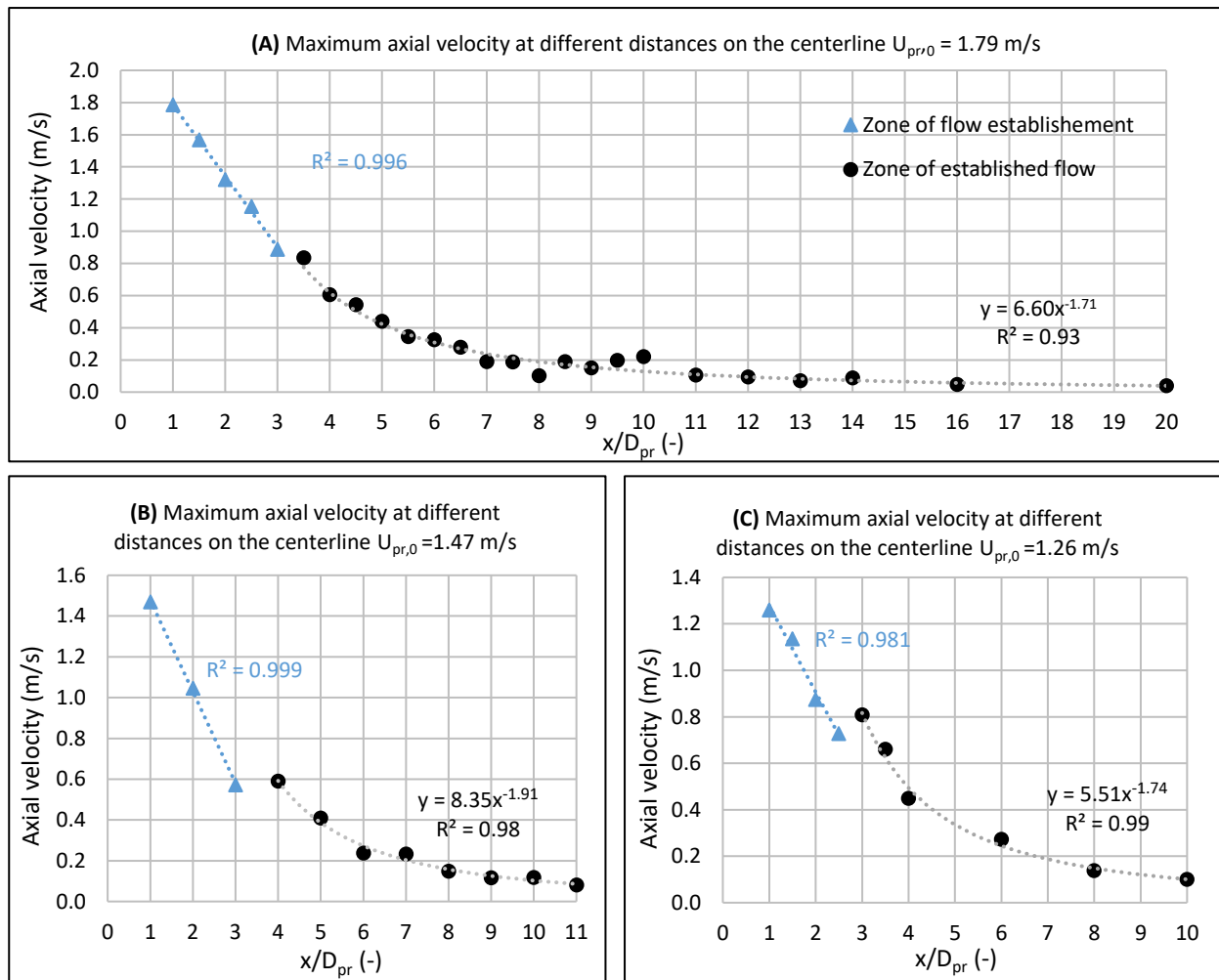


Figure 16: Time-averaged axial flow velocities at different distances from the propeller (x/D_{pr}) on the centerline with varying efflux velocities of the propeller (Plot A, B, C).

A power distribution is fitted in the zone of established flow which clearly corresponds with the obtained data. An abrupt transition is seen between the zone of flow establishment and the zone of established flow at approximately $x/D_{pr} = 3$ due to a change in position of the maximum axial velocity (see Figure 6 in paragraph 2.2). From the fitted equations in the graphs can be seen that the a_{pr} and b_{pr} coefficients from Eq. 5.1 do not correspond with previous research. Both obtained values for the coefficients are significantly larger than those found in literature. One of the reasons that could explain this difference is that the established maximum axial velocity decaying formulas are based on experiments carried out in free water without any obstruction from bottom or walls. This contradicts with the measurements carried out in this research where the bottom, walls and water level were clearly influencing the currents. Visual observations during the measurements revealed circulation of water in the flume and this might explain the different values of the coefficients. It is concluded that until now there is no proper agreed formula to calculate efflux velocities and the decay of the maximum axial velocity along the centerline of specific propellers. The data in this research might be used for validation of existing formulas, however for the purpose of this research the velocity data obtained from the EMS measurements will be used for further analysis on the erosion profiles caused by the ship's propeller.

Appendix F contains extra measurements regarding the decay of the axial velocities in longitudinal direction at different heights with respect to the bottom needed to determine the critical velocities on the bottom. This appendix also contains extra measurements in both width and depth to get confidence in the applied velocities of the propeller wash.

5.1.2 Erosion profiles

The velocities induced by the propeller lead to erosion of bed and banks in navigation channels. Past research of ship-induced erosion on the bed has focused on sand bottoms rather than sand-clay mixtures. However for this research the erosion of sand-clay mixtures related to the propeller wash behind sailing ships is of interest. Hereafter, the results are shown separately for every set of measurements (see Table 7). ‘Top’ and ‘Bottom’ respectively refer to the first and second session of the experiment at the same day where one parameter is varied but in which the sediment bed is not flattened between the sessions.

Experiment 1

| Keel clearance (h_k) | Efflux velocity ($U_{pr,0}$) | Sailing speed (V_s) |
|--------------------------|--------------------------------|-------------------------|
| 2.0 cm | 1.47 – 1.89 m/s | 0.1 m/s |

The erosion profile according to the parameters above is depicted in Figure 17 with the top plot corresponding to an efflux velocity of 1.47 m/s and the bottom plot corresponding to an efflux velocity of 1.89 m/s.

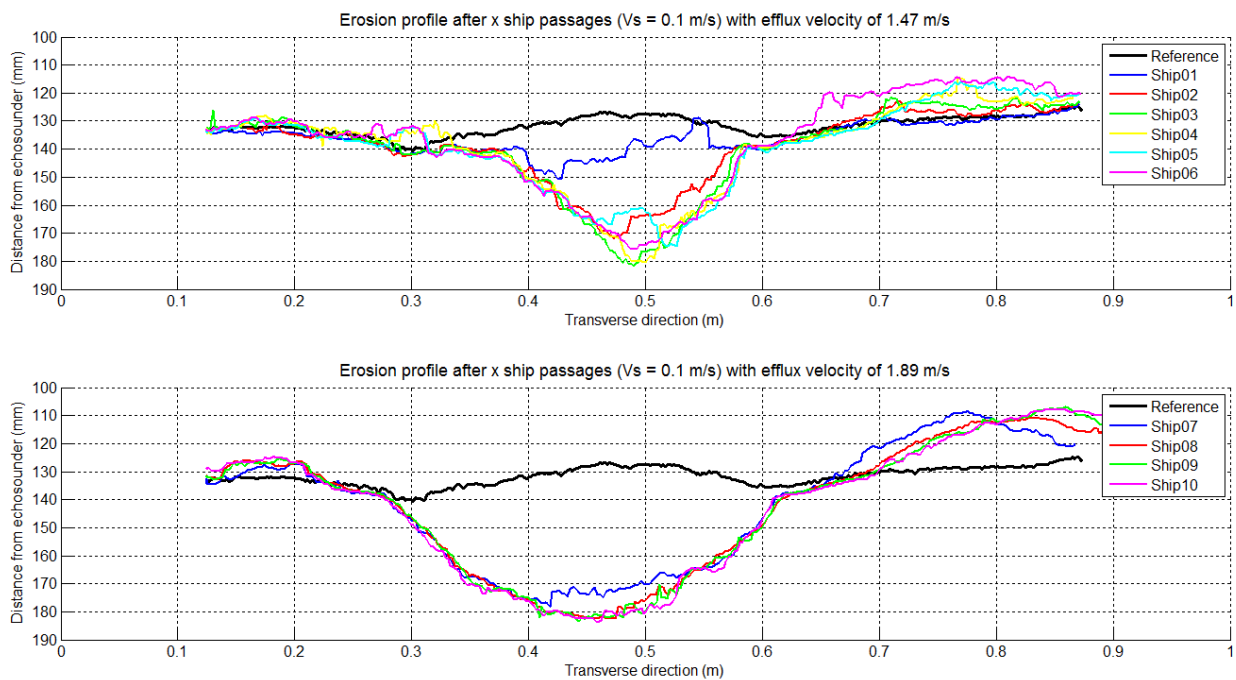


Figure 17: Erosion profiles Exp. 1 (propeller axis located at 0.5 m).

(Top) What can be seen from these figures is that the magnitude of the erosion per ship passage is large in the beginning compared to later ship passages. A logical phenomenon because the distance between the propeller axis and the bed also increases after a ship has passed. Furthermore it shows that approximately after three or four ship passages the ‘equilibrium erosion depth’ has been reached in the top situation (= 5 cm). The term equilibrium depth or maximum scour depth is arguable because only six ship passages have been investigated for this set of parameters. Nevertheless, depth changes due to more ship passages are in the order of millimetres as can be clearly seen in the bottom figure which is negligible for the purpose of this research. Last observation is that after the fourth ship passage the erosion depth decreases again which can be explained by the fact that the slopes of the profile are unstable and have collapsed before the bathymetry measurement is executed.

(Bottom) After six ship passages the efflux velocity was raised to 1.89 m/s, an increase of roughly 30%. It resulted in a much wider scour hole and the depth slightly increased, logically caused by higher flow velocities in the propeller wash. Moreover, the location of the maximum depth is shifted to the left looking towards the back of the ship which is probably caused by the deflection of the propeller wash to the left due to the left-handed propeller. What is also seen in both figures is the so-called ‘kattenrug’ profile as described in paragraph 1.2 where the eroded material below the ship is deposited besides the ship. The figures are somewhat misleading because it seems that the deposition only takes place at the right side of ship, however the same occurs at the left side which is not measured because it fell outside the measuring range of the echo sounder. Extra comment here is that sediment is not only transported to the sides but also backwards signifying that sediment is deposited at the measurement location due to the forward movement of the ship’s propeller.

▪ **Experiment 2**

| Keel clearance (h_k) | Efflux velocity ($U_{pr,0}$) | Sailing speed (V_s) |
|--------------------------|--------------------------------|-------------------------|
| 4.2 cm | 1.79 m/s | 0.45 – 0.1 m/s |

The erosion profile according to the parameters above is depicted in Figure 18 with the top plot corresponding to a sailing speed of 0.45 m/s and the bottom plot corresponding to a sailing speed of 0.1 m/s.

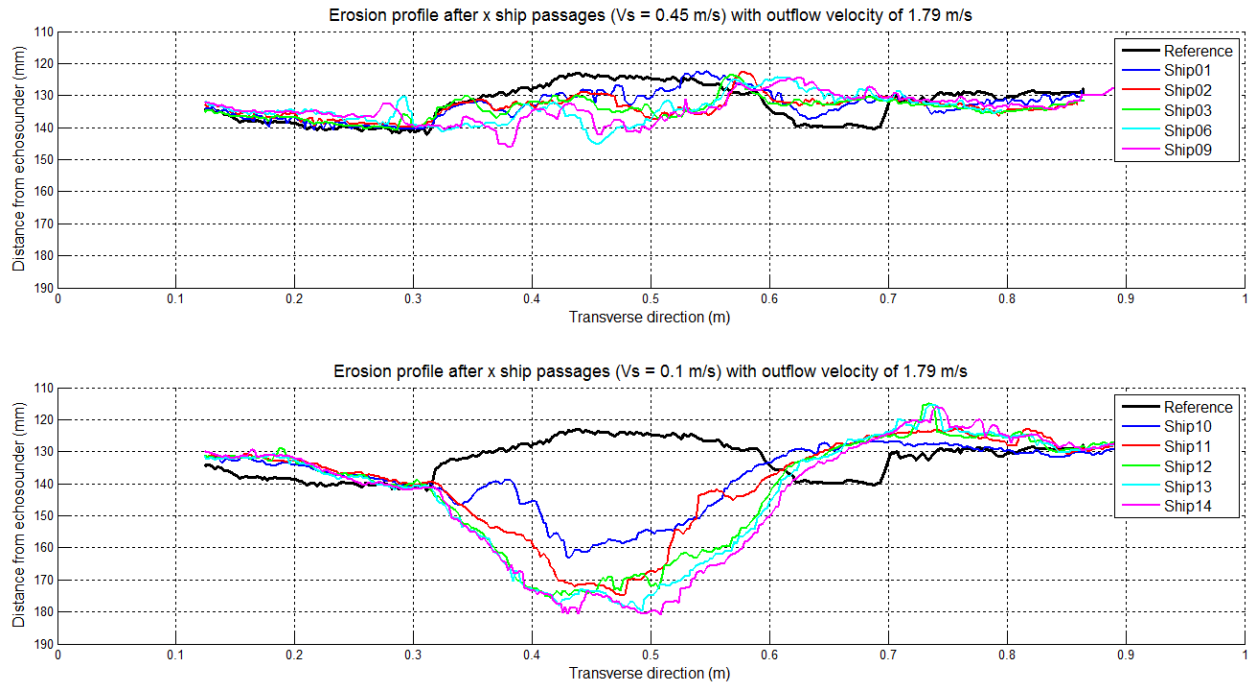


Figure 18: Erosion profiles Exp. 2 (propeller axis located at 0.5 m).

(Top) No clear scour hole has been detected here and the profile itself is defined as irregular. Nevertheless, compared to the reference line approximately 2 cm erosion took place. The chaotic structure of the profile is likely caused by the return current generated by the ship (also visible) rather than the propeller wash. In other words, the propeller wash was not able to pick up sediment particles and the return current is dominant which might be explained by the larger sailing speed resulting in larger return current. Moreover, higher sailing speed results in a decrease of the propeller wash velocities on the bottom with constant efflux velocity. At high sailing speeds the exposure of the sand-clay mixture to the propeller wash velocities (impact time of the propeller wash) is shorter.

(Bottom) After nine ship passages the sailing speed is decreased to 0.1 m/s. Directly after one ship passage the expected more regular scour hole starts to develop and it is assumed that after approximately five ship passages (Ship14 in the total experiment) the maximum depth has been reached (=5 cm). The reason for this rapid increase in erosion depth can be found in the relative velocity of the propeller wash and the larger impact time of the propeller wash on the bottom. As mentioned in paragraph 2.3 the bottom velocity caused by the propeller is dependent on the sailing speed of the vessel. The bottom velocity should be reduced with 0.5 times the sailing speed of the ship according to CUR 201 (CUR, 1999). Hence, bottom velocities and impact time are larger in the bottom plot of Figure 18 due to the lower sailing speed compared to the top plot of Figure 18.

Experiment 3

| Keel clearance (h_k) | Efflux velocity ($U_{pr,0}$) | Sailing speed (V_s) |
|--------------------------|--------------------------------|-------------------------|
| 2.0 cm | 1.79 m/s | 0.45 – 0.1 – 0.015 m/s |

The erosion profile according to the parameters above is depicted in Figure 19 with the top plot corresponding to a sailing speed of 0.45 m/s and the bottom plot corresponding to a sailing speed of 0.1 m/s.

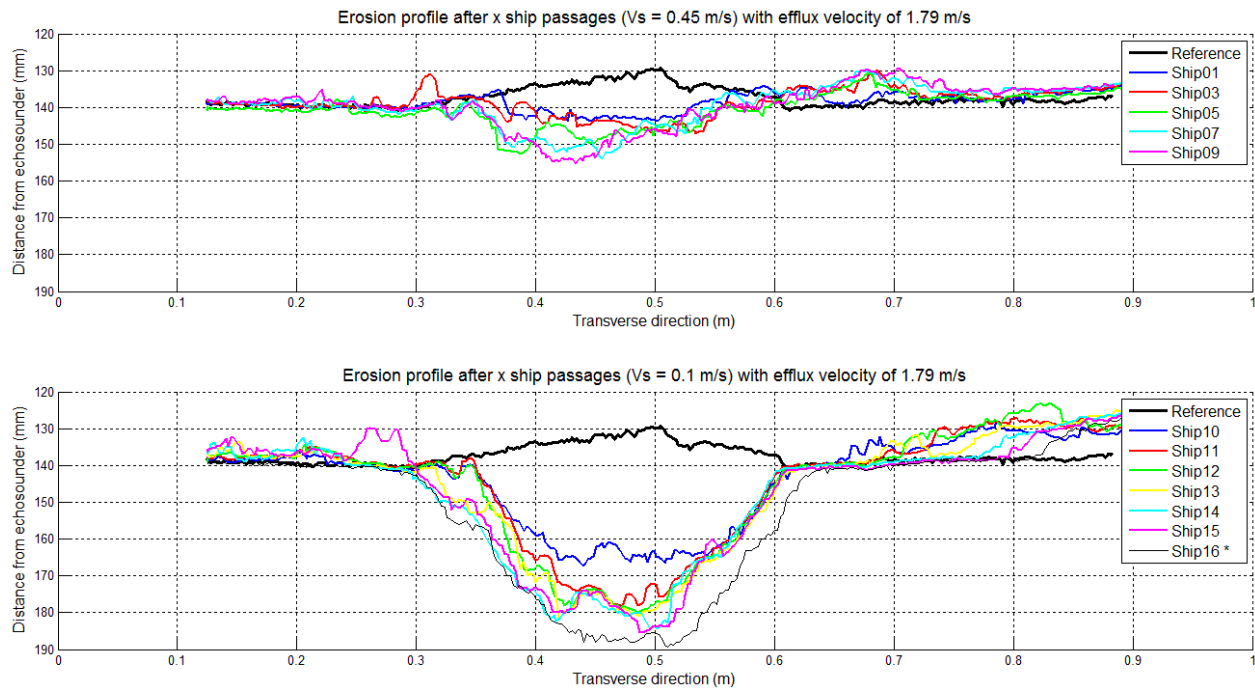


Figure 19: Erosion profiles Exp. 3 (propeller axis located at 0.5 m). *Ship 16 is marked because the sailing speed was decreased to 1.5 cm/s for this passage.

(Top) Again an irregular erosion profile, however relative to the reference line approximately 2.5 cm of erosion took place. Compared to the same situation, but with different keel clearance in the top plot of Figure 18, the erosion increased with approximately 0.5 cm likely caused by larger flow velocities at the bottom originating from the propeller wash rather than the return current. Logical reasoning would be to expect approximately 2 cm more erosion because of the 2 cm lowered keel clearance compared to the top plot of Figure 18. From what is shown here, this hypothesis cannot be verified because it seems that the maximum depth has not been reached yet plus the characteristics of the return current differ.

(Bottom) Lower sailing speeds directly result in a clear scour hole quickly increasing in depth with the amount of ship passages. From the fourteenth to the fifteenth ship passage hardly any change was detected, thus it is assumed that the equilibrium depth is reached here. To be able to assess the effects of the sailing speed on the scour hole formation it is chosen to sail once with a speed of 1.5 cm/s. It appears that the scour hole becomes wider again and also increases in depth. The reason is the larger impact time of the propeller wash on the bottom and higher flow velocities in the propeller wash itself. However, this statement refutes the earlier assumption of the attainment of the equilibrium depth, hence the equilibrium depth is based on a specific set of parameters. On the other hand the possibility of slope instability exists whereby (parts of) the slope collapses subsequently flattens the profile which slows down reaching the equilibrium depth. The theoretical equilibrium depth does not change assuming a fixed set of parameters, however it is questionable if this depth will be reached due to the above factors. Additionally, the scour hole is expected to be approximately equal to the situation in Figure 17 and Figure 18 which appears to be partly true. Remarkably the erosion depth stagnates at 180 mm from the echo sounder (approximately 5 cm of erosion) despite the fact that the keel clearance is decreased. It was expected that the erosion depth would increase compared with Exp. 2. One of the reasons could be that the sediment at this depth is suddenly more resistive to erosion, e.g. change in sand-clay ratio, signifying changes in the critical erosion stress due to for instance consolidation and cohesive properties as is studied by Mitchener and Torfs (1996) and Jacobs et al. (2011). Another reason could be that the magnitude of turbulence (i.e. more or less peaks in the velocity of the propeller wash) differs during the execution of the experiment.

▪ **Experiment 4**

| Keel clearance (h_k) | Efflux velocity ($U_{pr,0}$) | Sailing speed (V_s) |
|--------------------------|--------------------------------|-------------------------|
| 5.5 cm | 1.79 m/s | 0.45 – 0.1 m/s |

The erosion profile according to the parameters above is depicted in Figure 20 with the top plot corresponding to a sailing speed of 0.45 m/s and the bottom plot corresponding to a sailing speed of 0.1 m/s.

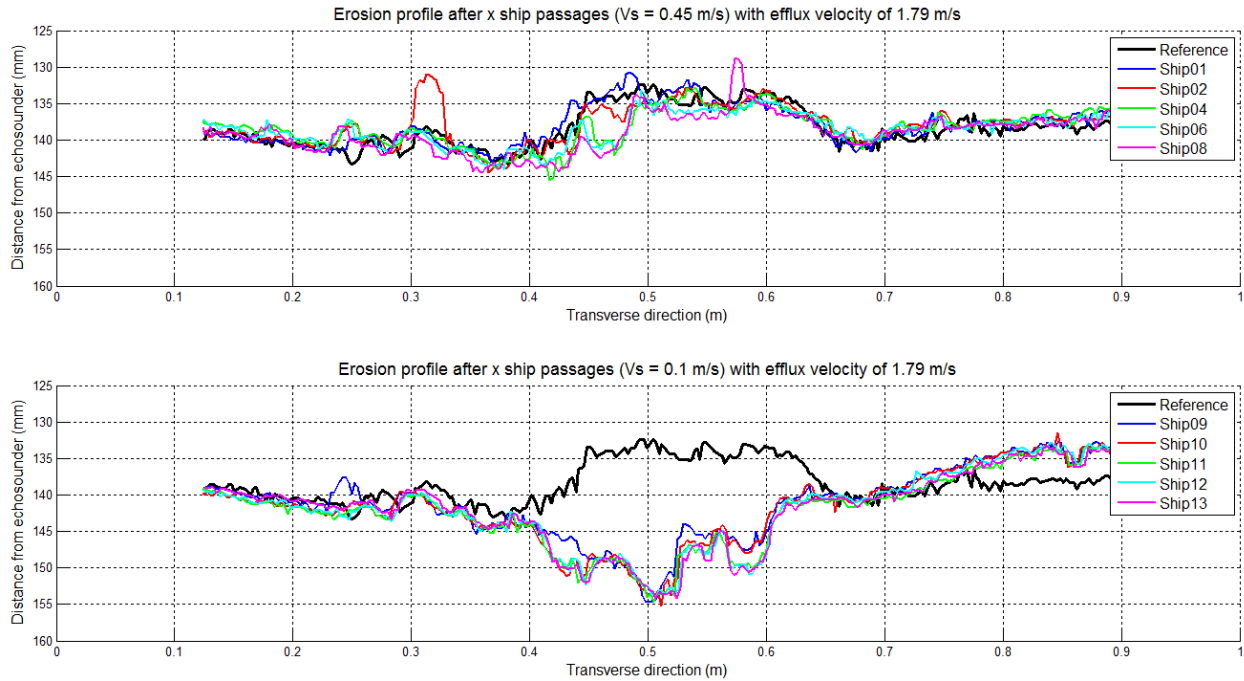


Figure 20: Erosion profiles Exp. 4 (propeller axis located at 0.5 m).

(Top) The increase in keel clearance results in less erosion as in the similar cases of Figure 18 and Figure 19. With a keel clearance of 2 cm in Exp. 3 some erosion was visible however with increasing keel clearance the erosion becomes less and less. Erosion according to this set of parameters is only 0.5 cm at maximum which is almost negligible. The propeller wash hardly influences the bottom and apparently the return current is not severe enough to move the sediment.

(Bottom) Decreasing the sailing speed results in a longer impact time of the propeller wash on the sediment bed. Already after one ship passage the erosion appears to be significant and results in a scour hole with a depth of approximately 2 cm. More ship passages hardly changes the erosion profile and it is assumed that the equilibrium depth has been reached even after one ship has passed. A possible explanation for this is the fluid character of the top layer which gets suspended quickly and the penetration depth of the propeller wash is only in this liquidised slurry.

Experiment 5

| Keel clearance (h_k) | Efflux velocity ($U_{pr,0}$) | Sailing speed (V_s) |
|--------------------------|--------------------------------|-------------------------|
| 2.0 cm | 1.26 m/s | 0.1 m/s |

The erosion profile according to the parameters above is depicted in Figure 21.

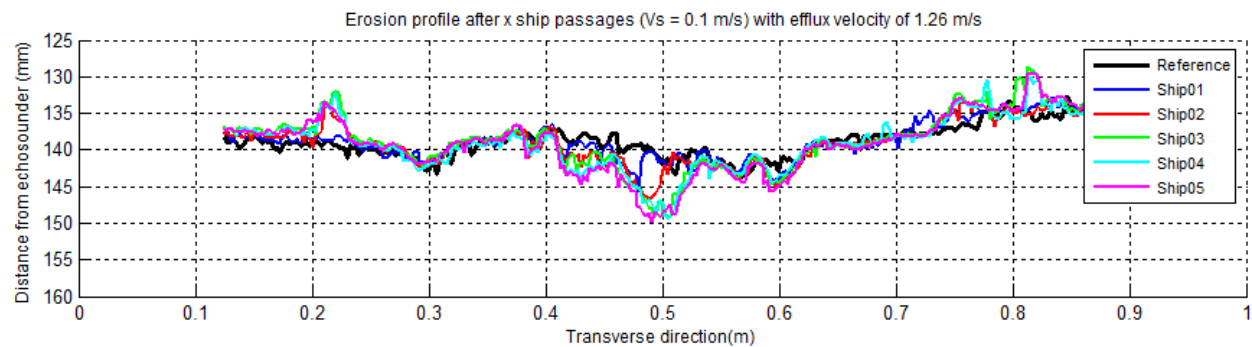


Figure 21: Erosion profile Exp. 5 (propeller axis located at 0.5 m).

The plot shows a chaotic pattern but erosion certainly takes place. The maximum depth of erosion is around 1 cm with respect to the reference situation and its position is specifically in line with the position of the propeller axis. The decrease in erosion depth is expected because the efflux velocity is smaller than in the previous experiments, however the magnitude of erosion is much smaller compared with for instance the erosion depth according to the set of parameters in Exp. 1. The efflux velocity in this experiment is decreased with approximately 15% whereas the erosion depth has decreased with 80% (5 cm in Exp. 1 and 1 cm in this experiment). Two possible reasons are (1) the so-called equilibrium depth has not been reached or (2) the erosion depth is very sensitive to the efflux velocity at small sailing speeds.

Summary erosion experiments

Generally, the erosion track and depth in the sand-clay mixture starts to develop directly after a ship has passed, relatively fast in the beginning and reduces with every ship passage eventually resulting in an equilibrium depth. Underneath the ship the bottom erodes and eroded sediment is transported to the sides of the channel. Additionally, slope instability of the scour hole is observed which limits the erosion depth (see for instance Exp. 1) and is related to the strength of the sediment. Five experiments were carried out in which either the efflux velocity, sailing speed or the keel clearance is varied. The following conclusions are drawn:

- 1) Increasing the efflux velocity results in a wider scour hole and increases the scour depth which is attributed to larger flow velocities in the propeller wash. The maximum scour depth is located at the axis of the propeller, however in Exp. 1 is observed that due to increasing the efflux velocity the location of the maximum scour depth is shifted to the left caused by the left-handed propeller. Moreover, in Exp. 5 is seen that the efflux is decreased with 15% whereas the erosion depth decreased with roughly 80%. Hence, it emphasizes the importance and sensitivity of the efflux velocity on the erosion depth.
- 2) Increasing the sailing speed results in a decrease of the scour depth caused by both shorter impact time and smaller flow velocities of the propeller wash on the bottom. Larger sailing speed results in smaller flow velocities on the bottom originating from the propeller assuming constant efflux velocity (BAW, 2005) and consequently smaller scour depth whereas a decrease in sailing speed directly results in a deeper scour hole (Exp. 2 and Exp. 3). Hence, the propeller wash is in particular of importance for bottom erosion when sailing speed is small. On the other hand, however, larger sailing speed results in an increase of the return current which could in turn be the dominant erosion mechanism.
- 3) Increasing the keel clearance results in a decrease of the scour depth because the distance between the propeller axis and the bottom increases consequently resulting in smaller flow velocities on the bottom (Exp. 2 and Exp. 3).

5.1.3 Erosion formula

Paragraph 2.3 summarized the most used erosion formulas to predict scour holes due to propeller wash in a sand bed, however this research focusses specifically on sand-clay mixtures with different (erosion) characteristics. For sand erosion the median particle diameter (D_{50}) is an important parameter and included in many erosion formulas. Erosion formulas for sand-clay mixtures frequently hold the dry or bulk density, percentage of mud or the Plasticity Index as parameter as is summarized in the literature study of Nijborg (2016). The exact values of the latter parameters have not been retrieved. Nevertheless, a comparison is made with existing erosion formulas for sand and fitted to the previous experiments. The formulas of Verheij (1983) and Hamill (1987) consists of the following parameters which are also known in this research and follow a power relationship (see Eq. 5.2):

$$\frac{d_{max}}{z_b} = \alpha \left(\frac{F_0}{z_b/D_0} \right)^\beta \quad (5.2)$$

With:

d_{max} = maximum scour depth [m]; z_b = offset height [m]; F_0 = densimetric Froude number = $U_{pr,0}/\sqrt{g\Delta d_{50}}$ with $U_{pr,0}$ = efflux velocity [m/s]; g = gravitational constant [m/s^2]; Δ = relative density [-]; d_{50} = median particle diameter [m]; D_0 = effective propeller diameter [m]

The coefficients α and β are empirically determined and are dependent on the experimental circumstances as can be seen in Table 2.

Table 9 presents the relevant parameters needed to develop a formula similar to Eq. 5.2 but also presents the initial time-averaged velocity at the bottom before erosion and the bottom velocity in the scour hole after erosion measured with the EMS. The latter can be interpreted as the time-averaged critical velocity because the scour hole does not increase in depth.

Table 9: Relevant parameters for erosion formula in experiment due to propeller wash of a sailing vessel with 0.1 m/s.

| | Exp. 1-1 | Exp. 1-2 | Exp. 2 | Exp. 3 | Exp. 4 | Exp. 5 |
|---|----------|----------|----------|----------|----------|----------|
| Keel clearance (h_k) | 2.0 cm | 2.0 cm | 4.2 cm | 2.0 cm | 5.5 cm | 2.0 cm |
| Effective propeller diameter (D_0) | 9.1 cm |
| Offset height (z_b) | 8.5 cm | 8.5 cm | 10.7 cm | 8.5 cm | 12 cm | 8.5 cm |
| Efflux velocity (U_0) | 1.47 m/s | 1.89 m/s | 1.79 m/s | 1.79 m/s | 1.79 m/s | 1.26 m/s |
| Densimetric Froude number (F_0)* | 25.8 (-) | 33.2 (-) | 31.5 (-) | 31.5 (-) | 31.5 (-) | 22.1 (-) |
| Initial bottom velocity ($U_{pr,b0}$) | 0.33 m/s | - | 0.3 m/s | 0.43 m/s | 0.3 m/s | 0.22 m/s |
| Critical erosion velocity in scour hole after erosion ($U_{pr,b1}$) | 0.24 m/s | - | 0.25 m/s | 0.25 m/s | 0.25 m/s | 0.2 m/s |
| Maximum scour depth (d_{max}) | 5 cm | 5.4 cm | 5 cm | 6 cm | 2 cm | 1 cm |

* The d_{50} is estimated at 200 μm .

The time-averaged critical velocity is more or less equal in the different experiments and assumed at 0.25 m/s. This is expected since erosion continues when the bottom velocity is larger than the critical velocity. Hence, this supports the statement regarding attainment of the 'maximum' erosion depth in all experiments. However, it is almost impossible that the equilibrium depth has been reached within this timeframe since the experiments of Hamill (1987) lasted for 24 hours in which the scour depth still significantly increased in the last hours. In other words, the 'maximum' erosion depth will most likely be underestimated. It should also be noted that small errors in the order of 1 or 2 mm are likely because of an irregular sediment bed instead of an exactly flat bottom which subsequently affects the applied keel clearance, and the initial bottom velocity is determined at the average height of the sediment bed after execution of the erosion experiments. Moreover, the turbulence intensity ($r_u = \sqrt{\overline{u'^2}}/\bar{u}$) caused by the propeller wash varied roughly between 0.2 - 1 on the line of the propeller axis, indicating that flow velocities randomly could be much larger than the time-averaged flow velocity. In turn these peaks in velocity influence the maximum scour depth and time-averaged bottom velocity. Nevertheless, possible small errors in offset height and efflux velocity ($R^2 = 0.96$, see Figure 15) which are of interest regarding the erosion formula do not affect the results significantly. The formula developed in Figure 22 is based on six measurements which is fairly limited. More data points are necessary to support and validate this formula, and minimize the influence of turbulence and measurement errors. However for the purpose of this research the erosion formula can serve as an indication for the effects of shipping directly after reconstructing the new layer.

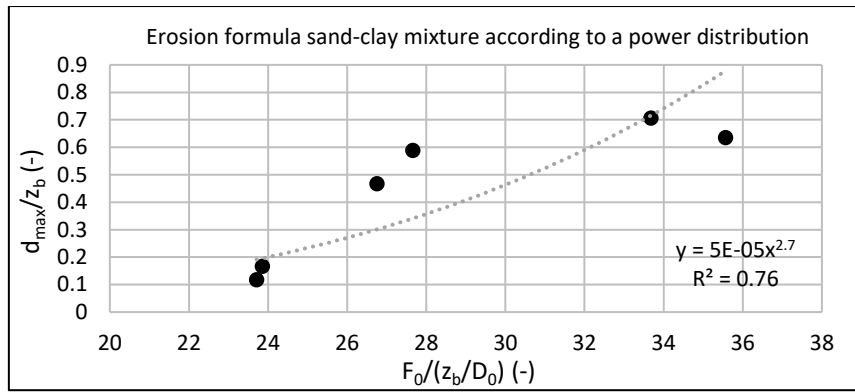


Figure 22: Empirically determined erosion formula with sailing speed of 0.1 m/s (Power distribution).

The erosion formula in dimensionless form valid in the range $23 < F_0 < 36$ after more or less six shipping passages with sailing speed of 0.1 m/s and yield strength of the sediment bed of approximately 100 Pa looks as follows (Eq. 5.3):

$$\frac{d_{max}}{z_b} = 5 * 10^{-5} \left(\frac{F_0}{z_b/D_0} \right)^{2.7} \quad (5.3)$$

Exponent β lies between the existing scour depth formulas of Verheij (1983) and Hamill (1987) regarding sand which give respectively values of 2.9 and 1.39 for β (see Table 2). However, the α coefficient is a factor 100 – 1000 lower, resulting in much smaller scour depths. Four possible reasons are proposed:

The first reason is that the maximum erosion depth has not been reached in the experiments because of very small impact time of the propeller (order of minutes) on the bottom compared to the formulas of Verheij (1983) and Hamill (1987) in which a continuously rotating propeller is used (impact time order of hours / days). On the other hand the erosion profiles show that the scour depth is hardly changing after certain amount of ship passages that could be allocated to slope instability of the scour hole. Again, this contradicts with the continuously rotating propeller used in literature which ensures slope stability due to continuous flow pressure on the slopes.

Second reason is the movement of the ship which consequently means that the sediment is transported not only to the sides but also behind the ship at the location of the measurements. In other words, at the location of the measurement the sediment is eroded first but when the ship has passed, sediment in front of the measurement location is transported or 'pushed' backwards due to the propeller wash to the measurement location again. In addition, possibly the flow velocities during sailing might not be severe enough for a longer time period in order to transport the sediment out of the scour hole. Therefore it is difficult to compare with the formulas of Verheij (1983) and Hamill (1987) because there the propeller is fixed at one position and continuously rotated meaning that sediment is only eroded and deposition takes place outside of the scour hole.

Third reason is the validity range in terms of the densimetric Froude number. The erosion experiments in this study are carried out with relatively large densimetric Froude numbers ($23 < F_0 < 36$) compared to the densimetric Froude numbers applied in the scour depth formulas found in literature ($5.12 < F_0 < 7.73$).

The fourth reason might be the increased erosion resistance due to different sand-clay ratios (Mitchener & Torfs, 1996) influencing the maximum scour depth compared to sand. The downward movement of sand particles (increasing strength with depth) in the bed due to their weight might be an explanation for the different sand-clay ratio and could possibly be better described with a log-function as can be seen in Figure 23. Moreover the log distribution fits the data slightly better with respect to R^2 value compared to the power distribution.

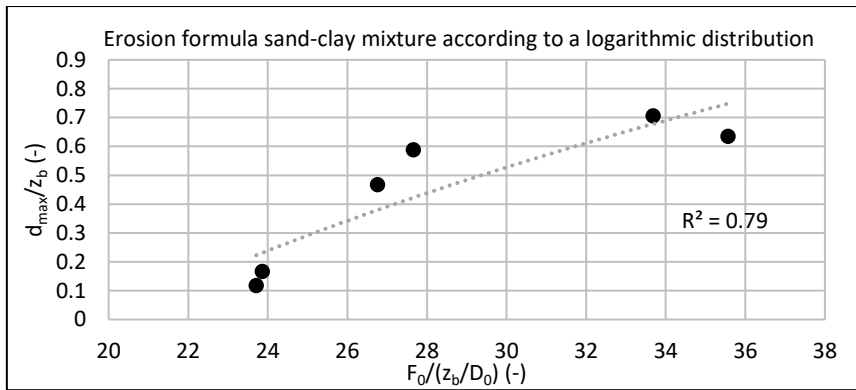


Figure 23: Empirically determined erosion formula with sailing speed of 0.1 m/s (Logarithmic distribution).

On the one hand it seems that a power distribution fits the data well, however a logarithmic distribution fits the data slightly better due to taking into account the downward movement of sand particles which consequently results in different sand-clay ratios. However, it is based on limited data points and ship passages, and only for one sediment type so no hard conclusions can be drawn. Moreover, despite the major importance of clay characteristics the above equations do not hold any clay characteristic. Concluding, a clay mixture has other F_0 values and perhaps need a totally different shape to determine the maximum erosion.

5.1.4 Particle size distribution over the width of the flume

Due to time constraints it was not possible to conduct a quantitative analysis on the grain size distribution over the width of the flume after the experiments. However, from visual observation it appeared that smaller particles were distributed to the sides while in the middle of the flume (where the scour hole developed) larger sand particles were found. Figure 24 shows images where the left image is retrieved from the sides and the right image is retrieved from the middle of the flume.

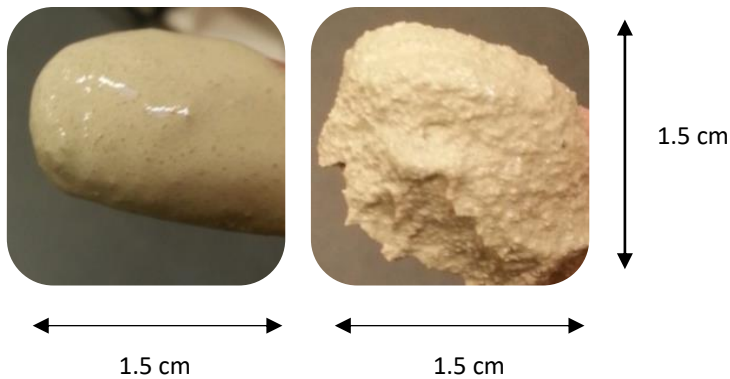


Figure 24: (Left) sediment retrieved from the side; (Right) sediment retrieved from the axis of the channel.

5.2 Results plastering experiment

This paragraph presents the results of the executed plastering tests from which an overview can be seen in Table 8. The original time series of Exp. 1 and 2 are presented in Figure 25 to show the occurring plastering process and in which the experimental procedure can be seen, however the original time series for the other experiments can be found in Appendix K. The relevant data to assess the hydraulic conductivity are the pressure differences over the height of the plastering cell and the weight of collected water in time.

Experiment 1 & 2

| Exp. 1 | Exp. 2 |
|----------------------|--|
| Clean Itterbeck sand | Clean Itterbeck sand + sand-clay mixture |

The first test that has been carried out is related to the clean Itterbeck sand and could be seen as a reference case for the first four experiments. In the second test an artificial sand-clay mixture (composition see Table 5) of approximately 4.5 cm in thickness was poured on the sand filter. The results of both tests can be seen in Figure 25 in which the plots (A) and (B) are related to the pressure recorded by the pressure sensors and the plots (C) and (D) are related to the weight of the collected water. Nevertheless, following the NEN 5123 (Laboratory determination of permeability of soil by constant head method) it appeared that the hydraulic conductivity value obtained during the first plastering test was fairly similar to the value given by the manufacturer. For example, according to the manufacturer the hydraulic conductivity of the Itterbeck sand was 10 m/day and the value that was obtained in the first experiment with clean Itterbeck sand was approximately 17 m/day. One of the reasons for this difference could be the different preparation of the soil sample in the perspex tube, e.g. the saturation and compacting of the soil layers. Additionally, the obtained hydraulic conductivity is also fairly similar to the hydraulic conductivity values of the sand present in the Twentekanalen (Appendix B).

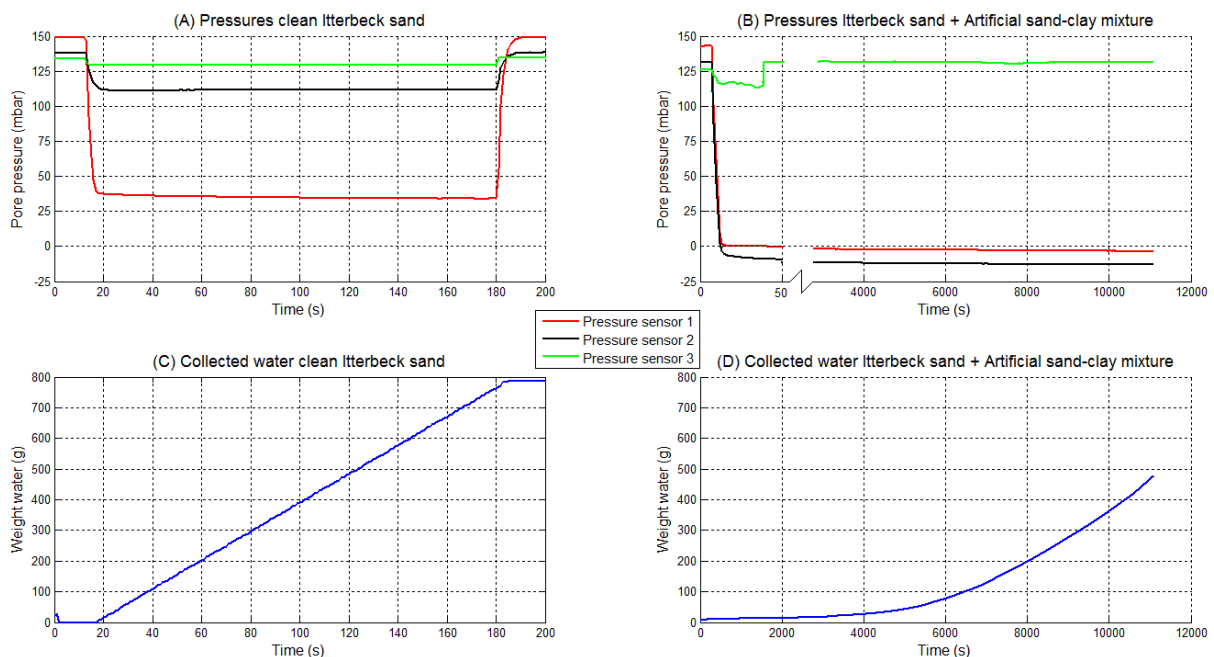


Figure 25: Exp. 1 (plot A and C) and Exp. 2 (plot B and D).

Figure 25A shows the pressures starting at a water pressure of 150 mbar slightly above the valve. At the moment of opening the bottom valve the pressure drops instantly to a more or less constant value and after the bottom valve is closed again the pressure immediately increases to the situation in the beginning. In Figure 25B the scale is clipped in order to see both the start and end of the measurement series. Furthermore, a pressure drop can be seen during the first 1800 seconds which can be allocated to a closed valve which ensures adding water to the system. Additionally, Figure 25C regarding clean Itterbeck sand shows also that when the valve is opened water starts to drain into the collection container and almost directly reaches a linear line, i.e. constant outflow in time. In contrast to the situation where an artificial sand-clay mixture is poured on top of the sand filter (Figure 25D), here the outflow of water shows a linear trend after more or less 7000 seconds. The first 4000 seconds shows a significant drop in the outflow of water compared to the situation of pure sand and outflow of water is linear related to the time. However, after approximately 4000 seconds the outflow of water suddenly increases with time indicating that the subsoil is not completely sealed anymore. The first reason could be allocated to small canals that might develop within the soil sample (e.g. along the perspex). A second reason could be allocated to the amount of clay particles

which might not be large enough to cover the surface of the perspex tube. The latter seems unlikely because during the experiments a stable layer of sand-clay mixture was continuously observed. The third reason could be that the clay particles are flown through the entire soil sample and dropped in the collection container. This reason is rejected because the water in the collection container was clean and transparent. Nevertheless, the hydraulic conductivity was still lower than in case of pure sand due to the presence of clay particles.

Figure 26 shows the pressure distribution over the height of the plastering cell of Exp. 1 and 2. The y-axis presents the height of the plastering cell in which 0 cm is the outflow opening at the bottom valve and the other markers represents the location of the pressure sensors in Figure 14. The pressures are different with the exception of pressure sensor 3 in top of the column indicating the constant water pressure. The grey line illustrates the situation in which the bottom valve is closed and results in the hydrostatic pressure. When the bottom valve is opened the pressure at the bottom is always equal to the atmospheric pressure (= calibrated to 0 mbar here). The blue line illustrates the situation with clean Itterbeck sand while the orange line represents the situation with Itterbeck sand + sand-clay mixture poured on top of it. In case of the sand-clay mixture, sensor 1 reaches approximately a pressure of 0 mbar because it is close to the outflow opening (2 cm = 2 mbar). Sensor 2 detects a negative pressure indicating that the water adheres below the poorly permeable clay layer. In other words, the clay layer is poorly permeable shown by the large pressure change over 5 cm between sensor 2 and 3 indicating that water poorly passes the layer while underneath the clay layer the water experiences negligible friction, and only the hydrostatic pressure remains. Hence, Figure 26 quickly shows which part is dominant in terms of (poor) permeability; the area between sensor 1 and 2 in which only sand is present or the area between sensor 2 and 3 in which the clay or sludge layer is present. In Figure 25B / Figure 26 the large pressure difference is taking place over the sand-clay layer signifying that this layer is dominant.

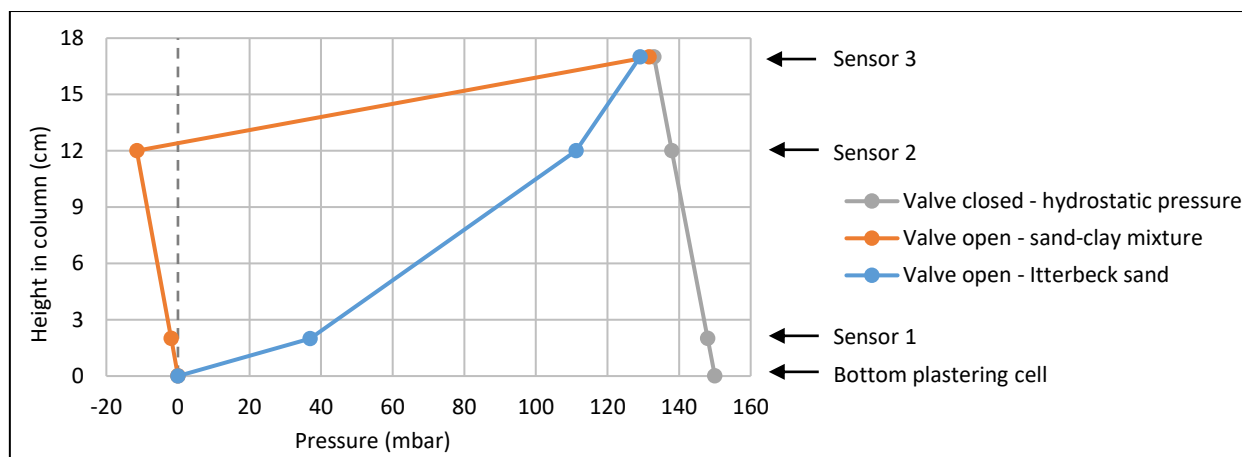


Figure 26: Pressure distribution closed and open valve in plastering experiments.

As described in the paper of Talmon et al. (2013) the mud spurt takes place quickly while consolidation is more slowly. Figure 27 shows a close up of plot Figure 25D where \sqrt{t} is chosen for the horizontal axis to visualize the consolidation process.

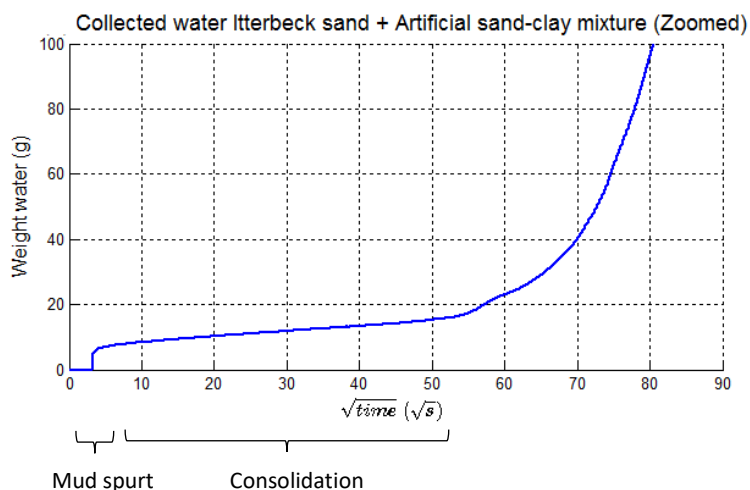


Figure 27: Close up of plot Figure 21D with respect to the first two hours plotted as the square root of time.

Figure 27 shows the initial mud spurt and the consolidation part representing the plastering process similar to that presented by Talmon et al. (2013). However, in their tests the measurement time was 30 minutes while the duration of the test conducted in this research was much longer and specifically after approximately $\sqrt{2500 s} = 50 \sqrt{s}$ the pattern changed, possibly due to the formation of small canals within the soil. However, the formation of small canals is not proven and remain uncertain. The permeability of the sand-clay layer can be found after the initial mud spurt and corresponds to a permeability value of 0.0026 m/day which is approximately a factor 6500 lower than in case of clean Itterbeck sand. This permeability is found over a layer of 5 cm and should only be interpreted as the average permeability of this specific layer, and should not be interpreted as the permeability for the total soil sample or for thin poorly permeable layers within this section.

▪ **Experiment 3 & 4**

| Exp. 3 | Exp. 4 |
|---|--|
| Clean Itterbeck sand + natural sludge TK (stable) | Clean Itterbeck sand + natural sludge TK (stirred) |

In Exp. 3 and 4 the artificial sand-clay mixture was replaced by the natural sludge originating from the Twentekanalen. In Exp. 3 approximately 4 cm sludge was poured on top of the Itterbeck sand filter and measurement duration was approximately 4.5 hours. Results are shown below in Figure 28 in which only the first 500 seconds are plotted. The complete measurement series can be found in Appendix K. The hydraulic conductivity is reduced from 17 m/day in the reference situation with clean sand to 0.25 m/day with the natural sludge poured on top, approximately a factor 70 lower. Note that the calculated permeability is the average value over the sludge layer of approximately 5 cm.

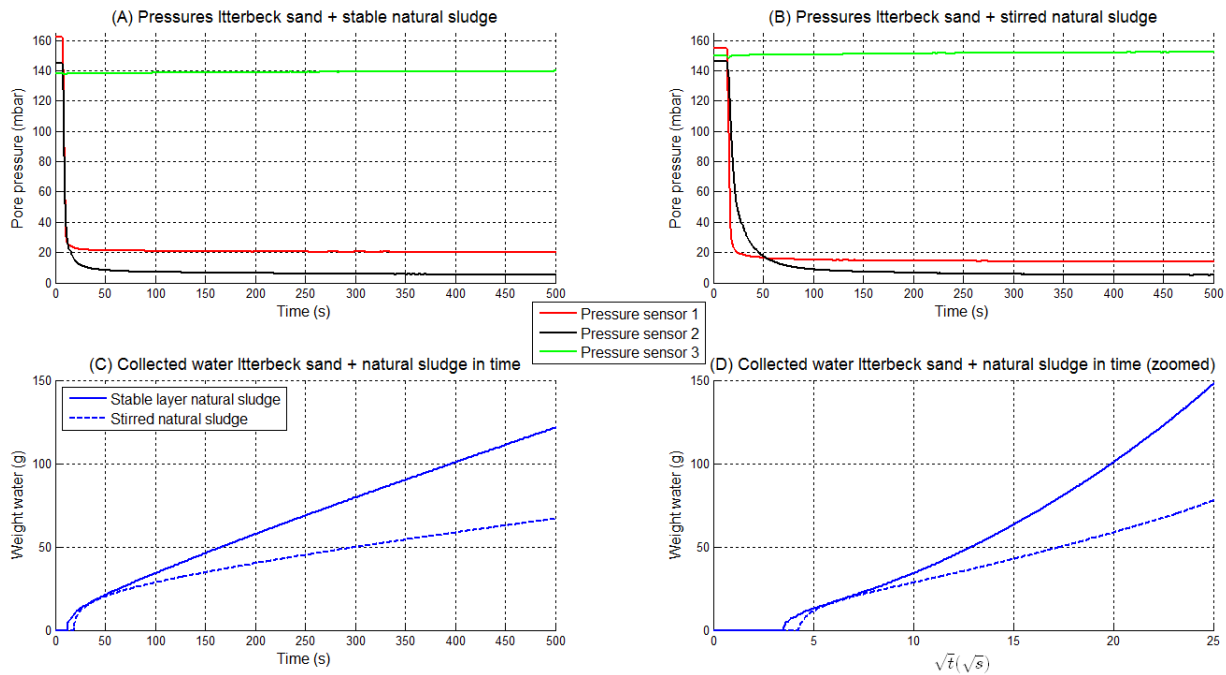


Figure 28: Exp. 3 (plot A) and Exp. 4 (plot B); collected water of both (plot C) and zoomed of plot C (plot D).

The difference between Exp. 3 and Exp. 4 was that in the latter case the (same) sludge was stirred up (≈ 4 cm), consequently mixing with the sand layer. What can be seen from this is that when the sludge is stirred up and mixed with the sand the hydraulic conductivity is lower compared to the situation where the sludge forms a stable layer. The hydraulic conductivity changes from approximately 0.25 m/day in the previous case to approximately 0.15 m/day in the stirred case which is a decrease of roughly 40% in this specific layer. However comparing Figure 28D to Figure 27D it can be seen that the plastering process with the artificial sand-clay mixture is better represented than in this case with the natural sludge. The most likely explanation lies within the grain size distribution because the artificial mixture contains more clay particles that can invade the sandy subsoil while the natural sludge contains proportionally larger particles as is investigated by Tauw (2016). In other words, the artificial sand-clay mixture has a larger effect regarding clogging of the pores within the sand filter while the obstruction due to the natural sludge is smaller because the relatively larger particles are not able to invade the soil.

▪ **Experiment 5,6 & 7**

| Exp. 5 | Exp. 6 | Exp. 7 |
|---------|--------------------------------------|---------------------------------------|
| Sand TK | Sand TK + natural sludge TK (stable) | Sand TK + natural sludge TK (stirred) |

The last three experiments are carried out with the soil samples originating from the Twentekanalen. The sandy part of the sample (see Appendix H, Figure 56) is used as sand filter while the clayey part is used as sludge poured on top of the sand. Figure 29 shows the recorded pressures in plot A, B and C of respectively only TK sand, TK sand + natural sludge in the form of a stable layer and TK sand + natural sand which is stirred up beforehand, hence mixed with the sediment bed. Figure 29D shows the collected water during the experiment over a period of 1000 seconds (see Appendix K for total measurement series). Figure 29D shows large differences in collected water over time between these three situations in which sand TK is most permeable followed by sand TK + stable sludge and lowest permeability is reached with the stirred case. Calculating the magnitude of the hydraulic conductivity it appears that the changes are minimal regarding TK sand ($=0.18$ m/day) and TK sand + stable sludge ($=0.17$ m/day), however a significant decrease of roughly 80% in permeability is found when the sludge is stirred ($=0.03$ m/day). The difference in permeability of the TK sand compared to the Itterbeck sand in Exp. 1 can be explained by clay particles already present in the soil sample whereas the Itterbeck sand is free of clay particles. The TK soil sample is moreover retrieved from the top layer of the sediment bed. Plot B shows that despite more sludge is poured on top of the TK sand filter and the pressure difference between sensor 2 and 3 increases relative to TK sand in plot A, the permeability barely changes because the TK sand layer is still dominant. The pressure differences in case of the stable and stirred sludge is clearly visible in plot B and C signifying the shift of the dominant layer. In the situation with the stirred sludge in plot C, the mixed top layer (layer between sensor 2 and sensor 3) is dominant above the TK sand (layer between sensor 1 and 2) while in plot B with stable sludge it was the other way around. Hence, stirred sludge with sand results in lower hydraulic conductivity in compliance with Exp. 3 and 4.

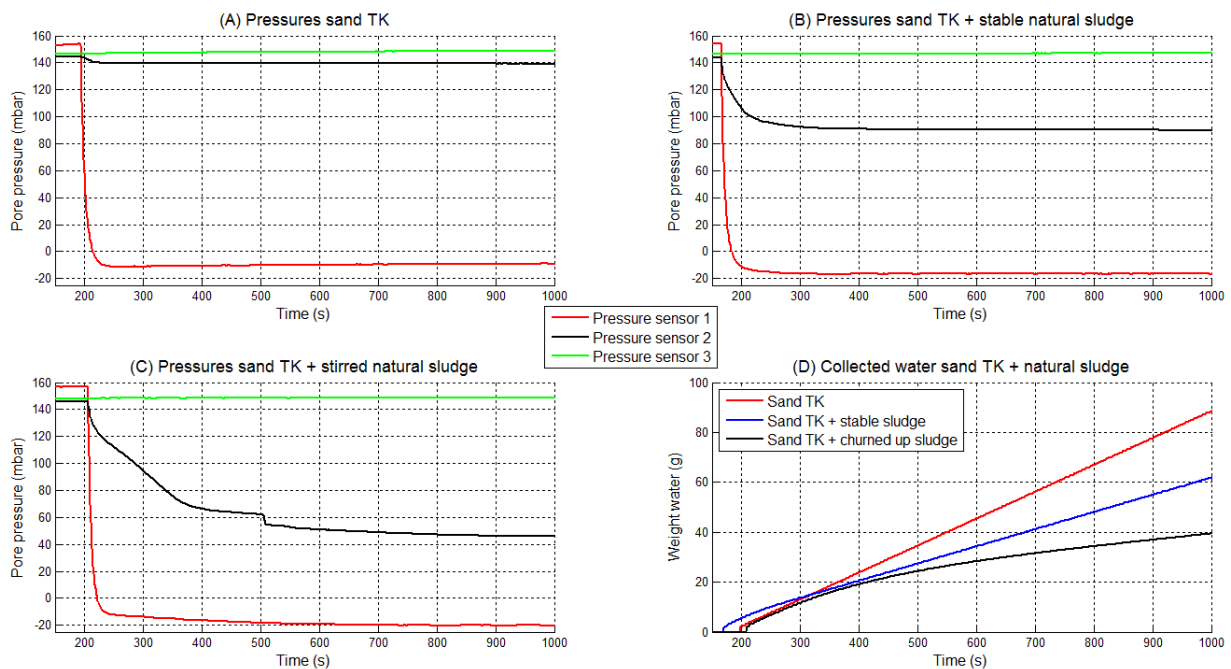


Figure 29: Exp. 5 (plot A), Exp. 6 (plot B) and Exp. 7 (plot C); Collected water of all three in plot D.

Summary plastering experiments

Summarizing, the plastering experiments show three main results:

- 1) Exp. 2 shows that the plastering process as is described by Talmon et al. (2013) is also applicable to the seepage problem of the Twentekanalen.
- 2) Higher percentage of clay (or small particles) reduces the hydraulic conductivity significantly referring to Exp. 1 and 2. Moreover, at Exp. 5 in which sand originates from the top layer of the Twentekanalen, it appeared that clay particles were present in the sample signifying the plastering process and explains the difference between the Itterbeck sand with comparable hydraulic conductivity as pure sand from the Twentekanalen.
- 3) The difference in permeability with respect to a stable sludge layer or stirred sludge is interesting. The situation in which the sludge was stirred, hence mixed with the sandy subsoil, resulted in a lower hydraulic conductivity in comparison to the stable sludge layer which might be attributed to more evenly distributed clay particles blocking the pores (see Figure 30).

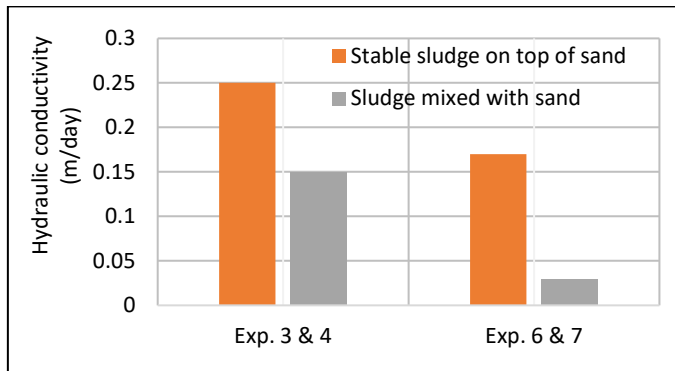


Figure 30: Comparison hydraulic conductivity values in case of a stable sludge layer on top of a sand filter and sludge mixed with the sand filter. Exp. 3 & 4 with clean Itterbeck sand and Exp. 6 & 7 with sand originating from the Twentekanalen.

6 Case Twentekanalen vs Experimental results

In the beginning of 2016 a temporary sludge layer was applied on the bottom of the Twentekanalen to reduce the amount of seepage and consequently lower the groundwater level in the area close to the dikes. Monitoring the groundwater levels revealed that the groundwater levels lowered. However, the decrease was not sufficient to mitigate problems for farmers. Paragraph 1.2 mentions, based on practical experiments with respect to the side channel of the Twentekanalen, that the amount of seepage mainly depends on four aspects (Rijkswaterstaat, 2003):

- 1) Composition of the sludge layer
- 2) Settling velocity of the specific sediment fractions within the sludge layer
- 3) Distribution of the sludge layer over de canal bed (thickness)
- 4) Time (consolidation / compaction)

Additionally, from these experiments is concluded that in particular the composition of the sludge layer is of great influence rather than the thickness of the sludge layer. It was found that especially the fine sediment fraction in the sludge is important to limit seepage water. Hence, requirements were established based on these practical experiments in the side channel. Rijkswaterstaat tested 14 soil samples of the temporary sludge layer on their physical characteristics to figure out the cause of the limited groundwater level reduction. It appeared that the requirements were far from met (Tauw, 2016). Table 10 shows the requirements and the average values of the 14 soil samples.

Table 10: Comparison sludge requirements and sludge encountered in the Twentekanalen.

| Description | Requirements | Average values in side channel |
|--|--------------------|--------------------------------|
| Clay content (<2 μm) | 10 - 15% | 4.2% |
| Sand fraction (63 – 2000 μm) | 35 – 50% | 75% |
| D50 | <100 μm | 152 μm |

In addition, the report of Tauw (2016) also mentions the thickness of the sludge. The water depth should be decreased due to adding the sludge to the channel. However measurements revealed an increase of the water depth. The mentioned possible explanation are the shipping movements which transport sediment to the sides.

This section gives insights in the ship-induced erosion in the Twentekanalen (paragraph 6.1) and the effects of clay plastering on the hydraulic conductivity in which also consolidation is taken into account (paragraph 6.2) in order to answer RQ. 4. The observations and results of both the erosion experiment and the clay plastering experiment are translated to the situation in reality. However, the erosion experiments are carried out with an artificial created sand-clay mixture, and scaling issues might result in errors. Moreover, the formulas developed in experiments are only applicable within a certain validity range of the densimetric Froude number and are highly dependent on experimental conditions (see Table 2, paragraph 2.3). Therefore, the scour depth is also assessed by the formula of Hoffmans and Verheij (1997) which is validated with full-scale ships in the Julianakanaal by Schroevers et al. (2015). Besides, the scour depth formula of Ducker and Miller (1996) is used which is applied regarding the Amsterdam-Rijnkanaal by Verheij et al. (2012). Both scour depth formulas shown in Table 2 are based on cohesionless soil, however the bottom in the Twentekanalen contains of sand when it is assumed that the sludge layer is eroded. The calculated scour depth serves as indication for the Twentekanalen and as comparison with the erosion depth observed during the erosion experiments.

6.1 Erosion profile Twentekanalen

Clear erosion patterns in the experiment are observed when the sailing speed is low and thus consequently small return current but relatively large propeller wash. The scour hole is formed below the location of the propeller axis and the eroded material is transported to the sides. Extra comment here is that sediment is also transported backwards, meaning that due to sailing of the ship the development of a scour hole in time is significantly slower than for a moored ship. In addition, the impact time of the ship's propeller on the bottom is also of influence and affected by the sailing speed.

However, in reality the occurring velocities of the return current cannot be neglected. Exp. 2 (Figure 18 top) corresponds to the occurring situation in reality (scaled). Extra comment here is that the most extreme scenario is chosen with loaded ships, sailing at maximum speed and minimum keel clearance. Moreover, the ships always sails exactly in the middle of the channel which is most likely not the case in reality. During the experiment was found that when the sailing speed increased, hence (1) return current increased, (2) magnitude of the propeller wash decreased and (3) impact time of propeller wash on the bottom decreased, the erosion profile became irregular. A clear scour hole was not detected but erosion occurred over a larger part of the cross section. This could be

explained by the fact that the return current also caused erosion of the sediment bed and / or the sediment eroded caused by the propeller wash (sediment in suspension) was distributed over the cross section by the return current. This statement also corresponds with the empirical formulas to estimate flow velocities at the bottom in which a larger sailing speed results in smaller velocities of the propeller wash on the bottom assuming constant efflux velocity.

6.1.1 Stability sludge layer

Rijkswaterstaat is interested in the stability of the seepage reducing sludge layer after reconstruction. An important issue here is the critical erosion velocity which is difficult to determine accurately. Different factors affects the critical velocity for which the sludge layer starts to erode such as clay content, sand-clay ratio, dry or bulk density, activity of the clay, Plasticity Index, organic material, particle sizes, sediment structure, kitting of clay-clay or clay-sand particles, compaction etcetera (see e.g. Mitchener and Torfs (1996); Jacobs et al. (2011)). For the purpose of this research an indication is made based on literature, the conducted experiment, and reports by Deltares with respect to the Amsterdam – Rijnkanaal (Verheij et al., 2012) and Julianakanaal (Schroevens et al., 2015), see Table 11.

Table 11: Critical velocities.

| | | |
|--|--|---|
| Critical velocity experiment | 0.25 m/s | Artificial sand-clay mixture |
| Critical velocity report Deltares (Amsterdam-Rijnkanaal) | 0.2 m/s | Natural sludge |
| Critical velocity report Deltares (Julianakanaal) | 0.75 m/s | Clay gravel mixture |
| Critical velocity for uniform flow used by Arcadis (2015) (low turbulence) | 0.30 m/s 0.50 m/s 0.40 m/s 0.60 m/s 0.80 m/s (1.0 m/s for short duration) 1.20 m/s (1.5 m/s for short duration) | Sand Peat Sandy clay Loose clay Moderate compacted clay Compact clay |

Paragraph 3.2 has shown that the velocities at the bottom ranges from 0.4 to 1.3 m/s in the current situation and with respect to shipping class IV for sailing vessels. In the future situation after enlarging and with respect to shipping class Va the bottom flow velocities ranges from 0.5 – 1.9 m/s for sailing vessels. The conclusion based on Table 11 and predicted flow velocities is rather simple, the sludge layer is, in all probability, not stable in future situation. Also in the current situation it is known, based on bathymetry measurements that the sludge layer is not stable, see also the suspended sediment caused by ship currents on the cover page. An estimation of the future erosion depth is described in paragraph 6.1.3.

6.1.2 Possible measures to stabilize sludge layer

Measures that could help to stabilize the seepage reducing layer should be found in (1) dimensions of the channel, (2) characteristics of shipping, e.g. keel clearance (restriction to amount of loading) and sailing / efflux velocities and (3) other measures besides sludge, e.g. bentonite mats or asphalt mats that can handle larger flow velocities. Logically, Rijkswaterstaat enlarges the channel especially accounting for characteristics of shipping class Va so this part cannot be adjusted and must be dealt with. The third aspect is found too costly and preference is given to insert sludge in the channel, so initially also this aspect is ruled out. The first aspect however, the dimensions of the channel could possibly be adjusted affecting the ship-induced flow velocities. The (extra) costs in quantitative sense of adjusting the channel are disregarded in this research.

Measure: deepening canal

Table 4 shows that the velocity on the bottom due to the propeller will increase with approximately 60% to 1.9 m/s compared to the current situation. It is likely that this increase in flow velocity affects the seepage reducing sediment layer in terms of erosion and influences the amount of seepage. An option to reduce this flow velocity on the bottom is to make the channel deeper than currently designed. The sensitivity related to the magnitude of the propeller wash and return current with respect to deepening of the canal is shown in Figure 31. Requirement for minimum depth according to “Richtlijn Vaarwegen” (Rijkswaterstaat, 2011) is 1.3 times the draught of the ship, thus 3.64 m. The depth is varied from 3.64 to 4.5 m and flow velocities are calculated according to the formulas in Appendix D.

It should be noted here that the results are only related to the future situation for loaded and unloaded vessels, and that the trapezium profile remains equal. With this is meant that deepening of the channel is modelled by raising the water level.

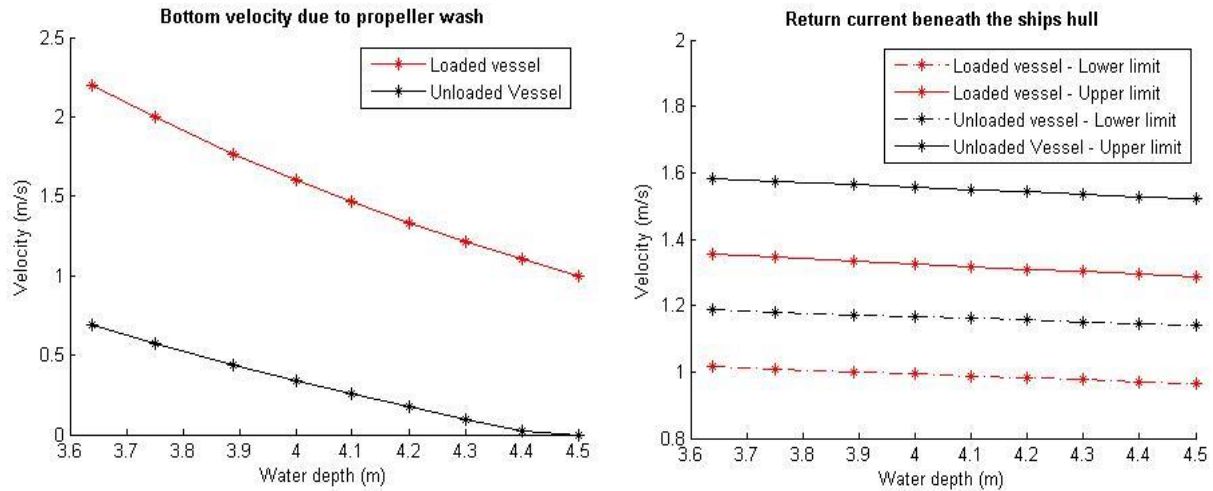


Figure 31: (Left) bottom velocity due to propeller wash and (right) return current velocity beneath the ship’s hull related to the water depth.

What stands out of the above figures is that the bottom flow velocity due to the propeller wash is very sensitive to deepening in comparison to the return current where the sensitivity is minimal. The return current is approximately linearly related with the water depth however also minimally affected while the bottom velocity due to propeller wash is strongly related.

When the depth is increased with 30 cm to 4.2 m the flow velocities on the bottom caused by the propeller reduces with 30% to 1.33 m/s (comparable with current situation). From the latter can be concluded that again in all probability the sludge layer will not be stable. More deepening could be an option, however even then it is very doubtful that a stable sludge layer will be achieved unless considerably deepened (e.g. more than 1 m). Most likely, costs will increase significantly and problems with sheet piles can occur, hence it seems not a feasible option.

Measure: widening canal

Another option, besides deepening, to reduce flow velocities is to widen the canal. The sensitivity related to widening is modelled in Figure 32. Only the bottom width is widened here which means that the slope remains equal (1:3) and that the trapezium profile is maintained. It can be seen that the propeller wash on the bottom is barely influenced by this widening measure. Actually the propeller wash on the bottom for sailing ships is only indirectly affected because the theoretical sailing speed of the vessel increases by this widening measure resulting in these minor changes. For both velocities hold that there is approximately a linear relationship with widening of the bottom.

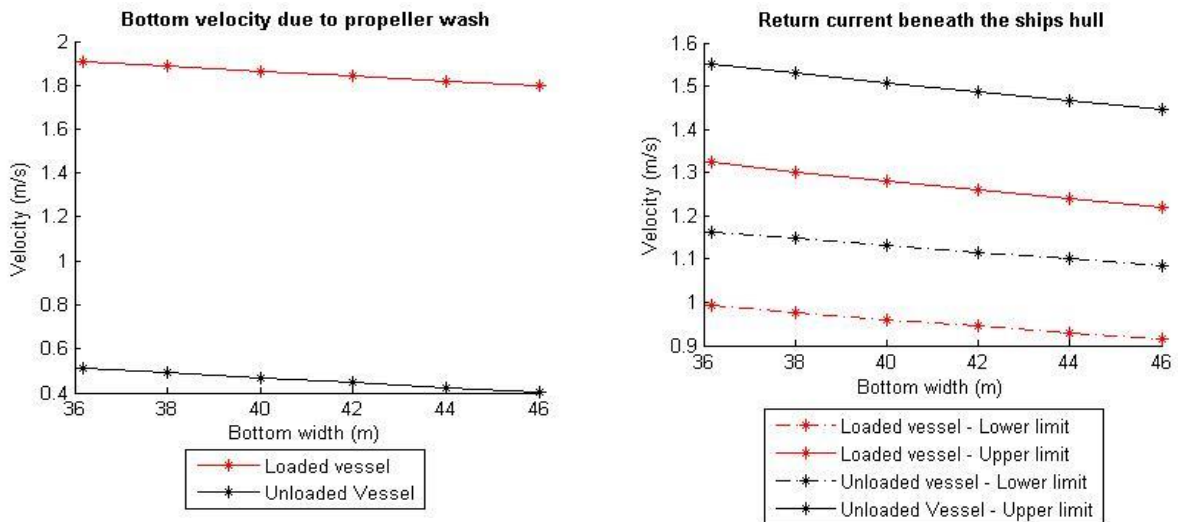


Figure 32: (Left) bottom velocity due to propeller wash and (right) return current velocity beneath ship’s hull related to bottom width.

With widening it is also possible to change the slope of the profile resulting in a wider waterline while keeping the bottom width the same. This is shown in Figure 33 where the slope is varied between 1:2 and 1:7.

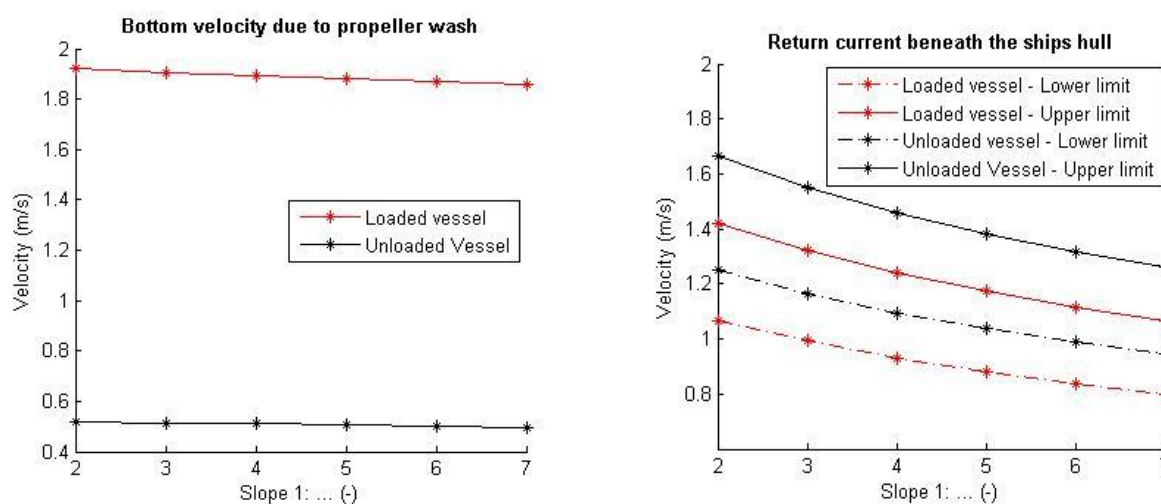


Figure 33: (Left) bottom velocity due to propeller wash and (right) return current velocity beneath ship's hull related to slope of the profile.

Again it stands out that the propeller wash is hardly affected while the return current is more sensitive to a change in slope. Furthermore, it can be seen that the return current is not linearly related to the slope of the banks.

As regards to widening of the channel, it does not affect the bottom velocity caused by the propeller (assuming no change in sailing speed) and changes in the return current beneath the ship's hull are relatively smaller compared to deepening. In other words, it is also not expected that (extra) widening will result in a stable sludge layer on the bottom of the Twentekanalen.

6.1.3 Depth scour hole

It is interesting for Rijkswaterstaat to know the depth of the scour hole regarding the amount of seepage. Possible measure to cope with the amount of seepage is to apply a specific thickness of the seepage reducing layer. For example, when the scour hole reaches a maximum depth of 20 cm the possibility arises to create a seepage reducing layer of 30 cm, i.e. ensuring a stable layer of 10 cm.

The formulas derived by Verheij (1983), Hamill (1987) and Hong et al. (2013) are not applicable since the value of the densimetric Froude number in reality is far from the validity range. Furthermore, attempts to create an erosion formula based on the experiments is rather uncertain therefore is chosen not to apply it in case of the Twentekanalen. However, geometric dimensions and sediment strength were scaled to 1:20 which gave an erosion depth of 2 - 5 cm in erosion Exp. 2 for a sailing speed of respectively 0.45 and 0.1 m/s. Scaling this back to reality results in an erosion depth of 0.4 - 1 m in the most extreme situation (= minimum keel clearance of 0.84 m). Evidently scaling could result in errors of which the magnitude with respect to erosion depth is unknown. Nevertheless, two other formulas applied in similar cases of erosion in channels in the Netherlands caused by the return current and propeller wash. These formulas remain uncertain as well, however these are validated in reality as is described below.

Return current

The following assumptions are made to estimate the bottom erosion caused by the return current according to the formula developed by Hoffmans and Verheij (1997), see Table 12. It is assumed that in the side channel of the Twentekanalen there will be 22.4 ship passages per day in 2040 (= 4091 per year) (Arcadis, 2015). Subsequently, the results are presented in Figure 34 in which the scour depth is plotted against the amount of ship passages and with a specific critical velocity for erosion.

Table 12: Assumptions for parameters according to the study of Arcadis (2015) regarding ship velocities at minimum prescribed depth, see paragraph 3.2.

$$d_{max} = (\alpha U_{r,b} - U_c)^2 \sqrt{\frac{Ndt}{K\Delta^{1.7}}} \tag{6.1}$$

| | | |
|---------------|--|--|
| $U_{r,b}$ | Return current below the ship's keel [m/s] | 1.16 - 1.55 (=lower - upper limit return current) |
| U_{cr}^* | Critical flow velocity [m/s] | 0.2 – 1.2 |
| K^{**} | Erosion constant [m ² /s ⁴] | 330 |
| V_s | Ship's sailing speed [m/s] | 2.95 (unloaded situation) |
| L | Ship's length [m] | 110 |
| dt | L/V_s [h] | 0.0104 |
| α^{**} | Turbulence coefficient [-] | 2 |
| Δ | Relative density [-] | 1.65 |
| N | Amount of ship passages [1/year] | 4091 (prognosis for one year) |

* Large difficulty to find out the true value, therefore a range of velocities is investigated.

**The scour constant K and turbulence coefficient α are retrieved from the study of Deltares regarding stability of the Julianakanaal (Schroevens et al., 2015)

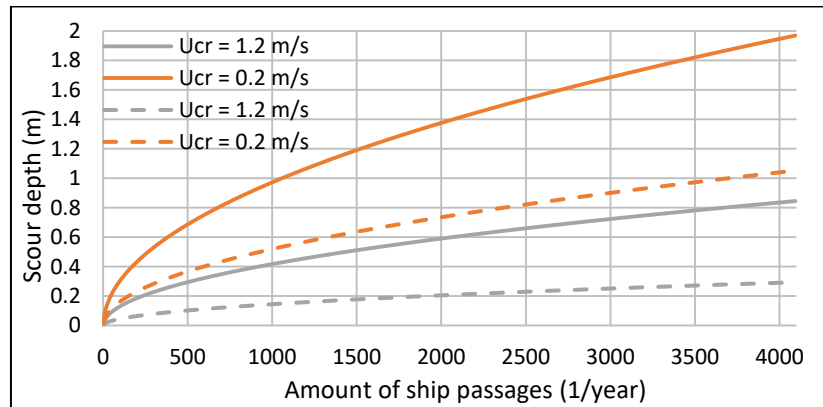


Figure 34: Scour depth plotted against the amount of ship passages. Solid line is based on the upper limit of the return current (1.55 m/s) and the dashed line is based on the lower limit of the return current (1.16 m/s).

The figure shows that especially in the beginning the erosion per ship passage is relatively large and is gradually slowing down with increasing ship passages, also seen in the erosion experiments. Nevertheless, the magnitude of erosion after 500 ship passages is around 0.1 - 0.7 m and after 4000 ship passages around 0.3 - 2 m. However, the lines presented in the figure are definitely an overestimation because first of all the amount of large ships sailing with maximum sailing speed will be limited (even a sailing restriction applies), besides the ships are not sailing exactly on the same line in the channel. The latter is also responsible for filling up the initial erosion track because the erosion track forms due to the lateral flow. In the study of Deltares regarding the stability of the bottom in the Julianakanaal an experiment on full-scale was carried out and it appeared that the observed erosion depth was around 50% lower than the theoretical erosion depth (Schroevens et al., 2015). The bandwidth is quite large due to the uncertainties summarized below:

- The erosion depth largely depends on the expected shipping;
- The erosion depth largely depends on the expected return current which in turn depends on the sailing speed;
- The erosion depth is largely dependent on the critical velocity of bottom material which in turn depends on cohesion, sediment structure, particle size etc.;
- The theoretical erosion depth is based on ships sailing exactly on the same line, while in reality this is not the case. Moreover, the theory does not include the particle displacement in longitudinal direction and filling up the erosion track. From experiments on full-scale it is observed that the theoretical erosion depth overestimates the erosion depth in reality with approximately a factor 2.

All in all, estimated is that after 500 ship passages the erosion depth is between 0.05 - 0.35 m and after one year (prognosis 4091 passages) between 0.15 and 1 m which seems reasonable compared with previous research regarding similar situations in the Amsterdam-Rijnkanaal (Verheij et al., 2012) and the Julianakanaal (Schroevens et al., 2014). Moreover, the observed erosion depth in the conducted experiment lies within the bandwidth of the calculated erosion depth.

Propeller wash

The formula of Römisch (1975) modified by Ducker and Miller (1996) is used to predict the erosion depth caused by the propeller wash (Eq. 6.2). The assumptions for the input parameters are summed in Table 13. A range of bottom velocities are investigated and presented in Figure 35. This formula is also applied in a more or less similar situation

with respect to the Amsterdam-Rijnkanaal by Verheij et al. (2012) and is used to compare outcomes with Eq. 6.1 and the erosion experiment.

Table 13: Assumptions for parameters regarding ship velocities at minimum prescribed depth, see paragraph 3.2.

$$\frac{d_{max}}{d_{85}} = C_m \cdot 4.6 \left(\frac{B^*}{B_{85}^*} \right)^{2.25} \quad (6.2)$$

| | | |
|-------------|--|------------------------------------|
| D_{85}^* | 85 th percentile of particle diameter [m] | $0.25 \cdot 10^{-3}$ |
| $U_{pr,b0}$ | Bottom velocity [m/s] | 0.2 – 1.9 |
| C_m | Constant for sailing vessels [-] | 0.3 |
| B^* | Load coefficient [-] | $U_{pr,b} / \sqrt{g\Delta D_{85}}$ |
| B_{85}^* | Stability coefficient [-] | 1.25 by definition |
| Δ | Relative density [-] | 1.65 |

*Estimated based on the study of Taww (2016) regarding Lake Dronten sludge.

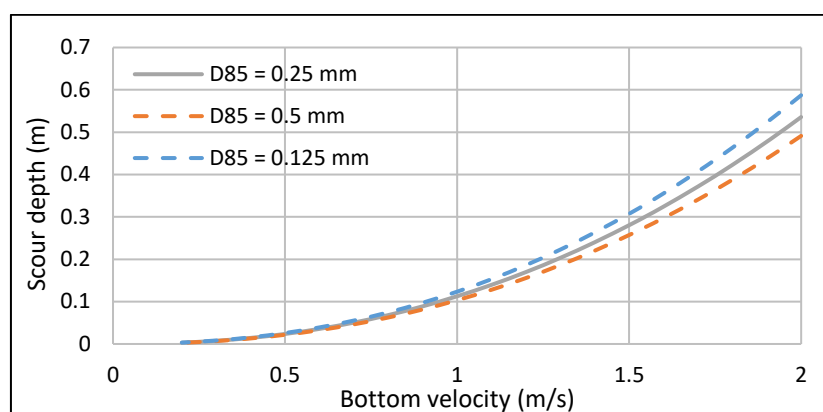


Figure 35: Scour depth plotted against bottom velocity.

The figure above presents the erosion depth with respect to the bottom velocity, and shows the sensitivity of the error in particle diameter. From this can be concluded that the effect of an error in particle diameter is rather small and accepted concerning the indication given here. The erosion depth varies between roughly 0 and 0.5 m given a bottom velocity of 0.2 and 1.9 m/s respectively. In the research of Deltares regarding the Amsterdam-Rijnkanaal (Verheij et al., 2012) is mentioned that similar to the estimation of return current erosion the uncertainty is quite large. Therefore, a factor 2 is applied resulting in an erosion depth of 0 - 1 m, similar to the estimation above and the experimental results.

Summarizing

Table 14 presents the range of obtained erosion depth found in the formulas as well as the erosion experiment.

Table 14: Comparison erosion depths of erosion experiment and applied erosion formulas in reality.

| Erosion experiment | Return current (Eq. 6.1) | Propeller wash (Eq. 6.2) |
|------------------------------------|--------------------------|--------------------------|
| 2 – 5 cm = 0.4 – 1 m at full-scale | 0.15 – 1 m | 0 – 1 m |

Currently, erosion tracks of 0.2 - 0.5 m are detected in the middle of the side channel of the Twentekanal (see Appendix C). At places where ships sail at small sailing speed the erosion depths are even larger due to the larger impact time of the propeller wash on the bottom and larger flow velocities (assuming constant efflux velocity). An increase in erosion depth is expected because of larger flow velocities (see Table 4), so the obtained erosion depths seems reasonable. The bandwidth is more or less similar which give confidence in the results despite the varying background and conditions underlying Eq. 6.1 and 6.2. Moreover, Eq. 6.1 showed same erosion behaviour as is observed during the erosion experiments. In the beginning the erosion goes rapidly and gradually slows down which is incorporated in the square root function of Eq. 6.1. Attempts are made to validate Eq. 6.1 and 6.2 with the erosion experiment, however the range of outcomes varied significantly and did not corresponded with the outcomes of the erosion experiment. One of the reasons is that during the experiment the equilibrium depth is quickly reached (after more or less six shipping passages) while Figure 34 indicates very long time period for equilibrium. This could for example be allocated to the sediment mixture. In the experiments with the sand-clay mixture slope instability was observed which limits the erosion depth and could be different for sand. Nevertheless, it seems worthwhile to conduct more experiments with for example sand to validate Eq. 6.1.

6.1.4 Qualitative model for ship-induced erosion

A qualitative model is made to provide quick insights in the relation between the different parameters on the occurring flow velocities and corresponding erosion depth. Figure 36 below presents an overview of the different parameters and its influence in positive (+) or negative (-) sense. A positive relation means that an increase in the specific input parameter value also results in an increase of the output variable while a negative relation means that an increase in the specific input parameter value results in a decrease of the output parameter. This figure shows for example that the sailing speed restriction does either have a positive or negative effect on the flow velocities on the bottom. On the one hand it reduces the magnitude of the return current, however on the other hand it increases the propeller wash velocities. Furthermore, this figure also shows that the characteristics of the sediment layer, e.g. particle diameter and critical erosion velocity are important for the erosion depth.

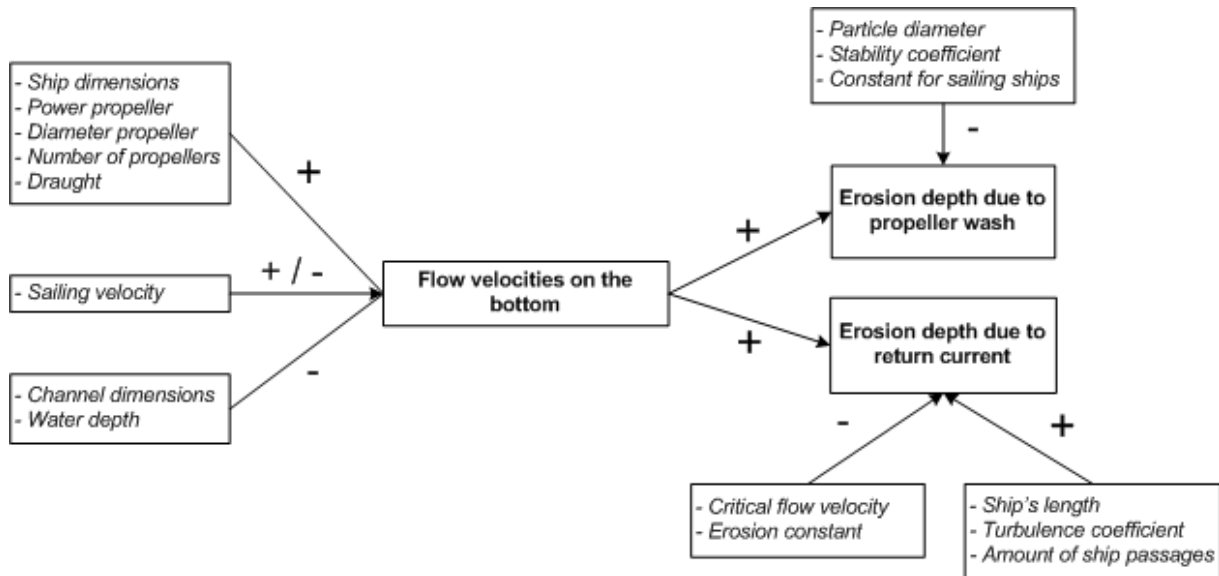


Figure 36: Qualitative model which gives insights in the relations between the input parameters (Italic) and output (Bold).

6.2 Plastering of clay particles in Twentekanalen

One of the main concerns after enlarging the Twentekanalen is the amount of seepage which should not increase but restored to the situation before maintaining dredging in 2010 or even lower. The hydraulic resistance of sludge might decrease the amount of seepage and largely depends on the composition with respect to particle size (i.e. clay, silt, sand, gravel). The expectation is that sludge applied on the channel bottom leads to sealing of the bottom. How this process happens exactly is not known and also the time period in which this will happen is unknown. It is expected that clay particles are entrained by the leaking groundwater and deposited in the upper layer of the sandy subsoil. In this research reference is made to the paper of Talmon et al. (2013) in paragraph 2.4, which in fact supports the above statement based on experiments. The term plastering is used for the deposition of clay particles in the top layer of the sandy subsoil. In addition, the concern exists that natural existing impermeable thin clay layers will be removed due to dredging activities resulting in higher permeability and consequently increases the seepage. Related to the Twentekanalen it is expected that when the sludge (or clay slurry) is inserted in the water column, from e.g. a bulk carrier, the sludge becomes in suspension and slowly deposits on the sandy bottom. Hereafter, due to leakage of groundwater the clay particles invades (drawn into) the pores of the granular soil. The clay particles basically block the pores which consequently means that the permeability decreases, and in turn the amount of seepage water decreases. The time period in which this happens, once the clay particles have reached the bottom is in the order of seconds to minutes signifying that also the permeability decreases with time. This mud spurt, however, is slowed down by itself because besides water, also clay particles cannot invade the soil anymore. Nevertheless, as described by Talmon et al. (2013) the clay suspension commences to consolidate during this process and a filter cake will be formed (see Figure 8). Consolidation is a process of soil compaction under the influence of gravity forces with a simultaneously expulsion of pore water (due to the weight of the deposit itself) and a gain in strength of the bed material. The consolidation process is strongly affected by the (Van Rijn, 1993):

- initial thickness of the mud layer;
- initial concentration of the mud layer;
- permeability of the mud layer (sediment composition and size, content of organic material, temperature).

The process of consolidation goes relatively fast in the beginning (after deposition) but gradually slows down. The progress of consolidation is usually indicated by a variable known as the degree of consolidation (U). A consolidation degree of $U = 0$ indicates the start of consolidation and $U = 1$ indicates the end of the consolidation process. To approximate the time of consolidation the 1D consolidation theory is used in which formula 6.3 corresponds well until a consolidation degree of 70%, $U = 0.7$ (Verruijt, 1999).

$$U \approx \frac{2}{\sqrt{\pi}} \cdot \sqrt{\frac{c_v \cdot t}{h_s^2}} \quad (6.3)$$

Where, U = degree of consolidation (varies between 0 and 1) [-]; c_v = Terzaghi consolidation coefficient [m^2/s]; t = time [s]; h_s = thickness sediment layer [m]

The consolidation coefficient and void ratio were determined via the Capillary Suction Time (CST) apparatus and water content respectively. The consolidation theory applied to the CST apparatus is described in the paper of Huisman and Van Kesteren (1998). Appendix G shows the CST apparatus and explains the use of it including the determination of the void ratio (e) and Terzaghi consolidation coefficient (c_v). The Terzaghi consolidation coefficient is a measure at which the consolidation rate process proceeds and is related to the permeability of the soil and could be helpful in evaluating the suitability of the sludge. Larger consolidation coefficient is often related to larger permeability (Eq. G.4 in Appendix G).

Appendix H presents the findings of the natural sludge parameters. Because of uncertainties in the consolidation coefficient and thickness of the sludge layer a sensitivity analysis is carried out and results are summed in Table 15. The thickness of the sludge layer is varied to 0.1 m, 0.25 m and 0.5 m. Additionally, the time of consolidation is calculated according to a consolidation degree of 30% and 70%. The table below shows that the consolidation is in the order of hours to days according to the applied consolidation coefficient and thickness of the sludge layer. Rijkswaterstaat could decide to establish a no-sailing zone for a certain period to enhance the consolidation of the sludge layer because the consolidation of the sludge layer (1) decreases the permeability and (2) increases the erosion resistance. However, it is expected that the increase in erosion resistance is too small to be able to form a stable layer on the bottom of the Twentekanalen because the ship-induced flow velocities on the bottom are significantly larger than the critical velocities of natural sludges (Table 4 vs Table 11). Nevertheless it could enhance the infiltration of very fine particles into the sandy subsoil.

Table 15: Consolidation time of current sludge in the side channel of the Twentekanalen based on Eq. 6.3.

| * c_v (m^2/s) | h_s (m) | Consolidation time (hours) | |
|--------------------------------------|--------------|-------------------------------|-----|
| | | 30% | 70% |
| $2.9 \cdot 10^{-7}$ | 0.1 | 1 | 4 |
| $2.9 \cdot 10^{-7}$ | 0.25 | 4 | 23 |
| $2.9 \cdot 10^{-7}$ | 0.5 | 17 | 92 |

* Average value of c_v values

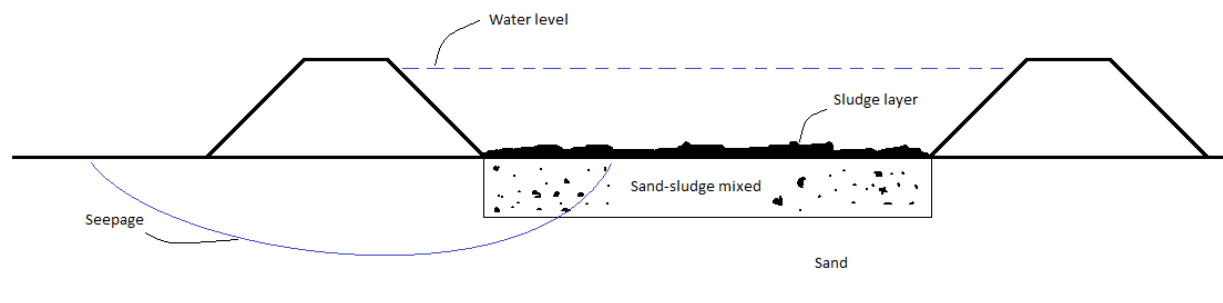


Figure 37: Schematic representation of specific layers after sludge is poured in the Twentekanalen.

Evidently, the sludge is stirred up by the shipping flow velocities which is also confirmed visually. Besides, it is likely to assume that the sludge is also mixed with the sandy subsoil (Figure 37). The plastering experiment in this research showed that the permeability is decreased by this mixing. To sketch the process one can say that due to the passage of a vessel clay particles are picked up from the bed into suspension, and will gradually deposit on the bottom again when flow velocities are lower. However, the larger particles (i.e. sand or larger clay flocs) deposit quicker on the

bottom compared to the smaller particles (i.e. clay and silt particles) because of their larger fall velocity. Additionally, the particles which were too heavy to pick up, or which were more erosion resistant due to for instance cohesion (kitting of clay – clay or clay – sand particles) remain on the bottom. Despite that these particles are not brought into suspension these could be displaced and mixed. Eventually, also the fine material will be deposited on the bottom of the channel. The effects of such a process is simulated in plastering Exp. 4 and 7 and showed a decrease in permeability. The deposition of fine materials in which flocculation processes play a role is not studied here.

The plastering tests showed that when the sludge was stirred with the sand, the permeability decreased compared to the situation of a stable sludge layer on top of the sand filter in that specific layer. Most likely, the interaction between the sand and (very) fine particles is intensified meaning that more pores are filled or blocked due to the fine particles which was also found in the plastering tests of Talmon et al. (2013). It implies again the importance of the percentage fine particles within the sludge corresponding to the practical experiments in the side channel of the Twentekanaal by Rijkswaterstaat (2003). Concluding, it is not proven that shipping has a direct negative relation to the amount of seepage. Since, shipping could mix the sediment on the bottom which might lead to a decrease of the permeability and clay particles can in turn infiltrate deeper in the sediment. A point of discussion is the height of the plastering cell used in the experiments because in reality it is reasonable to assume that fine particles are suspended high in the water column indicating much larger deposition times in comparison to the plastering cell.

7 Discussion

The objective of this research was “to visualize the erosion profile and estimate the equilibrium erosion depth of a sand-clay sediment mixture under the influence of shipping in the axis of the side channel of the Twentekanalen, and to test whether clay particles are infiltrated into the sandy subsoil affecting the hydraulic conductivity”. The research succeeded in visualizing the erosion profile and determining the equilibrium erosion depth after certain amount of ship passages in the experiment. Plastering experiments succeeded in testing whether clay particles infiltrated the sandy subsoil that reflects the sand in the Twentekanalen. Nevertheless, uncertainties in results were unavoidable and could be allocated to different reasons which will be discussed in this section. In addition, the translation to reality should be done with caution due to some factors which will be discussed as well. In this section the experiments are reviewed, uncertainties discussed and results are compared with existing literature. The first paragraph is related to the erosion experiment in which the propeller wash is of importance, the second paragraph is related to the plastering experiment and the third paragraph discusses the difficulties regarding translation of the experimental results to reality and the usability with respect to the side channel of the Twentekanalen.

7.1 Erosion experiment

Comparing the results of the propeller wash with existing literature reveals that the decay of the axial velocities in longitudinal direction especially differs in the zone of flow establishment. In the zone of flow establishment a linear relationship was found which is either supported or contradicted in literature (Lam et al, 2011) signifying there is no consensus about this statement in the scientific community. Nevertheless, in this research the velocity at one propeller diameter behind the propeller is assumed equal to the efflux velocity which can be questioned. Moreover, the empirically determined coefficients in the decay functions of the axial velocities do not correspond with values found in literature (see e.g. Lam et al, 2011) which is likely caused by the influence of bottom and walls. Small differences in the velocities of the propeller wash appeared not of significant influence for the purpose of the results. Nevertheless, the gathered velocity data under the given circumstances are valuable in understanding the velocity distribution behind a propeller and are useful to validate existing formulas. The relevant velocities in this research were separately measured, i.e. close to the propeller, on the initial bottom and in the bottom of the scour hole. The velocity close to the propeller showed good agreement between the amount of propeller rotations and the velocity ($R^2 = 0.96$). Moreover, the measured axial velocities at the bottom of the scour interpreted as the time-averaged critical velocity in all experiments hole were similar which give confidence in the results.

The experimental set-up with respect to the model ship and its propulsion requires consideration. In this research the ship was fixed in a frame underneath the moving measuring bridge. Consequently, the ship could not move vertically and is towed instead of driven by the propeller which could be criticized. One of the consequences of towing the model ship is that the propeller wash is more severe. The propulsion of water, hence the velocities in the propeller wash are larger for moored ships than for sailing ships. In other words, when the sailing speed of the model ship due to towing is smaller than the velocity of the propulsion system, the velocities in the propeller wash are higher compared to the situation when the model ship would be driven by the propulsion system itself and vice versa. With regard to this part the conclusion reads that the observed erosion depth is likely to be overestimated in a situation with smaller sailing speed and underestimated in a situation with larger sailing speed relative to the propulsion speed induced by the propeller.

The results of the erosion experiment showed a clear erosion pattern with deepening underneath the ship and elevation at the sides corresponding to bathymetry measurements in practice and literature with respect to sand erosion (Verheij, 1983; Hamill, 1987; Hong et al., 2013). Moreover, it appeared that the efflux velocity and offset height are of importance as expected. However, it is also expected that the specific characteristics such as plasticity index and strength (consolidation and sand-clay ratio) should have its influence on the erosion depth. Erosion formulas with respect to sand of Verheij (1983) and Hamill (1987) were applied to the available data points and the empirical coefficients were estimated. The differences in especially α were large which might be attributed to small impact times of propeller wash on the bottom due to sailing vessels compared to the earlier experiments by Verheij (1983) and Hamill (1987) in which the propeller is continuously rotating for at least 24 hours at the same position. The latter indicates that the slopes of the scour hole could not collapse while in the conducted experiments in this research the slopes could collapse after a ship has passed (also seen in one of the experiments) resulting in smaller erosion depths indicating the importance of the strength of the sediment mixture. Hence, impact time and slope instability definitely influences the eventual erosion depth. Another reason might be that the particles in the scour hole are eroded but not transported out of the hole which limits the eventual erosion depth. All in all, a clear erosion formula could not be developed, partly because of limited amount of data points and partly because it is expected that besides particle diameter also clay characteristics (cohesive properties) are of influence regarding scour holes in sand-clay mixtures. Additionally, different kind of processes could limit the erosion depth which need further

attention. Nevertheless, the erosion experiment succeeded with respect to the purpose of this research in visualizing the erosion profile and exploring the development of the erosion depth owing to shipping currents.

7.2 Plastering experiments

The results of the plastering experiments correspond well with the theory described by Talmon et al. (2013). In particular, the experiment with an artificial sand-clay mixture agrees with the expected plastering process found in literature. It should be mentioned that the plastering theory by Talmon et al. (2013) is based and tested on sediment mixtures with relatively smaller yield strength (order 0 - 30 Pa) in comparison to the sediment mixtures used in the plastering experiments conducted in this report (>100 Pa). Nevertheless, the plastering process of the artificial sand-clay mixture is well represented in the first part of the experiments (1 - 1.5 hours), however in the second part there is a clear change in the pattern which might be allocated to the development of small channels within the soil, insufficient amount of clay particles to cover the surface or clay particles might be washed out of the soil. Prior reasoning is rather uncertain and needs further attention. The latter is however not substantial for the purpose of this research because relevant information is retrieved from the first part. The experiments involving the natural sludge also agree with the theory, however the process was less intense. The mud spurt was clearly visible but the consolidation (filter cake formation) was less intense compared to the experiment with the artificial sand-clay mixture. The explanation lies in all probability in the percentage of clay within the sediment. The artificial sand-clay mixture contains more clay than the natural sludge and therefore the filter cake formation is better represented. Consequently, the calculated hydraulic conductivity of the natural sludge appeared to be much higher than the artificial sand-clay mixture.

Furthermore, a lower hydraulic conductivity is obtained when the sludge is stirred with the sand. Exp. 6 and 7 in particular demonstrate that when the sludge is stirred up the permeability decreases compared to the situation with a stable sludge layer on top of the subsoil. Most likely this is caused by a better distribution of clay particles over the surface consequently clogging larger amount of pores. Foregoing indicates that the infiltration depth of clay particles is also of great importance and should be measured to draw conclusions.

7.3 Usability experimental results for reality

The calculation of occurring flow velocities and erosion depths in the side channel are based on normative situations and empirical formulas. Flow velocities of ship-induced currents on the bottom of the side channel of the Twentekanalen increase from 0.4 - 1.3 m/s in the current situation based on shipping class IV to 0.5 - 1.9 m/s in future situation based on shipping class Va. These flow velocities represent the situation for sailing vessels while flow velocities for ships at rest are even higher. In addition, it is assumed that all the ships sail exactly in the axis of the channel which is most likely not true.

A direct translation of the erosion results obtained in the experiments to the situation in reality is questionable. First of all, relevant parameters in reality are scaled according to Froude's law in the experiment which consequently results in impurities either in resistance or in occurring return current and propeller wash (Delefortie, 2007; Starke, 2004). Moreover, the sediment mixture is not the same as in reality and the used model ship did not exactly match the dimensions of a ship according to class Va. However, impurities were small and accepted for this research because the main purpose for Rijkswaterstaat was to provide insights in the processes around erosion of sand-mud mixtures. The obtained erosion depth in the erosion experiments varied roughly between 2 - 5 cm which would be 0.4 - 1 m on full-scale (scale 1:20). This value should serve as rough indication because it is likely to be overestimated as is discussed above and it is also uncertain due to scale effects. Nevertheless, comparing this value with empirical formulas applied and validated in situations in reality, under more or less same circumstances, it appears that it is fairly similar.

The plastering experiments clearly showed that the natural sludge from the Twentekanalen contained less clay particles compared to the artificial sand-clay mixture. Furthermore, it appeared that the situation of stirred sludge the permeability decreases compared to the situation of stable sludge. It is an interesting finding with regard to the Twentekanalen in which the sediment on the bottom might be stirred up and mixed due to sailing ships which could ensure a better distribution of clay and subsequently lower hydraulic conductivity. Remark is the imposed pressure which is based on the maximum observed difference between water level in the canal and surrounding groundwater level. The question is if similar conclusions can be drawn when smaller pressures are applied. Arcadis (2015) mentioned that it is likely that clay particles are entrained into the subsoil due to the seepage flow. This statement could not be confirmed visually, however it is expected based on the plastering theory that clay particles are indeed infiltrated in the soil. The applied natural sludge however appeared to be sandy instead of clayey (Tauw, 2016) which was requested by Rijkswaterstaat. Moreover, the Itterbeck sand used in the plastering set-up did not exactly match with sand in the Twentekanalen, the hydraulic conductivity however was fairly similar. Having discussed this, the found values of hydraulic conductivity should serve as comparison between the conducted experiments and should not be interpreted as the true value.

8 Conclusions and recommendations

To answer the main question of this research and to comply with the objective of this research four sub questions were established. Paragraph 8.1 answers the sub questions and the main research question in succession. Paragraph 8.2 presents recommendations for future research and ends with recommendations for Rijkswaterstaat related to the issues in the side channel of the Twentekanalen.

8.1 Conclusions

RQ. 1 What are the ship-induced flow velocities under and around the ship in the side channel of the Twentekanalen assuming stagnant water in current and future situation?

Table 16 shows the occurring flow velocities under and around the ship in which shipping class Va is normative. The findings show that the maximum flow velocities for sailing ships increases in future situation with approximately 20% with respect to the return current beneath the ship and increases with roughly 60% for the propeller wash on the bottom. In addition, the highest velocity on the bottom is caused by the propeller in case of loaded ships.

Table 16: Ship-induced flow velocities in the current and future situation regarding different shipping class and profile.

| | Current situation Class IV | | Future situation Class Va ('Krap' profile) | |
|--|-------------------------------|-----------------|---|-----------------|
| | <i>Loaded</i> | <i>Unloaded</i> | <i>Loaded</i> | <i>Unloaded</i> |
| Actual sailing speed [m/s] | 2.1 | 2.8 | 2.1 | 2.9 |
| Max. Return current canal [m/s] | 0.5 | 0.7 | 0.7 | 0.8 |
| Return current underneath ship (lower limit) [m/s] | 0.8 | 1.0 | 1.0 | 1.2 |
| Return current underneath ship (upper limit) [m/s] | 1.1 | 1.3 | 1.3 | 1.6 |
| Velocity directly behind propeller [m/s] | 7.2 | 7.2 | 7.2 | 7.2 |
| Velocity on the bottom due to the main propeller for ships at rest [m/s] | 2.2 | 1.8 | 2.9 | 2.0 |
| Velocity on the bottom due to the main propeller for sailing ships [m/s] | 1.2 | 0.4 | 1.9 | 0.5 |

RQ. 2 How does the erosion profile and equilibrium depth in a sand-clay mixture develop under influence of ship-induced currents during the experiment in the flume?

After the first ship passage it was seen that the profile of the channel starts to erode and that an erosion track developed. Underneath the ship at the location of the propeller, the bottom eroded and the eroded sediment was transported to the sides of the channel. Foregoing was caused by the propeller wash which is especially dominant when sailing speeds are low. Moreover, it was observed that smaller particles were transported to the sides while larger particles were located in the axis of the channel. The development of the erosion track is decreasing after every ship passage. In other words, in the beginning the erosion is relatively fast and reduces with every ship passage, because the distance from the propeller tip to the bottom increases. Moreover, the equilibrium erosion depth and width of the track is dependent on the velocities within the propeller wash. Higher efflux velocity of the propeller results in a wider and deeper scour hole. Additionally, the sailing speed is also of influence. On the one hand an increase in sailing speed results in smaller flow velocities of the propeller wash on the bottom and shorter impact time. On the other hand the return current starts to play a role when the sailing speed increases. Erosion was observed when the sailing speed increased, however a clear scour hole did not develop. The erosion depth is also dependent on the slope stability of the erosion hole, hence the strength of the sediment. Collapsing slopes limit the equilibrium erosion depth. In addition, the sand-mud ratio changing with depth could limit the erosion depth. No clear relation between the maximum erosion depth and the propeller wash was found due to the variety of reasons mentioned above. Comparison with existing erosion formulas for sand seems to give fairly reasonable results, however these are established for continuously rotating propellers located on the same location contradicting to the conducted erosion experiment in this research and might be an explanation for the large difference in one of the empirical coefficients in these formulas.

RQ. 3 How does clay plastering affect the hydraulic conductivity over time?

Clay plastering appeared to be of great importance regarding the hydraulic conductivity. The mud spurt of clay particles into the sandy subsoil takes place within seconds (when deposited on the bottom) while consolidation (creation of filter cake) takes place within hours to days. The hydraulic conductivity is directly affected by the clay particles; more clay particles results in lower hydraulic conductivity. Furthermore, the findings show that the hydraulic conductivity decreases when the sludge (or clay layer) is stirred up and better mixed with the sandy subsoil. Hence, also the distribution of clay particles within the sandy subsoil is of importance for the hydraulic conductivity.

RQ. 4 How will the seepage reducing natural sand-mud mixture which is used in the Twentekanalen develop over time regarding erosion and hydraulic conductivity?

The erosion of the seepage reducing natural sand-mud mixture, which is used in the Twentekanalen, due to ship-induced currents starts directly. In the beginning the erosion is fast signifying the first ship passage and decreases after every ship passage eventually resulting in an equilibrium depth. However, it is questionable if the equilibrium depth is reached because ships will not sail all the time exactly in the axis of the channel. Nevertheless, the seepage reducing natural sand-mud mixture is transported to the sides. The latter indicates that the presence of clay particles decreases in the axis of the channel consequently meaning that the hydraulic conductivity increases in the axis of the channel while it decreases at the sides. The hydraulic conductivity could decrease over time due to the infiltration of clay particles deeper in the sandy subsoil and mixing caused by ships currents.

Main question

What will be the effect of ship-induced hydraulic loadings on the erosion profile, equilibrium erosion depth and hydraulic conductivity of the sand-mud mixture in the Twentekanalen after enlarging and construction of the new layer?

Applying a sand-mud mixture on the bottom of the Twentekanalen after enlarging will directly be eroded due to ship-induced hydraulic loadings. It is unlikely that a natural sand-mud mixture will develop to form a stable layer on the bottom of the Twentekanalen because occurring flow velocities are much higher than the critical erosion velocity of (natural) sand-mud mixtures. Mixtures of clay with sand or gravel, or compacted clay increases the erosion resistance significantly, however in all probability not enough to create a stable layer. The erosion profile can be described as follows: an erosion track develops in the axis of the channel where the ships are sailing and the eroded sediment is transported towards the sides resulting in elevation near the banks (Figure 2). Currently, erosion tracks in the axis of the side channel of the Twentekanalen ranges from 0.15 to more than 0.5 m (near locks and bridges erosion tracks are deeper caused by intensified propeller wash to manoeuvring of the ships) based on obtained bathymetry data. After enlarging of the channel and giving access to shipping class Va the flow velocities on the bottom become higher, hence it is reasonable to assume that the erosion tracks will become deeper in the future. Erosion depths of 0.4 - 1 m seem reasonable based on the executed experiments and existing erosion formulas.

The plastering experiments showed that in case of sludge stirred with sand the permeability decreases compared to the situation of a stable sludge layer. Related to the Twentekanalen this means that ship-induced currents does not have direct negative consequences for the amount of seepage because it could mix the clay particles with the sandy subsoil and therefore decreasing the hydraulic conductivity.

8.2 Recommendations

Future research is divided into three themes and in succession described: propeller wash, ship-induced erosion and plastering experiment. The last subparagraph presents recommendations for Rijkswaterstaat with respect to the side channel of the Twentekanalen.

Propeller wash

In this research an extensive data set of velocities in the propeller wash is obtained. However, this research only focussed on the axial flow velocities because from literature it appears that these velocities affects bottom erosion the most. Nevertheless, tangential velocities were obtained simultaneously and could be used to elaborate further on the propeller wash. Currently, only empirical formulas are present to calculate velocities in the propeller wash which could be validated with the obtained data set. Additionally, the efflux velocity is an important parameter regarding bottom erosion. In this research it is assumed that the efflux velocity is equal to the measured velocity at one diameter behind the propeller as is proposed in specific literature but there is no consensus about this statement in the scientific community. Furthermore, in the flow of establishment a linear relationship was found which either is supported or contradicted. However, this relationship is based on three to five data points. Smaller resolution of measurements within the zone of flow establishment is advised to support the statement. The same holds for the efflux velocity formulas in combination with the axial momentum theory. In this research the thrust coefficient of the propeller was not determined, but when it is, it might help to validate existing formulas or to refine these.

Ship-induced erosion

Attempts to develop an erosion formula for sand-clay mixtures under influence of shipping currents, based on the available data appeared not to be straightforward. A power function similar to existing erosion formulas for sand showed fairly good agreement, however one of the empirical coefficients showed a large difference which might be

attributed to difference in experimental set-up. Besides, a logarithmic function supports the reasoning of increasing erosion resistance with depth (different sand-clay ratios), however cohesive properties are not incorporated. Slope stability limits the increase in erosion depth, hence the strength of the sediment is found to be relevant. Suggestion for further research is to carry out exactly similar experiments as in literature with continuously rotating propeller and meanwhile measuring the scour depth in time. Such experiments could give answers regarding the form of the distribution and magnitude of the coefficients but also the impact of factors described above. Additionally, experiments with sailing ships (i.e. smaller impact time of propeller wash and including the return current) can be carried out on different sand-mud mixtures, preferably on full-scale. Additionally it is advised to execute more experiments regarding the erosion of only sand because also for sand it appears that the empirical coefficients are highly dependent on experimental conditions. Moreover, the formula of Hoffmans and Verheij (1997) in Eq. 1 shows same erosion behaviour as observed in the experiments and it seems worthwhile to conduct more experiments to improve and validate this formula.

Another issue regarding the erosion with subsequent deposition is the particle distribution over the width of the flume (selected transport). It was expected that after ship passages a scour hole developed in the axis of the flume and that the sides levelled up (also seen in reality) due to deposition of particles. In fact, it was expected that due to relatively small fall velocities especially fine particles were transported to the sides which largely affects the permeability. The conclusion from tangible and visual observations heralded that indeed small particles (clay) were transported to the sides and that in the middle of the flume more sand was present. However, a quantitative analysis was not carried out. For the purpose of seepage in the Twentekanalen it could be of importance to know the particle distribution over the cross section after construction of the seepage reducing sludge layer.

Plastering experiment

The execution of the plastering tests are carried out with a pressure of approximately 150 mbar, however another interesting question is how this plastering evolve when smaller pressures are applied because the groundwater flow also takes account of a certain part of the total pressure. Moreover, varying sand-mud mixtures could give more insights in the plastering behaviour in different situations. Besides, due to installation of more pressure sensors over the plastering cell, especially near the location of the sludge or clay layer, more information can be retrieved regarding for instance the invasion depth of the clay particles. The invasion depth of clay particles in a sandy subsoil could be particularly of interest regarding seepage issues because this is found to be important for the permeability.

Recommendation Rijkswaterstaat with respect to side channel Twentekanalen

Possible measures to reduce flow velocities on the bottom such as widening or deepening the channel does not fulfil requirements to create a stable sludge layer or are expected to be too costly. Consolidation of the sludge layer results in higher erosion resistance, however it is unlikely that the erosion resistance is larger than occurring flow velocities. In other words, a sailing restriction does not seem worthwhile. The mud spurt of fine particles into the sand is important and takes place within seconds to minutes while consolidation (creation of filter cake) takes place within hours to days based on available data. Comparing the artificial sand-clay mixture with the natural sludge it appeared that the latter is much more permeable in which the explanation lies within the grain size distribution. The artificial sand-mud mixtures consists of more clay particles which closes of the pores much better than the larger particles within the natural sludge. Since, it seems that in particular the percentage of clay within the sludge is of importance in compliance with the practical experiments conducted in the side channel of the Twentekanalen by Rijkswaterstaat (2003) while the layer thickness is of less importance also taking into consideration the displacement of the sludge layer over the profile. Moreover, analysing soil samples of the temporary sludge applied in the side channel of the Twentekanalen also shows that the requirements such as minimum clay content are far from met (Tauw, 2016). Therefore, it is recommended to make use of a seepage reducing layer containing a significant amount of clay as is mentioned by experts which can infiltrate the sandy subsoil as is demonstrated in the plastering experiments. Further study to investigate the infiltration depth of clay particles and plastering of different sand-mud mixtures and its effects on the hydraulic conductivity under different conditions is recommended. Nevertheless, there are other possibilities to seal the bottom such as bentonite mixtures also applied in the Julianakanaal. These mixtures are beyond the scope of this research, however it seems worthwhile to investigate it.

The scope of this research was related to erosion and plastering, however re-sedimentation is also an extra factor influencing the amount of seepage. Past experience have shown that quick re-sedimentation of clay particles maintained the amount of seepage. In other words, erosion of the sludge layer does not have directly consequences for the amount of seepage when eroded particles are quickly deposited again. It is advised to study the deposition of fine particles under the influence of shipping currents.

9 References

- Albertson , M. L., Dai, Y. B., Jensen, R. A., & Rouse, H. (1950). Diffusion of a submerged jets. *Transcript of the ASCE (Paper No. 2409), Vol. 115*, 639-697.
- Arcadis. (2015). *Aanvullend verkennend waterbodemonderzoek en civieltechnisch onderzoek; Zijtak Deeltraject 4 en 5*.
- Arcadis. (2015). *Memo: Stroombelasting op kanaalbodem (onderdeel VTW-001 Kwel)*.
- Arcadis. (2015). *Planuitwerking en Voorbereiding Realisatie Twentekanelen 2e Fase - Analyse Kwelproblematiek (VTW-001)*.
- BAW. (2005). *Principles for the Design of Bank and Bottom Protection for Inland Waterways, No. 88*. Kalsruse, Germany: Bundesanstalt für Wasserbau.
- Bisschop, F., & van Kesteren, W. G. (1994). *Consolidatie Sliblaag*. Waterloopkundig Laboratorium |WL.
- Blaauw, H. G., & Van der Kaa, E. J. (1978). *Erosion of bottom and sloping banks caused by the screw race of manourving ships*. WL publicatie 202.
- Bouwmeester, J., Van de Kaa, H. J., Nuhoff, H. A., & Van Orden, R. G. (1977). *Recent studies on push towing as a base for dimensioning waterways*. WL| Delft Hydraulics, Delft.
- Brovchenko, I., Kanarska, J., Maderich, V., & Terletska, K. (2007). 3D non-hydrostatic modelling of bottom stability under impact of the turbulent ship propeller jet. *Acta Geophysica, 55 (1)*, 47-55.
- CIRIA. (2007). *The Rock Manual*. CIRIA.
- CUR. (1999). *CUR-publicatie 201 "Natuurvriendelijke oevers: belasting en sterkte"*. Gouda: Stichting CUR.
- Delefortie, G. (2007). *Manourving Behaviour of Container Vessels in Muddy Navigation Areas*. PhD Thesis, University of Gent, Gent.
- Ducker, H. P., & Miller, C. (1996). Harbour bottom erosion at berths due to propeller jets . *Proceedings of the 11th International Harbour Congress*. Antwerpen.
- Eloot, K., Verwilligen, J., & Vantorre, M. (2008). An overview of squat measurements for container vessels in restricted water. *International Conference on Safety and Operations in Canals and Waterways SOCW*. Glasgow.
- Fuehrer , M., & Römisch, K. (1977). Effects of modern ship traffic on islands and ocean waterways and their structures . *PIANC 24th Congress*, (pp. section 1-3). Leningrad.
- Hamill, G. A. (1987). *Characteristics of the screw wash of a manoeuvring ship and the resultant bed scour*. PhD Thesis, The Queen's University, Northern Ireland.
- Hasmi, H. N., Ghumman, A. R., Hamill, G. A., & Stewart, D. P. (2007). Propeller-wash induced erosion and method for its prediction. *Technical Journal*, 29-37.
- Hazen, A. (1892). *Some physical properties of sand and gravel, with special reference to their use in filtration*. 24th Annual Report, Massachusetts State Board of Health, Boston.
- Hill, R. (1950). *The mathematical theory of plasticity*. Oxford: Clarendon Press.
- Hoffmans, G. J., & Verheij, H. J. (1997). *Scour manual*. Rotterdam: A.A. Balkema.
- Hong, J.-H., Chiew, Y.-M., & Cheng, N.-S. (2013). Scour Caused by a Propeller Jet. *Journal of Hydraulic Engineering, 139 (9)*, 1003 - 1012.
- Huisman, M., & van Kesteren, W. G. (1998). Consolidation Theory Applied to the Capillary Suction Time (CST) Apparatus. *Water Science and Technology, 37, No 6 - 7*, 117-124.
- Jabocs, W., Le Hir, P., Van Kesteren, W., & Cann, P. (2011). Erosion threshold of sand-mud mixtures. *Continental Shelf Research 31*, 14 - 25.
- Jacobs, W., Le Hir, P., van Kesteren, W., & Cann, P. (2011). Erosion threshold of sand-mud mixtures. *Continental Shelf Research, 31 (10)*, S14-S25.

- Jol, C. (2014). *Verkeersbesluit voor een snelheidsbeperking op het Zijkanaal naar Almelo van de Twentekanalen, Rijkswaterstaat*. Koninkrijk der Nederlanden, Staatscourant nr. 17335.
- Lam, W., Hamill, G. A., Songyong-chen, Robinson, D. J., & Raghunathan, S. (2011). Experimental Investigation of the Decay from A Ship's Propeller. *China Ocean Engineering*, 25, (2), 265-284.
- Mitchener, H., & Torfs, H. (1996). Erosion of mud/sand mixtures. *Coastal Engineering*, 29, 1-25.
- Nijborg, N. A. (2016). *Literature study: The erosion and permeability of sand-mud mixtures*. Preparation MSc Thesis, University of Twente, Enschede.
- Paulsen, E. (2007). *Investigating the effect of coarse particle addition on the measured rheological parameters of fine clay slurries*. PhD Thesis, University of Stellenbosch.
- Powers, M. C. (1953). A new roundness scale for sedimentary particles. *Journal of Sedimentary Petrology*, 23 (2), 117-119.
- Rijkswaterstaat. (2003). *Twentekanalen baggeren; Kwelproblematiek profielverruiming, uitwerking maatregelen in het kanaal*. Waterbodems Advies en Uitvoering, Utrecht.
- Rijkswaterstaat. (2011). *Richtlijnen Vaarwegen 2011*.
- Rijkswaterstaat. (2015). *Verruiming Twentekanalen fase 2*.
- Robijns, T. (2014). *Flow beneath inland navigation vessels*. MSc Thesis, TU Delft , Delft.
- Römisch, K. (1975). *Der Propellerstrahl als erodierendes Element bei An- und Ablegemanövern in*. Berlin.
- Schiereck, G. J. (2004). *Introduction to Bed, Bank and Shore Protection*. London: Spon Press.
- Schijf, J. B. (1949). Paper presented at the XVIIth International PIANC Congress. *17 th International PIANC Congress*. Lisbon, Portugal.
- Schofield, A. N., & Wroth, C. P. (1968). *Critical state Soil Mechanics* . London: McGraw-Hill.
- Schroevers, R., Verheij, H., Berends, K., & Vermaas, T. (2015). *Stabiliteitsproeven Julianakanaal 2014*. Deltares, Delft.
- Starke, B. (2004). The prediction of scale effects on ship wave systems using a steady iterative RANS method. *7th Numerical Towing Tank Symposium*. Hamburg, Germany.
- Stewart, D. P. (1992). *Characteristics of a ships screw wash and the influence of quay wall proximity*. PhD Thesis, Queen's University of Belfast.
- Talmon, A. M., Mastbergen, D. R., & Huisman, M. (2013). Invasion of pressurized clay suspensions into granular soil. *Journal of Porous Media*, 16 (4), 351-365.
- Talmon, A., & Verheij, H. J. (2014). *Memo aan RWS, concept KPP 2014 Vlot en veilig gebruik vaarwegen*. Deltares, Delft.
- Tauw. (2014). *Oorzaken en oplossingen kweloverlast omgeving Twentekanaal*. Deventer.
- TAUW. (2016). *Slibdiktemetingen zijkanaal Twentekanaal richting Almelo*.
- Torfs, H. (1995). *Erosion of mud / sand mixtures*. PhD Thesis, Katholieke Universiteit Leuven.
- Van de Ree, T. H. (2015). *Deposition of high density tailings on beaches*. MSc Thesis, TU Delft.
- Van Rijn , L. C. (1993). *Principles of Sediment Transport in Rivers, Estuaries and Coastal Areas*. Oldemarkt : Aqua Publications.
- Verheij, H., Van Meerten, H., & Giri, S. (2012). *Onderzoek Bodemerosie Amsterdam-Rijnkanaal*. Deltares, Delft.
- Verhey, H. J. (1983). The stability of bottom and banks subjected to the velocities in the propeller jet behind ships. *Proceedings 8th Int. Harbour Congress*, (pp. 1-11). Antwerp, Belgium.
- Verruijt, A. (1999). *Grondmechanica*. Delft: Delft University Press.
- Wiertsema & Partners. (2015). *Geotechnisch laboratorium onderzoek; Twentekanalen 2e fase in Twente te Enschede*. VN-63497.

Winterwerp, J. C., & van Kesteren, W. G. (2004). *Introduction to the Physics of Cohesive Sediment in the Marine Environment*. Amsterdam: Elsevier.

WL| Delft Hydraulics. (1987). *Erosion of cross sections of navigation channels: systematic test serie of water motions by three different types of inland navigation vessels (In Dutch)*. WL| Delft Hydraulics, Delft.

10 Appendices

| | | |
|-------------|--|----|
| Appendix A. | Seepage judgement Twentekanalen | 56 |
| Appendix B. | Characteristics side channel Twentekanalen..... | 57 |
| Appendix C. | Erosion track Twentekanalen..... | 62 |
| Appendix D. | Calculation ship-induced velocities | 63 |
| Appendix E. | Preparation flume..... | 65 |
| Appendix F. | Axial velocities propeller wash in width and depth..... | 69 |
| Appendix G. | Determination void ratio and consolidation coefficient | 70 |
| Appendix H. | Summary of sludge parameters | 72 |
| Appendix I. | Itterbeck sand properties..... | 74 |
| Appendix J. | Deposition effects during experiment..... | 75 |
| Appendix K. | Original measurement series plastering experiments | 76 |

Appendix A. Seepage judgement Twentekanalen

The parts of the Twentekanalen which will be enlarged in 'phase 2' are shown in Figure 38 where the amount of seepage / drainage is analysed by Tauw (2014). The legend in the figure is in Dutch, hence Table 17 is a translation into English language.

Table 17: Translation legend in Figure 38 to English. Note terminology here: seepage = water leakage from canal to surrounding area; drainage = water leakage from surrounding area to canal.

| | |
|---|--|
|  | Strong seepage, side channel dredged in 2010 |
|  | Strong seepage |
|  | Slight seepage, side channel dredged in 2010 |
|  | Slight seepage |
|  | Changing seepage and drainage |
|  | Strong drainage |
|  | Slight drainage |

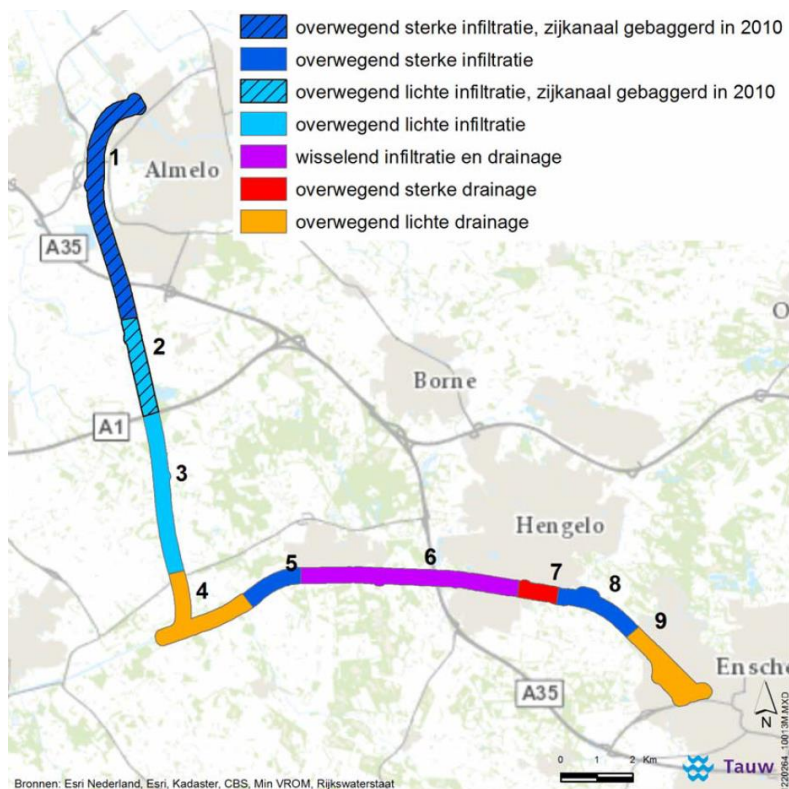


Figure 38: Amount of seepage / drainage in Twentekanalen (phase 2) analysed by Tauw (2014).

Appendix B. Characteristics side channel Twentekanalen

Subsoil side channel Twentekanalen

The subsoil of the side channel of the Twentekanalen is of interest regarding the occurring seepage because the hydraulic conductivity of the soil is to a great extent responsible for the amount of seepage (water level difference between canal and surrounding area is important as well). Arcadis (2015) investigated the soil properties along the total length of the side channel. Figure 39 shows the side channel divided into sections:

- “Deeltraject 4” --> starting at Delden at 0 km to 9.686 km;

Research of bed samples showed that in several parts of this section a limited quantity or even no sludge at all was found. Especially near bridges or places where ships need to manoeuvre to different positions in the channel, limited amounts of sludge were measured. Near the turning basins a large amount of sludge was encountered of about 0.6 m. All in all, on average over the remainder section Arcadis determined a thickness of the sludge layer of about 0.07 m. Below the sludge layer the subsoil consists of a moderate fine, weakly silty sand layer with locally small gravel.

- “Deeltraject 5” --> starting at 9.686 km to Almelo at 15.5 km.

The soil samples taken from deeltraject 5 showed that in several parts of this section a limited quantity or even no sludge at all was found. Measurements here showed more or less the same pattern in sludge thickness as in deeltraject 4: near bridges limited amounts of sludge were measured and near the turning basins large amounts of sludge of about 0.4 m was measured. On average over the remainder section Arcadis determined a thickness of about 0.15 m. Below the sludge layer the subsoil consists of a moderate fine, weakly silty sand layer with locally small gravel. It appears that especially in this section the nuisance of seepage is large due to the fact that sludge is absent in large parts along the channel (Tauw, 2014).

For more detailed information regarding bed samples at different places in the side channel is referred to soil survey carried out by Arcadis (2015).

Grain shape

The shape of the grain is determined according to the visual roundness scale of M. Powers (1953). Two parameters are important here 1) the sphericity of the grain and 2) the roundness of the grain. According to this scale it appears that the average grain shape in the side channel of the Twentekanalen was characterized as 1) low sphericity and 2) round corresponding to $R = 0.6$ on this scale (Wiertsema & Partners, 2015).

Grain size distribution

Consultancy firm Wiertsema & Partners determined the grain size distribution from specific soil samples of the side channel by means of 1) mechanically sieving for the particles $> 62 \mu\text{m}$ and 2) studying the settling velocity for particles $< 63 \mu\text{m}$ based on the Stokes Law. An example of the grain size distribution and location within the area of interest is shown in Figure 40, from which important parameters can be retrieved (e.g. D_{50}). Pay attention to the fact that along the channel the soil samples could be significantly different. Examples of grain sizes within sludge samples originating from the Twentekanalen can be seen in Figure 41.

Hydraulic conductivity

The hydraulic conductivity (k) of the soil samples can be determined in the laboratory using the constant head method for relatively permeable soil samples and using the falling head method for poorly permeable soil samples. It can also be calculated with the aid of empirical formulas based on the grain size distribution. Other methods are in the field itself which are not discussed here.

Wiertsema & Partners (2015) determined the hydraulic conductivity in the Twentekanalen according to the constant and falling head method and also used the empirical formula of Hazen (1892) to calculate the hydraulic conductivity (Eq. B.1):

$$k = C_H \cdot D_{10} \quad (\text{B. 1})$$

With:

k = hydraulic conductivity [m/s]

C_H = Hazen's empirical coefficient, according to the 'polytechnisch zakboekje' set to 0.01157 [-]

D_{10} = the particle size for 10% of the material is finer [mm]

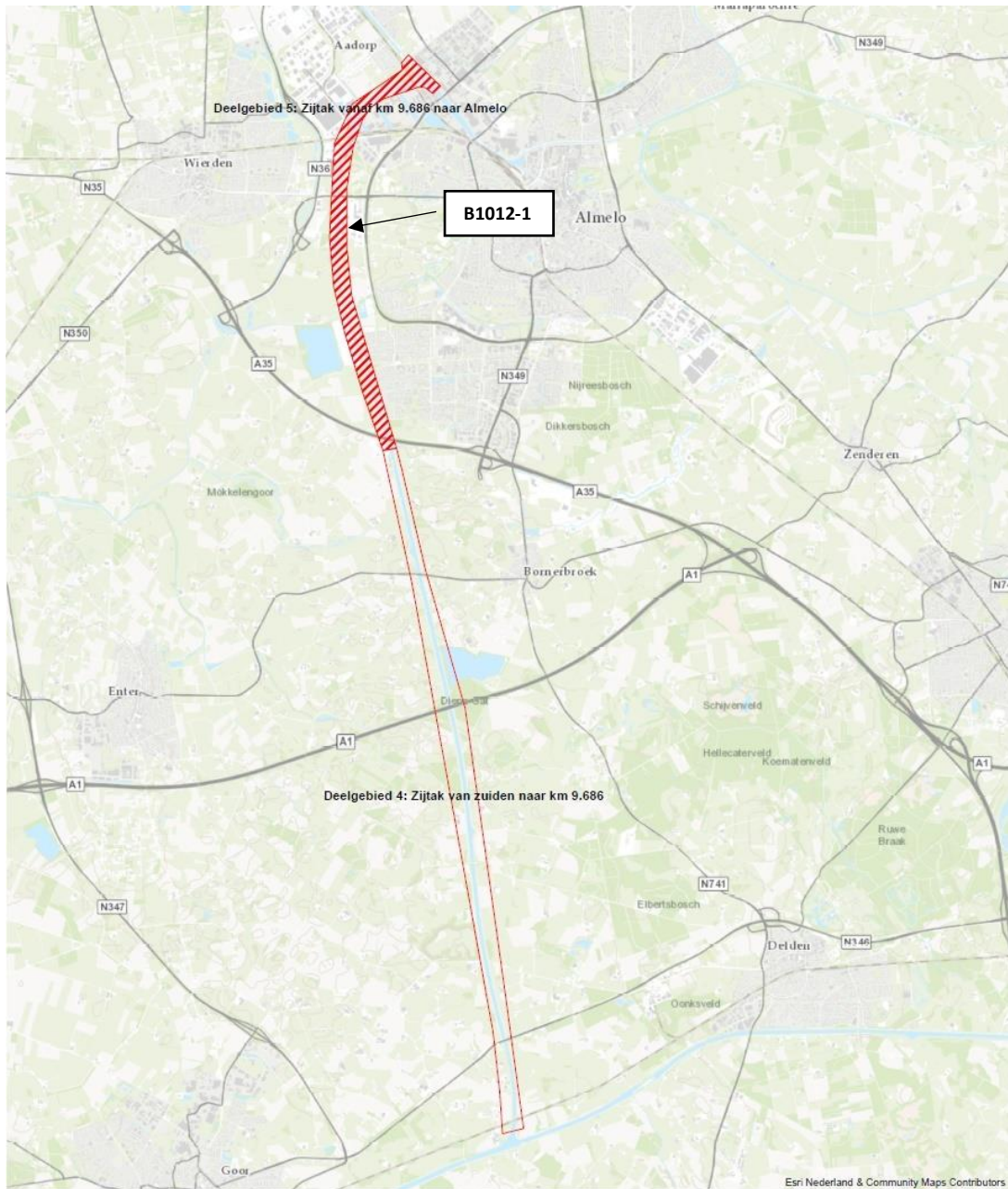
The measured k -value for predominantly sandy soil derived from the constant head method varies between 2 and 20 m/day. However, the calculated k -values with the Hazen equation are (much) larger than the measured

values. The calculated value is at the point with the largest difference about 4 times larger than the measured k-value. Based on the grain size distributions and the calculation according to Hazen, the k-value of predominantly sandy soil varies between 4 and 33.1 m/day.

The falling head method is applied on the soil layers which were considered as poorly permeable, based on the grain size distribution. It appears that the k-value of these samples is < 0.001 m/day. The calculation of the k-value of the sludge layer, and several loam layers in the subsoil according to the formula of Hazen could not be performed due to the large proportion of very fine sediments such as clay and silts. This implies that the hydraulic conductivity is small (< 0.1 m/day).

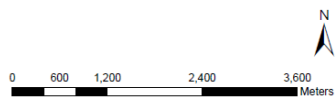
Summarizing, the hydraulic conductivity of the soil samples should be treated carefully because:

1. Only a confined sample is analysed which might not be representative for the entire bottom layer;
2. The measured k-values in the laboratory are (much) smaller than the k-values calculated with the formula of Hazen;
3. In general it can be said that, if there is no sludge or loam present in the subsoil, the hydraulic conductivity of the sandy soil is between 2 to 20 m/day. Locally sludge or loam layers are present which directly affect the hydraulic conductivity resulting in a k-value < 0.001 m/day. However, since these layers are not continuous in space it will not hamper the overall good permeability.



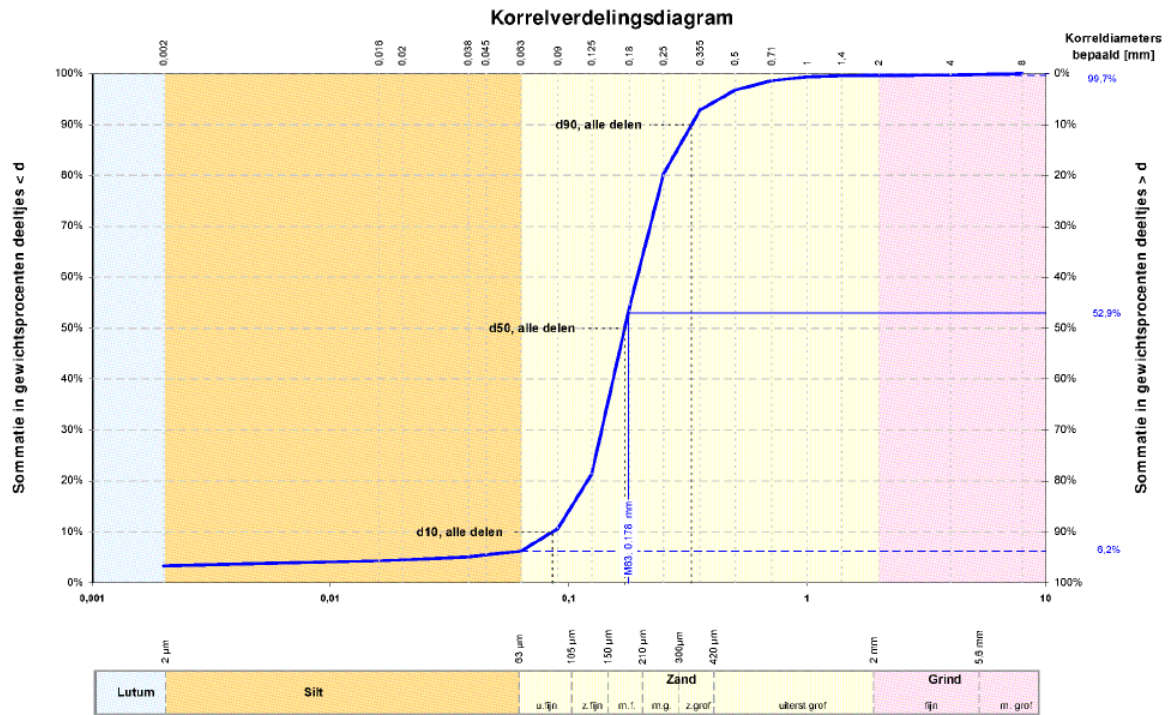
Legenda

- Deeltraject 4: Zijtak van zuiden naar km 9.686
- Deeltraject 5: Zijtak vanaf km 9.686 naar Almelo



| | | | | | | |
|---------------------------------------|---------------|---|------------|--------------------|-------------------|---|
| Tabel: Regionale ligging | | Projectnaam: Verruiming Twentekanalen, deelgebied 4 en 5: zijtak van zuiden naar Almelo | | Project: 203718-13 | Bijlage: 1 | Formaat: A3 |
| Gecontroleerd: | Getekend: EGU | X: 241.300 | Y: 474.000 | Schaal: 1:50.000 | Datum: 03-11-2015 |  <small>ingevuld met natuurlijke oeverbebating inland, water & wind</small> |
| Opdrachtgever: ARCADIS Nederland B.V. | | | | | | |

Figure 39: Side channel sections and location sample B1012-1.



| Alle fracties | |
|-----------------------------|--------|
| Kentallen | Waarde |
| d 10 [mm] | 0,065 |
| d 50 [mm] | 0,172 |
| d 60 [mm] | 0,194 |
| d 90 [mm] | 0,328 |
| $C_u = d_{60} / d_{10} [-]$ | 2,269 |
| $d_{90} / d_{10} [-]$ | 3,836 |
| $C_c [-]$ | 1,145 |

| Karakteristieke waarden | |
|--|-------|
| M_{63} [mm] | 0,178 |
| M_{2000} [mm] | 5,1 |
| D_n [mm] | 0,184 |
| $F_m [-]$ | 1,028 |
| $U_{16} [-]$ [10 $\mu\text{m} - 2\text{mm}$] | 64,63 |

| Zandfractie | |
|---|--------|
| Kentallen | Waarde |
| D 10 [mm] | 0,105 |
| D 50 [mm] | 0,178 |
| D 60 [mm] | 0,199 |
| D 90 [mm] | 0,331 |
| $C_u = D_{60} / D_{10} [-]$ | 1,907 |
| $D_{90} / D_{10} [-]$ | 3,162 |
| $U [-]$ [83 $\mu\text{m} - 2\text{mm}$] | 59,957 |

| | Fractie < 63 μm | | Zand | | Grind | | Stenen | |
|--------|----------------------------|-------|--------|-------|--------|-------|--------|-------|
| | d [mm] | % < d | d [mm] | % < d | d [mm] | % < d | d [mm] | % < d |
| Lutium | | | 0,075 | - | 2,8 | - | 125 | - |
| | 0,001 | - | 0,090 | 10,7 | 4,0 | 99,7 | | |
| | 0,002 | 3,3 | 0,106 | - | 5,6 | - | | |
| Silt | 0,004 | - | 0,125 | 21,3 | 8,0 | 100,0 | | |
| | 0,006 | - | 0,150 | - | 11,2 | - | | |
| | 0,008 | - | 0,180 | 54,1 | 16,0 | - | | |
| | 0,010 | - | 0,212 | - | 20,0 | - | | |
| | 0,016 | 4,3 | 0,250 | 80,3 | 22,4 | - | | |
| | 0,020 | 4,5 | 0,355 | 92,9 | 31,5 | - | | |
| | 0,030 | - | 0,500 | 96,8 | 45,0 | - | | |
| | 0,038 | 5,1 | 0,710 | 98,6 | 63,0 | - | | |
| | 0,045 | 5,5 | 1,000 | 99,4 | | | | |
| | 0,063 | 6,2 | 1,400 | 99,6 | | | | |
| | | | 2,000 | 99,7 | | | | |

| Aanvullende bepalingen | |
|------------------------|--------------|
| Humusgehalte | niet bepaald |
| Kalkgehalte | niet bepaald |

| Legenda | |
|------------|--------------------------------------|
| C_u | Gelijkmatigheidscoëfficiënt |
| C_c | Krommingscoëfficiënt |
| U | U-Filter of relatief korreloppervlak |
| F_m | Fijnheidsmodulus |
| M_{63} | Zand mediaan |
| M_{2000} | Grindmediaan |
| D_n | Mediane korrel diameter |

| Beschrijving uitvoering test | |
|-------------------------------|--------------|
| Beschrijving volgens NEN 5104 | Zs1g1 |
| Humusgehalte | niet bepaald |
| Kalkgehalte | niet bepaald |
| Bepaling fijne fractie | sedigraaf |
| Bepaling zand | zeven, nat |
| Bepaling grind | zeven, nat |

Figure 40: Grain size distribution sediment sample B1012-1; after Wiertsema & Partners (2015).

| | Eenheid | 583894 1 (0-0,1) | 583895 2 (0-0,2) | 583896 3 (0-0,3) | 583897 4 (0-0,2) | 583898 5 (0-0,25) |
|--|-------------------|---------------------|---------------------|---------------------|---------------------|----------------------|
| Algemene monstervoorbehandeling | | | | | | |
| Droge stof | % | 65,8 | 57,9 | 69,7 | 36,8 | 46,7 |
| Klassiek Chemische Analyses | | | | | | |
| Gloeiverlies (organische stof) | % Ds | 1,8 | 2,6 | 0,8 | 8,9 | 4,8 |
| Calciet (CaCO ₃) | % Ds | <1,0 | 3,2 | 1,4 | <1,0 | 5,2 |
| Dichtheid | g/cm ³ | 1,8 | 1,6 | 1,9 | 1,7 | 1,5 |
| Fracties (sedigraaf) | | | | | | |
| Fractie < 2 µm | % Ds | 1,5 | 4,6 | <1,0 | 14 | 7,2 |
| Fractie < 16 µm | % Ds | 2,2 | 6,8 | 1,9 | 27 | 11 |
| Fractie < 2 µm | % md | 1,6 | 5,0 | <1,0 | 19 | 8,6 |
| Fractie < 16 µm | % md | 2,3 | 7,4 | 1,9 | 36 | 13 |
| Fractie < 32 µm | % md | 3,4 | 9,6 | 2,4 | 45 | 18 |
| Fractie < 50 µm | % md | 4,4 | 14 | 3,3 | 52 | 27 |
| Fractie < 63 µm | % md | 4,8 | 17 | 3,4 | 56 | 32 |
| Fractie < 125 µm | % md | 15 | 47 | 13 | 80 | 63 |
| Fractie < 250 µm | % md | 51 | 81 | 41 | 95 | 88 |
| Fractie < 500 µm | % md | 97 | 97 | 87 | 99 | 98 |
| Fractie < 1 mm | % md | 100 | 99 | 98 | 100 | 99 |
| Fractie < 2 mm | % md | 100 | 100 | 100 | 100 | 99 |
| Fractie > 2 mm | % Ds | 2,2 | 1,6 | 3,8 | 0,6 | 3,2 |
| Overig onderzoek | | | | | | |
| M 50 | µm | 246 | 134 | 286 | 44 | 95 |

Figure 41: Examples of grain size distributions of different sludge samples of the Twentekanalen (Tauw, 2016).

Appendix C. Erosion track Twentekanalen

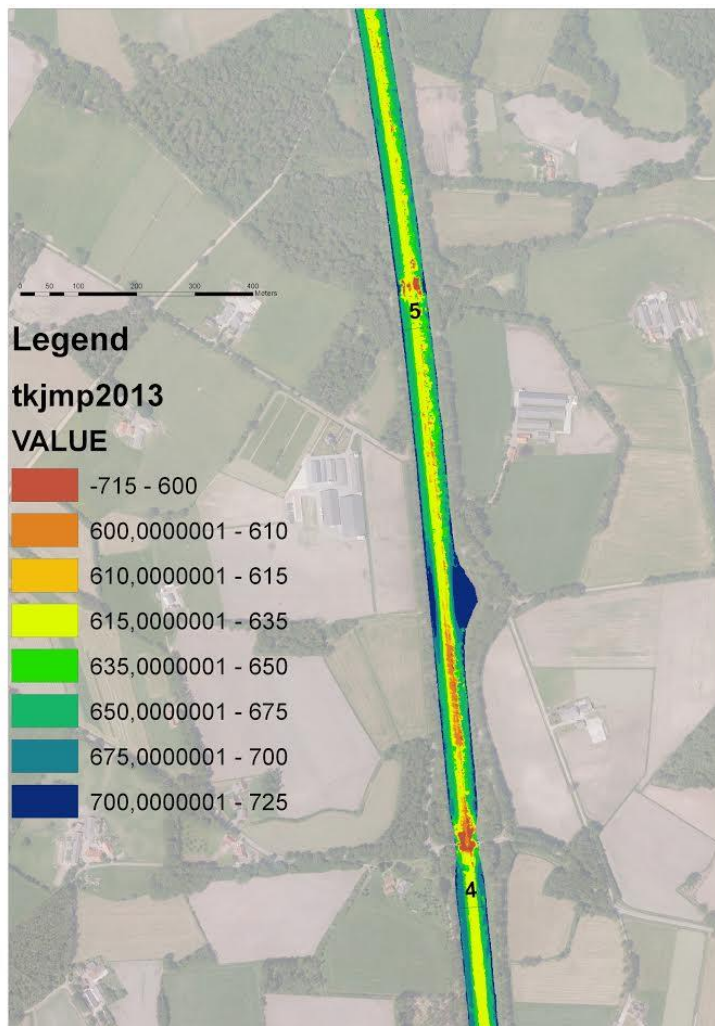


Figure 42: Erosion track side channel Twentekanalen.

Appendix D. Calculation ship-induced velocities

The calculation of ship-induced velocities is based on empirical formulas summarized in the Rock Manual (CIRIA, 2007, pp. 434-442) which most important formulas are summarized here. Three types of ship-induced currents are distinguished: (1) primary water movements, (2) secondary water movements and (3) propeller wash. An overview is shown in Figure 43. It is known that secondary water movements are of importance regarding bank protection but are not dominant with respect to bottom protection in inland navigation channels. Hence, the calculation for the primary water movements of especially the return current and the propeller wash is presented here, since these are important regarding bottom erosion.

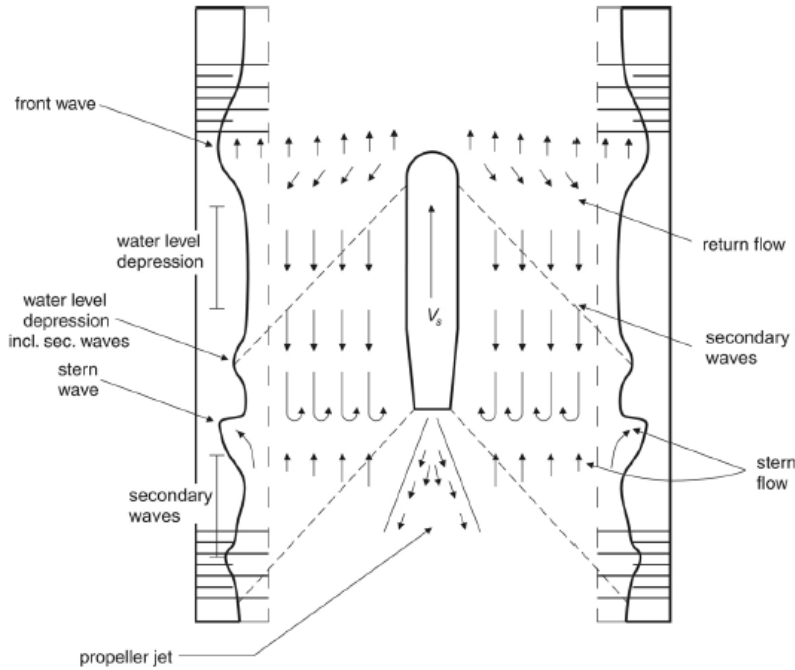


Figure 43: Overview of ship-induced currents; after the Rock Manual (CIRIA, 2007).

Return current

Formulas to calculate the return current are summarized below:

1. Vessel's submerged cross section (A_m):

$$A_m = C_m B_s T_s \quad (D.1)$$

where C_m = midship coefficient related to the cross section of the ship [-] (for inland vessels 0.9 to 1.0);
 B_s = beam width of the ship [m]; T_s = draught of the ship [m]

2. Limit speed of vessel, (V_L):

$$V_L = F_L \sqrt{\frac{g A_c}{b_w}} \quad V_L = \left(\frac{g L_s}{2\pi}\right)^{\frac{1}{2}} \quad V_L = (gh)^{\frac{1}{2}} \quad (D.2) \quad (D.3) \quad (D.4)$$

where $F_L = \left[\frac{2}{3} \left(1 - \frac{A_m}{A_c} + 0.5 F_L^2\right)\right]^{\frac{2}{3}}$; A_c = cross sectional area of the waterway [m²]; b_w = width of the waterway at the waterline [m]; g = gravity constant [m/s²]; L_s = ship length [m]; h = water depth [m]

The minimum value should be applied in further calculations.

3. Actual sailing speed, (V_s):

$$V_s = f_v V_L \quad (D.5)$$

Where $f_v = 0.9$ for unloaded ships and 0.75 for loaded ships.

4. Mean water level depression, (Δh) and mean return flow (U_r):

$$\Delta h = \frac{V_s^2}{2g} \left[\alpha_s \left(\frac{A_c}{A_c^*} \right)^2 - 1 \right] \quad U_r = V_s \left(\frac{A_c}{A_c^*} - 1 \right) \quad (D.6) (D.7)$$

Where:

α_s = factor to express the effect of the sailing speed V_s relative to its maximum [-]: $\alpha_s = 1.4 - 0.4 V_s/V_L$

A_c = cross sectional area of the fairway in the undisturbed situation [m²]

A_c^* = cross sectional area of the fairway next to the ship [m²]

5. Maximum water level depression, ($\Delta \hat{h}$) and maximum return current (\hat{U}_r):

$$\Delta \hat{h} / \Delta h = \begin{cases} 1 + 2A_w^* & \text{for } b_w/L_s < 1.5 \\ 1 + 4A_w^* & \text{for } b_w/L_s \geq 1.5 \end{cases} \quad (D.8)$$

Where $A_w^* = yh/A_c$ [-]

$$\hat{U}_r / U_r = \begin{cases} 1 + A_w^* & \text{for } b_w/L_s < 1.5 \\ 1 + 3A_w^* & \text{for } b_w/L_s \geq 1.5 \end{cases} \quad (D.9)$$

6. Return current underneath ships ($U_{r,b}$):

$$U_{r,b} = c \cdot U_r \quad (D.10)$$

Where $c = 1.5$ to 2.0

In the Netherlands, research is being conducted to develop more accurate prediction formulas.

Propeller wash

The following equations are used to estimate the time-averaged current velocities in propeller jets caused by main propellers for moored ships.

1. Velocity behind the propeller ($U_{pr,0}$):

$$U_{pr,0} = 1.15 \left(\frac{P}{\rho_w D_0^2} \right)^{\frac{1}{3}} \quad (D.11)$$

2. Maximum bed velocity along horizontal bed ($U_{pr,b}$):

$$U_{pr,b} = c \cdot u_{pr,0} \left(\frac{D_0}{z_p} \right)^n \quad (D.12)$$

Where P = applied power [W]; ρ_w = water density [km/m³]; D_0 = effective diameter of propeller: 0.7 (for free propeller without nozzle) to 1 (for propeller in a nozzle) times the real diameter D_p [m]; z_p = distance between the propeller axis and the bed [m].

In the Netherlands the following empirical coefficients are generally used for designing channels: $c = 0.3$ and $n = 1$ (Blaauw and Van der Kaa, 1978). For sailing vessels the bottom velocity should be corrected by half of the actual sailing speed. Additionally, an extra factor related to the number of propeller is added in accordance with Proceedings, 10th International Harbour Congress, Antwerp 1992. The bottom velocity should be multiplied with 1 for ships with one propeller, multiplied with 1.5 for ships with two propellers and multiplied with 2 for ships with more than two propellers.

Appendix E. Preparation flume

In order to simulate the reality as much as possible it is necessary to know the properties of the sludge layer in the side channel of the Twentekanalen and the properties of the available sand-clay mixture at Deltares. Rijkswaterstaat is responsible for delivering soil samples of the side channel in unremoulded state. This means that the soil samples have to be transported vertically and vibrations should be kept at a minimum otherwise the soil sample will be stirred and proper measurements cannot be done. The soil samples should be conserved at approximately 5 degrees Celsius. The first thing to do is to inspect the soil samples and describe the samples by visual observation. Properties of both mixtures can be compared based on the unremoulded and remoulded shear strength which can be determined by a so-called vane test described hereafter.

The peak shear strength (or yield stress) and the undrained shear strength c_u will be measured at different depths in the sample by means of a vane test (Figure 44). The vane shaft is mounted on a torque measuring head and slowly sub-merged in the sample. Subsequently the vane is rotated at constant rpm and the torque is measured. If the vane starts to rotate, the stresses will be redistributed and torque increases. This continues until the sample will yield. After yielding the clay, the particle structure is no longer continuous resulting in a weaker resistance and therefore a lower torque is measured which become continuous after a while signifying the remoulded strength (Figure 44). The peak in the torque measurement is therefore related to the yield stress. The underlying assumptions and equations can be found in the thesis of Paulsen (2007) for example.

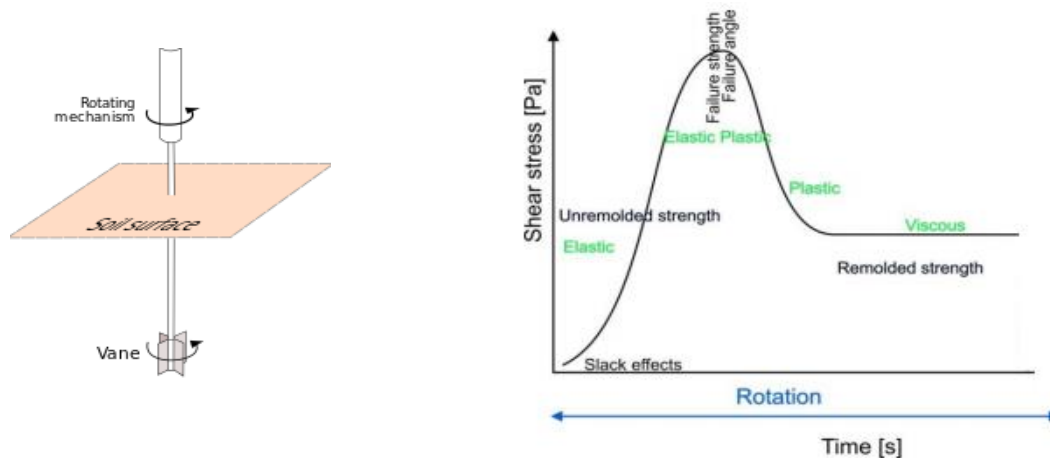


Figure 44: Schematic representation of vane test. (Right) Example of vane measurement results (after Cornelisse, 2011).

The undrained shear strength is used to prepare the water-soil flume because the sand-clay mixture was stored in another basin (Figure 45) with different strengths due to consolidation and evaporation of water. The undrained shear strength c_u is a material property at given water content of the sample (Winterwerp & van Kesteren, 2004) and is defined as the residual stress in the bed after failure of a sample. It gives an indication of the resistance of the sediment bed to erosion. The tests are carried out with the Rotovisco meter Haake M1500 (Figure 45).



Figure 45: (Left) storage basin of sand-clay mixture. (Right) Haake M1500 Visco device.

In order to create a sediment bed comparable to the sludge layer in the Twentekanalen the strength at different depths have to be determined. Two assisting students carried out vane tests in the storage basin at four different locations (Figure 46) with the Haake Visco device and vane FL10. The results showed the same behaviour as in Figure 44 and the results are summarized in Figure 47 below. Redundancy can help to feel comfortable and rely on results given by measurements such as the vane test. Simple methods are often applied to confirm/verify results from measuring equipment. The results of the vane test are checked by placing a measuring cup on top of the sand-clay mixture in the storage basin and fill it with water. When the measuring cup sinks into the soil or destabilizes peak shear stress can be determined. The surface tension of the water (+ measuring cup) divided by 5 results in the approximate yield stress (Hill, 1950, p. 222). The results are checked near location 5 were a yield stress of around 250 Pa is found which appears to be consistent.

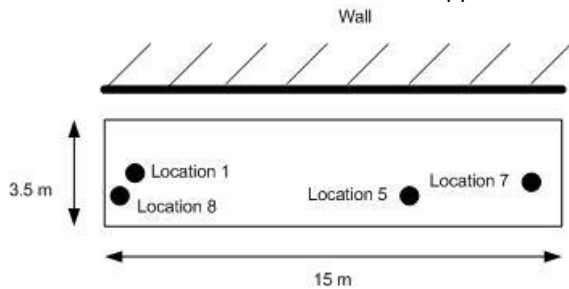


Figure 46: Measurement location within the storage basin.

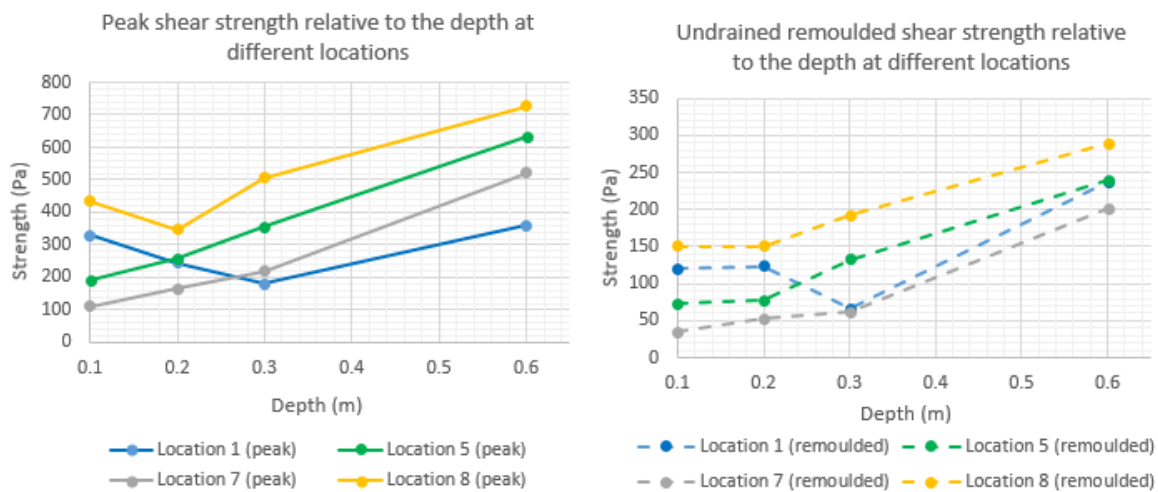


Figure 47: (Left) Peak shear strength relative to the depth. (Right) The undrained remoulded strength which has been computed by taking the average in the tail of the measurement.

What stands out of the above figures is the higher strength of the top layer for location 1 and 8 while it is expected that the strength increases with depth. This phenomenon might be explained by the fact that the top layer is dried up as also can be seen in Figure 45. Furthermore, it is evident that the strength of the sediment at the left hand side of the storage basin (location 1 and 8) is higher compared to the right hand side. It seems like the strength is gradually reducing from left to right. In order to compare with sludge in the Twentekanalen also vane tests are carried out on the soil samples retrieved from the side channel. It should be noted that some of the tests showed unexpected patterns, possibly caused by gravel, organic material or wrong execution of the test. Besides, also very high strengths (e.g. 13 kPa) were measured at larger depths indicating sand which is of minor interest here. From visual observation (after drying) it is concluded that the top layer in soil sample 2 and 13 showed most reliable results regarding sludge. Figure 48 shows the dry sediment of the top layer of the sediment from soil samples 2 and 7. After inspection it appears that the sediment in tube 2 and 13 was clayey while the sediment in tube 7 and 10 was sandy. All in all, only the properly executed tests are shown here from which relevant information is obtained (Figure 49).



Figure 48: (Left) clayey soil sample tube 2. (Right) sandy soil sample tube 7.

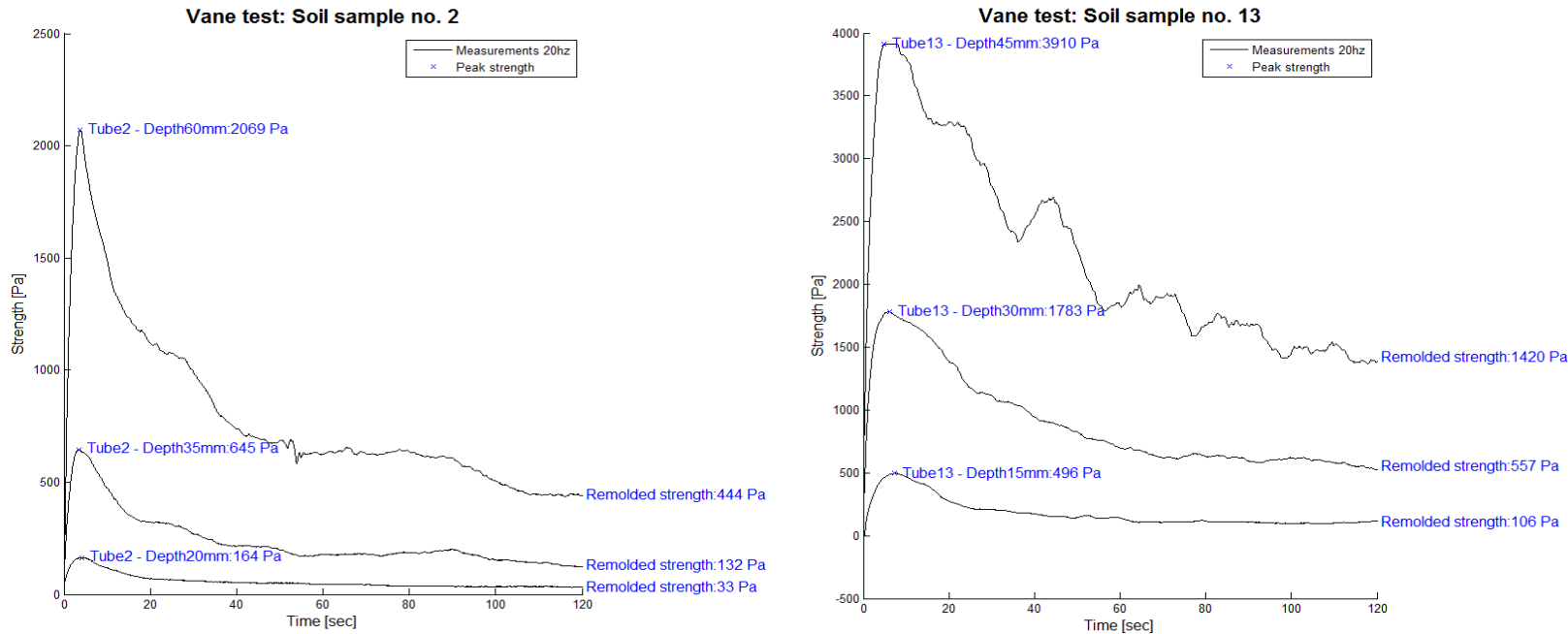


Figure 49: Results of executed vane tests. (Left) Soil sample 2 and (right) Soil sample 13.

The vane test of soil sample 2 indicates that the shear strength increases with depth which is expected in view of consolidation theory. The same behaviour can be seen in the vane test of soil sample 13 but at a depth of 45 mm more variation in strength with respect to time is visible, indicating an increase in the sand fraction. Visual observations helped to confirm this statement. However, relevant information is deduced from Figure 49 regarding the preparation of sand-clay mixture in the flume. Initially the idea was to pump the sediment from a specific location in the storage basin to the flume. However, based on the strength information and due to technical issues the choice was made to pull a large shovel through the storage basin. Figure 50 shows the flume without water and a smoothed sediment bed. Also the strength of the sediment has been checked with the vane on eight locations in the flume. The yield strength varied roughly between 80 and 140 Pa with an average of 110 Pa as can be seen in Figure 51. These differences in yield strength are most likely caused by a different sand-clay ratio as is discussed by Mitchener and Torfs (1996). Apparently, at specific locations the sand-clay ratio was different emphasizing the heterogeneous character.



Figure 50: Prepared sediment bed.

Vane tests sand-clay mixture poured in the flume

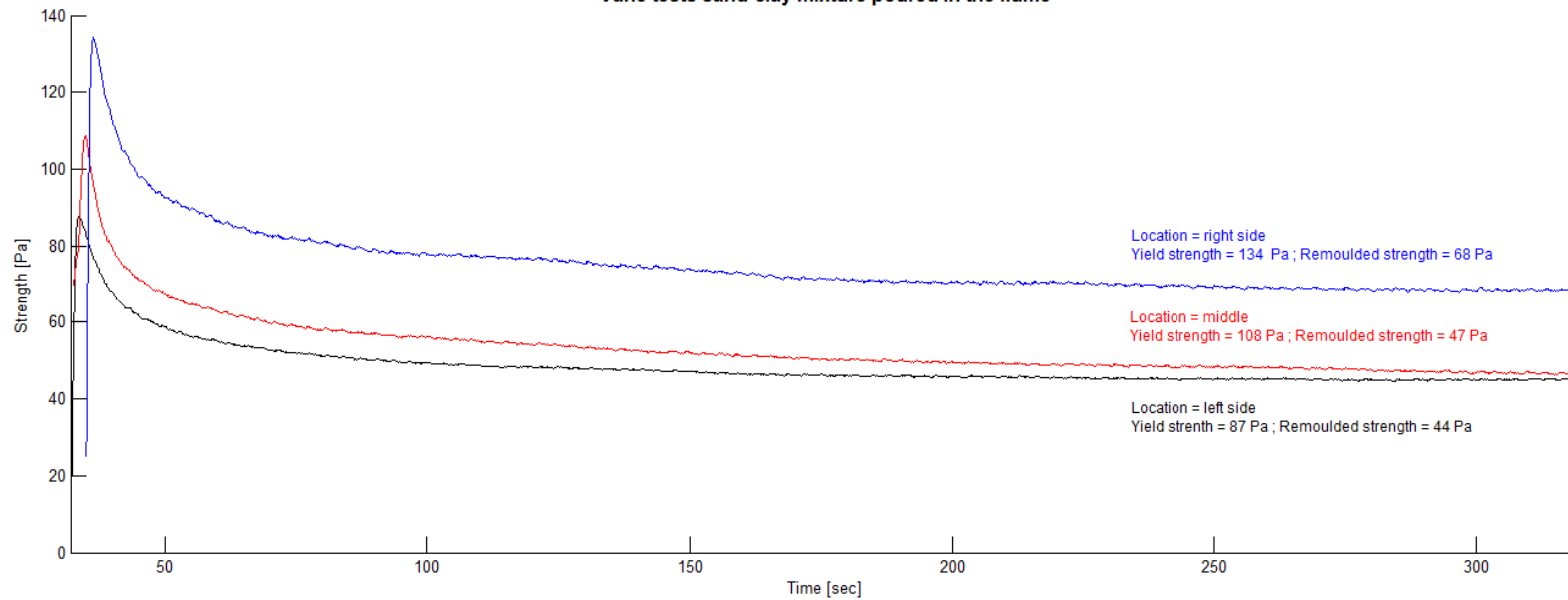


Figure 51: Strength of the prepared sediment at different locations in the flume. The locations left, middle and right are seen from the back of the ship.

Appendix F. Axial velocities propeller wash in width and depth

▪ Axial velocities with respect to the width of the ship (transverse (y-) direction)

As explained in paragraph 2.2 the axial velocities can be described as a Gaussian curve. However, the propeller turns anti-clockwise and during the measurements it seems that the propeller flow deflects to the left regularly (viewpoint behind the ship). For the erosion experiments this is essential information because when the average maximum axial velocity is not at the centerline of the propeller, the location of the maximum depth in the erosion profile would be different. Therefore, velocity measurements are carried out in transverse direction from the left side to the right side of the ship (0 - 56 cm) at ten transects. Figure 52 shows the time-averaged axial velocity measurements at the height of the propeller axis in transverse direction and at varying distance in longitudinal direction resulting in an overall view of the velocity profile. In the plot can be seen that at short distance in longitudinal direction ($x/D_{pr} = 1,2,3$) the velocity profile follows more or less a Gaussian curve as expected from theory. At larger distances behind the propeller the Gaussian curve flattens out and a more or less straight line develops meaning that the propeller flow velocities are uniformly in width. The effects of flow deflection to the left can be neglected because the highest flow velocities still occur along the centerline of the propeller.

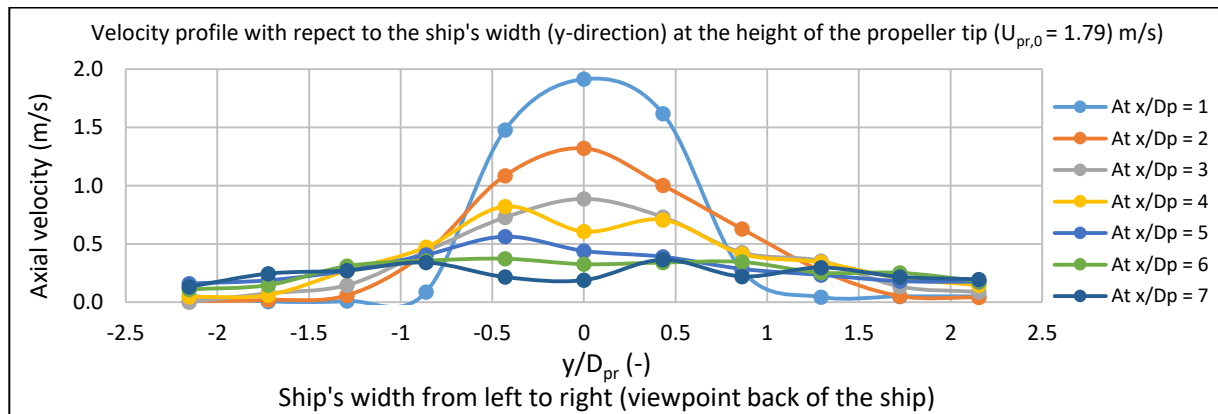


Figure 52: Axial flow velocities related to the transverse (y-) direction and propeller efflux velocity of 1.79 m/s.

▪ Axial velocities with respect to the depth (z-direction)

Similar to the axial velocity profile in transverse y-direction also the axial velocity profile in depth, or z-direction, follows a Gaussian curve according to theory (see paragraph 2.2). To confirm this measurements are carried out at different depths and in longitudinal direction, see Figure 53. Note that in this graph only measurements below the propeller axis are carried out. Especially the flow velocities obtained at these depths are relevant for the erosion of sand-clay mixtures. Again it can be seen that the flow velocities in depth follow more or less the Gaussian curve, however caution is advised with this confirmation because a limited amount of data points are obtained. Furthermore, the location for the maximum axial velocity is shifted to larger values of x/D_{pr} and just as in the previous figures the curve also flattens out at larger distance from propeller tip in longitudinal direction which is showed in the right plot of Figure 53.

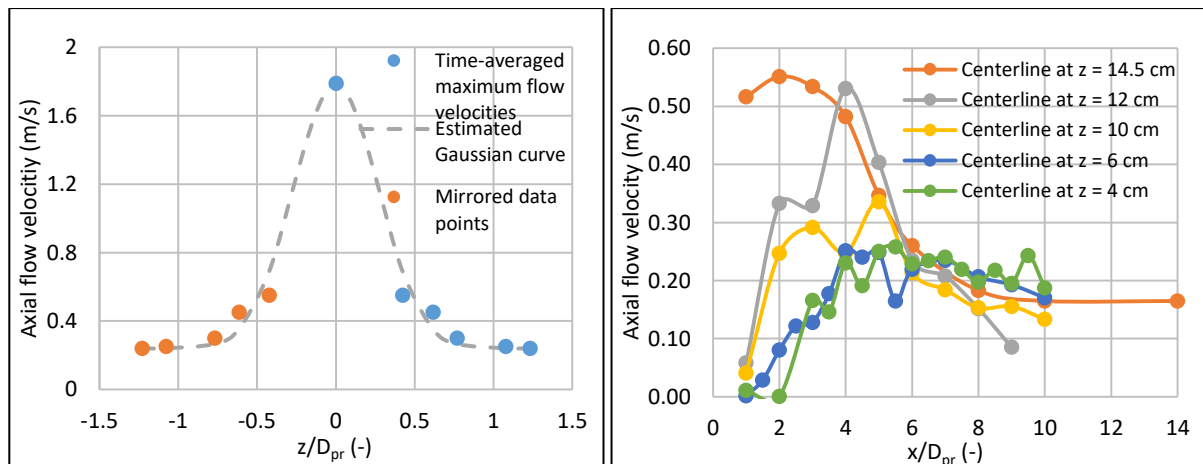


Figure 53: (Left) Time-averaged maximum axial flow velocities related to depth; (Right) Time-averaged axial flow velocities at different distances in longitudinal directions. Efflux velocity in both is 1.79 m/s.

Appendix G. Determination void ratio and consolidation coefficient

The consolidation coefficient is determined with the aid of The Capillary Suction Time (CST) Apparatus (Figure 54). It is a measure for the permeability of the sample at certain void ratio (or water content). Consolidation is a relevant process in soil plastering tests and causes an increase in strength of the sediment bed over time.

The way it works is that capillary suction pressure causes filtrate from the sludge to seep through the filter paper at a rate largely dependent on the filterability of the sludge, and almost independent of the hydrostatic pressure of the height of the sludge in the funnel. The probes in contact with the filter paper cause the timer to start as the liquid 'front' or interface reaches the first probe, and to stop as the interface reaches the second probe. The time interval recorded by the counter of the time taken for the liquid to pass over the distance between the probes is related to the filterability of the sludge. In the paper of Huisman and van Kesteren (1998) the consolidation theory is applied to the CST apparatus. The paper shows that from measurements with the CST-test, conducted on a series of samples of a certain sludge with different initial void ratios, the coefficient of consolidation (Gibson coefficient C_{gib}) of the soil can be deduced. They showed that when the void ratio is plotted against the $1/\sqrt{CST}$, a linear relation is obtained in which the slope of this line determines the Gibson coefficient. Furthermore it is noted that it only applies for preconsolidated soil samples. The equation relating the void ratio to the CST and Gibson coefficient is given by (Huisman & van Kesteren, 1998):

$$e_i = e_{CST}^{\infty} + \frac{L\sqrt{\pi}}{2\sqrt{C_{gib}}} \cdot \frac{1}{\sqrt{CST}} \quad (G. 1)$$

With :

e_i = initial void ratio [-]

e_{CST}^{∞} = void ratio with infinite capillary suction time [-]

L = characteristic length [m] dependent on CST device and filter paper

C_{gib} = Gibson coefficient [m²/s]

CST = capillary suction time [s]

The intercept of the line with the vertical axis is the void ratio for which the CST approaches infinity (e_{CST}^{∞}). For this research the Gibson coefficient is interesting and can be determined according:

$$C_{gib} = \left(\frac{L\sqrt{\pi}}{2 \cdot slope} \right)^2 \quad (G. 2)$$

In which the slope is in fact the slope of the void ratio against $1/\sqrt{CST}$ -line [s^{0.5}]

The parameter L is dependent on the properties of the CST device and the properties of the filter paper. In the paper of Huisman and van Kesteren (1998), a value of $1.3 \cdot 10^{-3}$ is suggested for a CST with the dimensions and filter paper that will be used in this analysis.

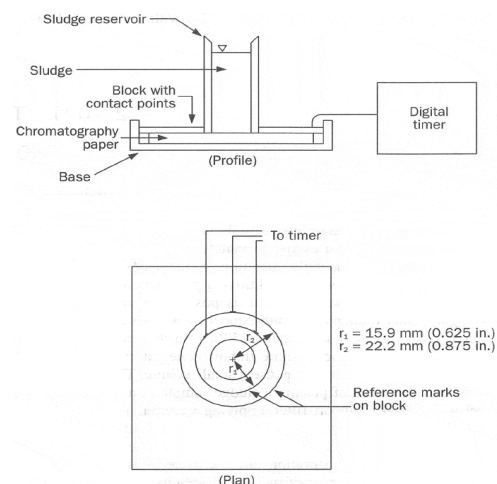
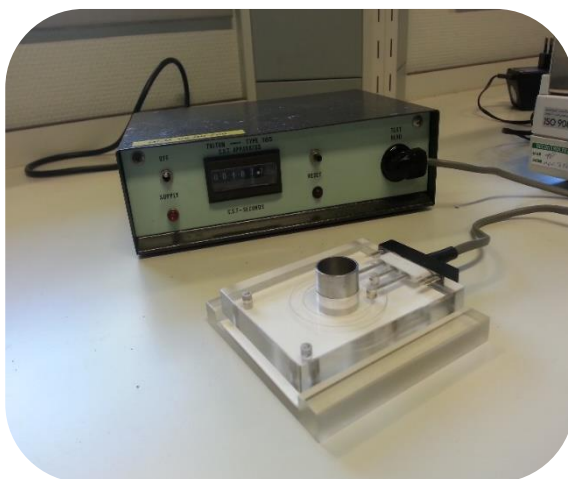


Figure 54: (Left) CST device. (Right) Schematic representation of CST device.

The Gibson consolidation coefficient found in the CST test can be translated to the Terzaghi consolidation coefficient which is more commonly used in consolidation formulas. The translation takes place via (Eq. G.3):

$$c_v = C_{gib} \cdot [1 + e_i]^2 \quad (G.3)$$

With: c_v = Terzaghi consolidation coefficient [m²/s]

The general formula for the Terzaghi coefficient is related to the permeability (Eq. G.4)

$$c_v = \frac{k}{m_v \gamma_w} \quad (G.4)$$

With: k = permeability [m/s]; m_v = compressibility [m²/kN] and γ_w = specific density of water [kN/m³]

Firstly, the consolidation tests were carried out. Secondly, the bulk properties of the soil sample were determined. The void ratio is determined by means of measuring the water content and assuming 2650 kg/m³ for the density of solids.

Bulk properties: water content / void ratio / density

After the CST test, the weight of the sludge is measured and subsequently placed in the oven at 105 degrees Celsius for 24 hours and subsequently measured to determine the mass of water (difference between saturated soil sample and dry soil sample). With the obtained data calculations can be done to determine the water content, densities and void ratio. The water content W is a parameter to quantify the amount of water in a soil sample and is defined as:

$$W = M_w / M_{s,dry} \quad (G.5)$$

With: W = water content [-]; M_w = mass of water [kg] and $M_{s,dry}$ = mass of dry solids [kg]

The dry and bulk density of the sediment is defined as the mass of dry and saturated material divided by the wet volume of the sample (Eq. G.6 and G.7 respectively):

$$\rho_{dry} = \frac{M_{s,dry}}{V_{wet}} = \frac{M_{s,dry}}{\frac{M_{s,dry}}{\rho_s} + \frac{M_w}{\rho_w}} \quad (G.6)$$

With: ρ_{dry} = dry density [kg/m³]

$M_{s,dry}$ = mass of dry solids [kg]

V_{wet} = volume of wet solids [m³]

ρ_s = density of solids [kg/m³], assumed to be 2650 kg/m³ in this study

ρ_w = density of water [kg/m³], assumed to be 1000 kg/m³

$$\rho_b = \frac{M_{s,w}}{V_{wet}} = \frac{M_{s,w}}{\frac{M_{s,dry}}{\rho_s} + \frac{M_w}{\rho_w}} \quad (G.7)$$

ρ_b = bulk density [kg/m³]

$M_{s,w}$ = mass of wet solids [kg]

The void ratio e_i of the samples is computed as follows:

$$e_i = \frac{M_w / \rho_w}{M_{mud} / \rho_{mud}} = W \cdot G_s \quad (G.8)$$

e_i = (initial) void ratio [-]

M_w = mass of water [kg]

ρ_w = density of water [kg/m³], assumed to be 1000 kg/m³

M_{mud} = mass of dry solids with $d < 63 \mu\text{m}$ [kg], assumed equal to $M_{s,dry}$ in this research

ρ_{mud} = density of solids with $d < 63 \mu\text{m}$ [kg/m³], assumed to be 2650 kg/m³

W = water content [-]

G_s = specific gravity of dry solids [-], assumed to be 2.65

Appendix H. Summary of sludge parameters

Undisturbed sludge samples (four tubes 2, 7, 10 and 13) contained in Ackerman tubes originating from the Twentekanalen were analysed by means of a vane test. The location of these samples can be found in the report of TAUW (2016). Firstly the Ackerman tubes were visually inspected and it appeared that two out of four soil samples were drained (no supernatant water), however vane tests were conducted on all four soil samples and at different depths in the tube (example is shown in Figure 49). First impression of the results is that only the top layer contained material corresponding to sludge because of relatively small values of the yield stress. Higher yield stress values were interpreted as larger amounts of sand. The vane results corresponded with visual observation after the soil samples were hydraulically pushed out of the tube. In Figure 56 four soil samples are shown. Note that before the soil sample was disturbed the consolidation tests have been carried out. However, the consolidation tests were only valid for the soil originating from tube 2 and tube 13 because it appeared that these soil samples contained some sludge while in the others the sludge was very limited. See for example Figure 48 in Appendix E in which the right soil sample (tube 7) contains only sand while the left soil sample (tube 2) clearly shows more clay. The characteristics of the soil samples such as the void ratio and water content are presented in Table 18. Comparing this data with existing data from Lake Ketel sludge⁶ it also appears that tube 2 and tube 13 correspond well while the soil samples from tube 7 and 10 certainly not match. Moreover, the sludge applied in the Twentekanalen initially originates from Lake Dronten which is located close to Lake Ketel. Figure 55 shows the results of the CST-tests on the Twentekanalen sludge. Only limited amount of CST-tests were carried out, hence results should be interpreted carefully.

The average yield strength of the sludge in the soil samples is approximately 2 kPa while the average yield strength of the applied sediment bed in the erosion experiment is approximately 100 Pa (see Figure 51). Hence, a scale factor of 20 is obtained similar to the length scale (assuming mass erosion).

Table 18: Soil sample characteristics.

| | Tube 2 | Tube 7 | Tube 10 | Tube 13 |
|--|---|--|---|--|
| Undrained yield strength* | 1.1 kPa | - | - | 2.8 kPa |
| Undrained remoulded shear strength* | 280 Pa | - | - | 400 Pa |
| Water content | 1. 137 % 2. 102 % 3. 135 % | 1. 54 % 2. 66 % 3. 64 % 4. 67 % | 1. 27 % 2. 27 % 3. 25 % 4. 40 % 5. 43 % | 1. 96 % 2. 85 % 3. 84 % |
| Void ratio | 1. 3.64 (-) 2. 2.72 (-) 3. 3.58 (-) | 1. 1.44 (-) 2. 1.74 (-) 3. 1.70 (-) 4. 1.77 (-) | 1. 0.72 (-) 2. 0.71 (-) 3. 0.66 (-) 4. 1.06 (-) 5. 1.14 (-) | 1. 2.6 (-) 2. 2.26 (-) 3. 2.21 (-) |
| Gibson consolidation coefficient C_{gib} | $2.29 \cdot 10^{-8}$ (m ² /s) | - | $8.41 \cdot 10^{-8}$ (m ² /s) | $1.18 \cdot 10^{-8}$ (m ² /s) |
| Terzaghi consolidation coefficient C_v | $4.33 \cdot 10^{-7}$ (m ² /s) | - | $2.39 \cdot 10^{-7}$ (m ² /s) | $1.31 \cdot 10^{-7}$ (m ² /s) |
| Infinite void ratio e_{∞} | 2.31 (-) | - | 0.61 (-) | 1.51 (-) |

*Average of the measurements in the top layer in the tube where the sludge was located from which an example can be seen in Figure 47. Only tube 2 and 13 are given because the others showed irregular behaviour indicating sandy soil. Note that these values should be treated as rough indication, not as the true value because of the large variability in space and depth.

⁶ Lake Ketel sludge: Average remoulded shear strength of 200 Pa; Average water content of 134 %; Void ratio of 3.28 [-]; e_{∞} of 3.58 [-] and a consolidation coefficient of $C_{gib} = 1.0 \cdot 10^{-8}$ m²/s (Bisschop & van Kesteren, Consolidatie Sliblaag, 1994)

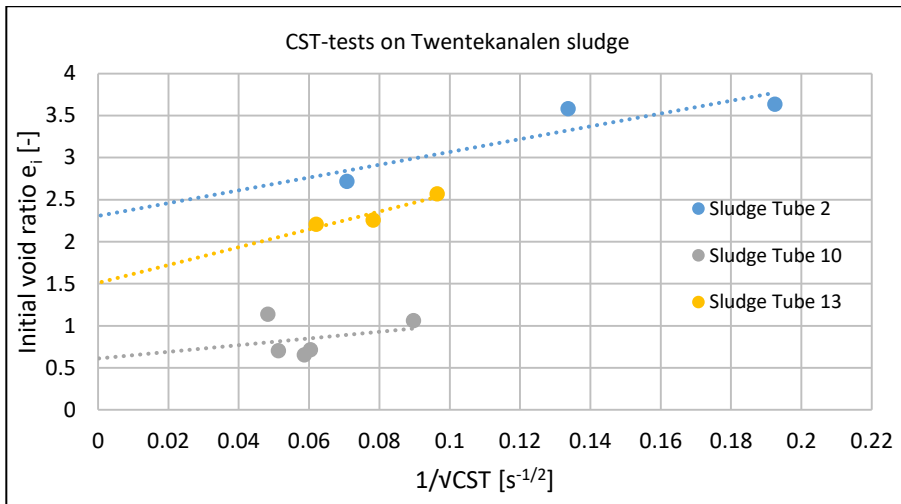


Figure 55: CST results.

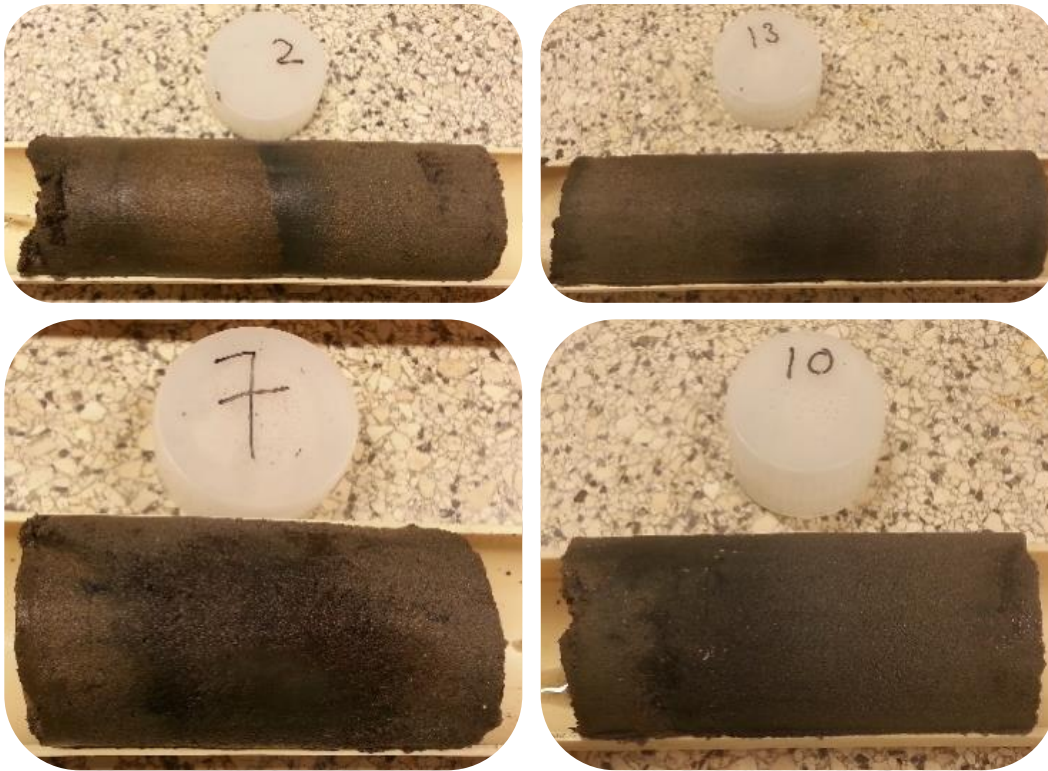


Figure 56: Soil samples Twentekanalen.

Appendix I. Itterbeck sand properties

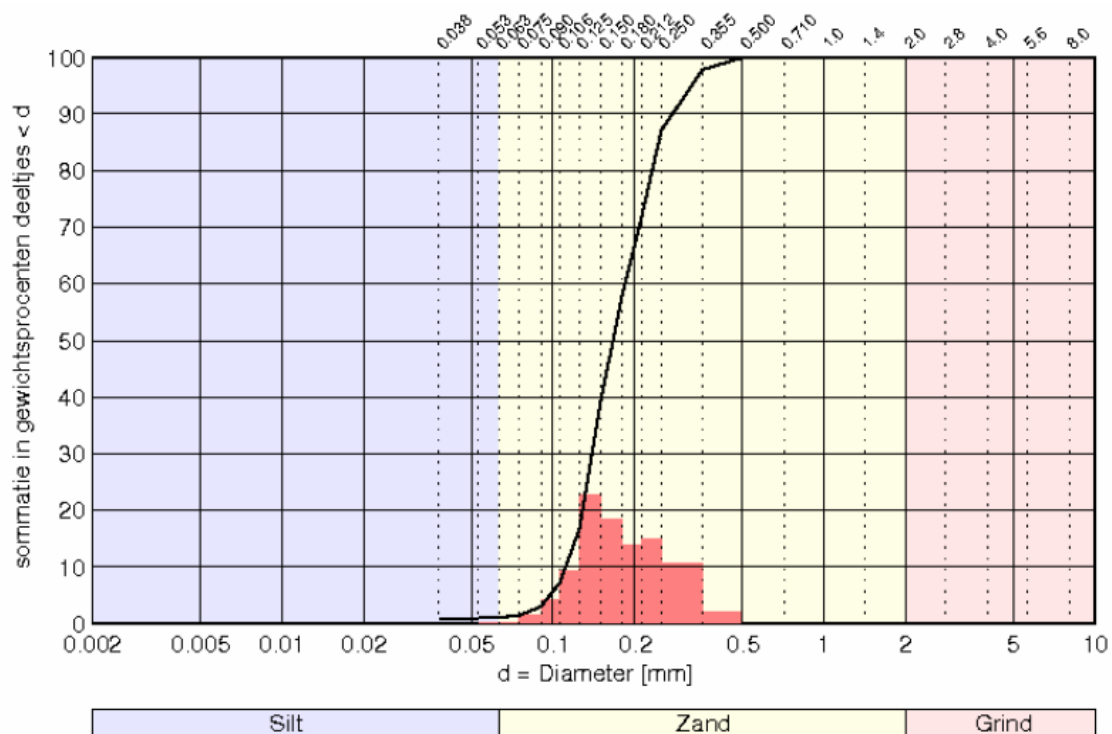


Figure 57: Grain size distribution Itterbeck sand.

Table 19: Key figures Itterbeck sand

| Kental | Waarde | Eenheid |
|----------|---------|---------------|
| d_{10} | 0.111 | mm |
| d_{15} | 0.121 | mm |
| d_{50} | 0.166 | mm |
| d_{80} | 0.184 | mm |
| Cu | 1.654 | - |
| Cu_z | 1.634 | - |
| p | 2.473 | - |
| Cc | 0.943 | - |
| Mz | 167.033 | μm |
| D_m | 0.177 | mm |
| Fm | 0.964 | - |
| U | 61.512 | mm^2 |

Cu: Coëfficiënt van uniformiteit (D_{80}/D_{10})
 Cu_z : Coëfficiënt van uniformiteit van zandfractie
 p : Gradatie (D_{80}/D_{10})
 Cc: Krommingscoëfficiënt $\frac{(D_{30})^2}{D_{60} \times D_{10}}$
 Mz: Zandmediaan
 D_m : Gemiddelde diameter
 Fm: Fijnheidsgetal
 U: Specifiek oppervlak

Table 20: Porosity n and density ρ of the Itterbeck sand.

| n_{\min} | n_{\max} | ρ [kg/m^3] |
|------------|------------|-----------------------------------|
| 0.3449 | 0.46465 | 2642.9 |

Appendix J. Deposition effects during experiment

The effect of deposition on the bathymetry measurements is presented in Figure 58. Directly after the sediment is stirred up either by a ship or due to equalizing of the sediment layer, a bathymetry measurement is executed. Then, 2.5 days later (over the weekend) again a bathymetry measurement is executed on the unaffected sand-clay mixture where particles had time to settle. It appears that the effects are negligible signifying that it is justified to measure relatively quick (about 30 minutes) after the ship has passed the measurement section. Hence, the majority of particles in suspension settle within 30 minutes. The difference in height is in the order of 2 mm which is approximately 4% of the obtained erosion depth of approximately 5.0 cm.

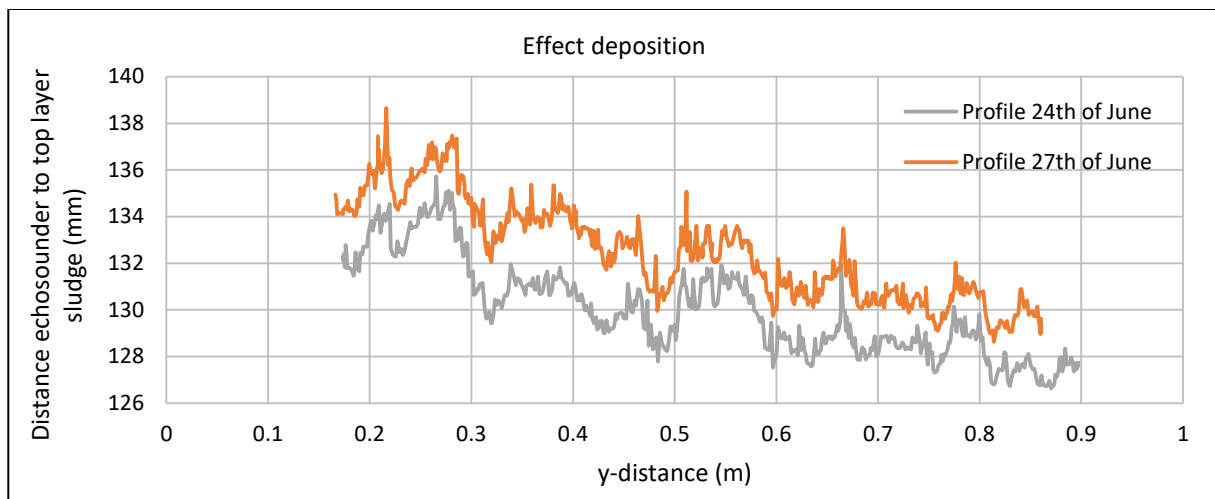


Figure 58: Deposition effects during the erosion experiments related to measurement gap of 2.5 days.

Appendix K. Original measurement series plastering experiments

In Figure 59 natural sludge of approximately 4 cm is poured on top of clean Itterbeck sand. The pressure differences and the amount of drained water over the plastering cell is recorded in time. The peaks in the figure shows the opening and closure of the valve. Reason for opening and closing the valve is to empty the water collection container. Subsequently, the sludge is stirred up and more mixed with the sand filter which can be seen in Figure 60.

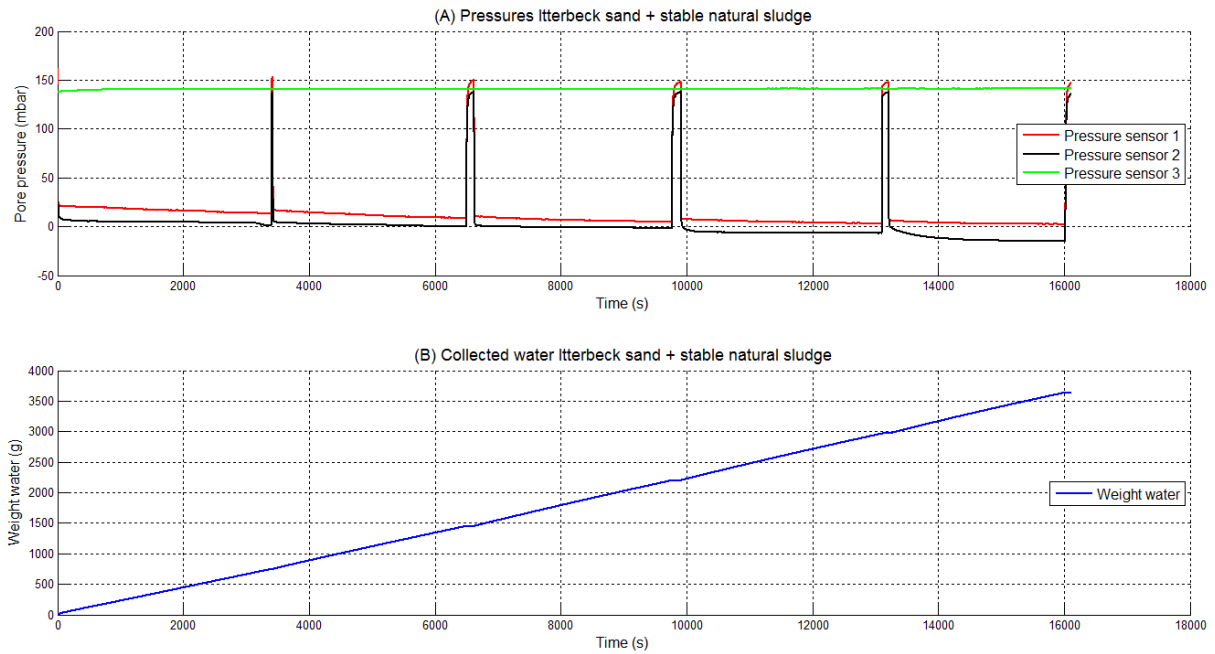


Figure 59: Complete measurement series Exp. 3.

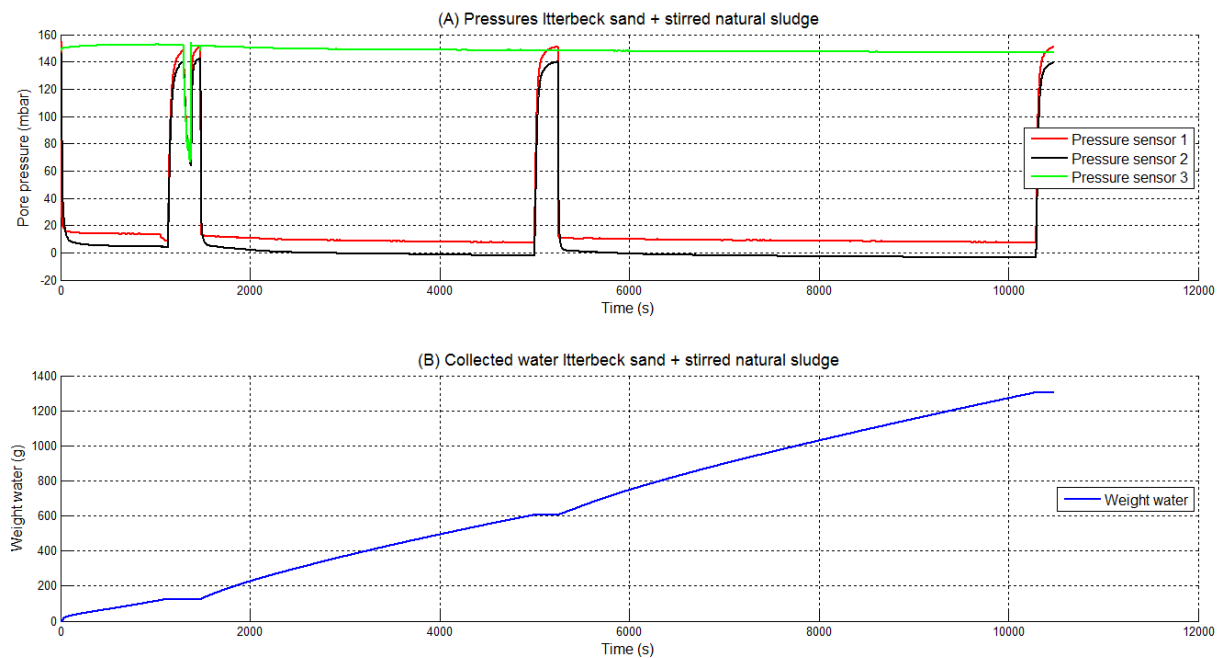


Figure 60: Complete measurement series Exp. 4.

Figure 61 shows the total measurement series of plastering tests 5, 6 and 7. The record time of the measurement started somewhat earlier in these experiments. Pressure is being built up in the beginning because the top valve of the plastering cell is opened attempting to reach to a stable situation. However, no stable situation is reached before opening the bottom valve allowing water to flow through the soil sample. This is not that important because the stable situation after opening the bottom valve is of interest.

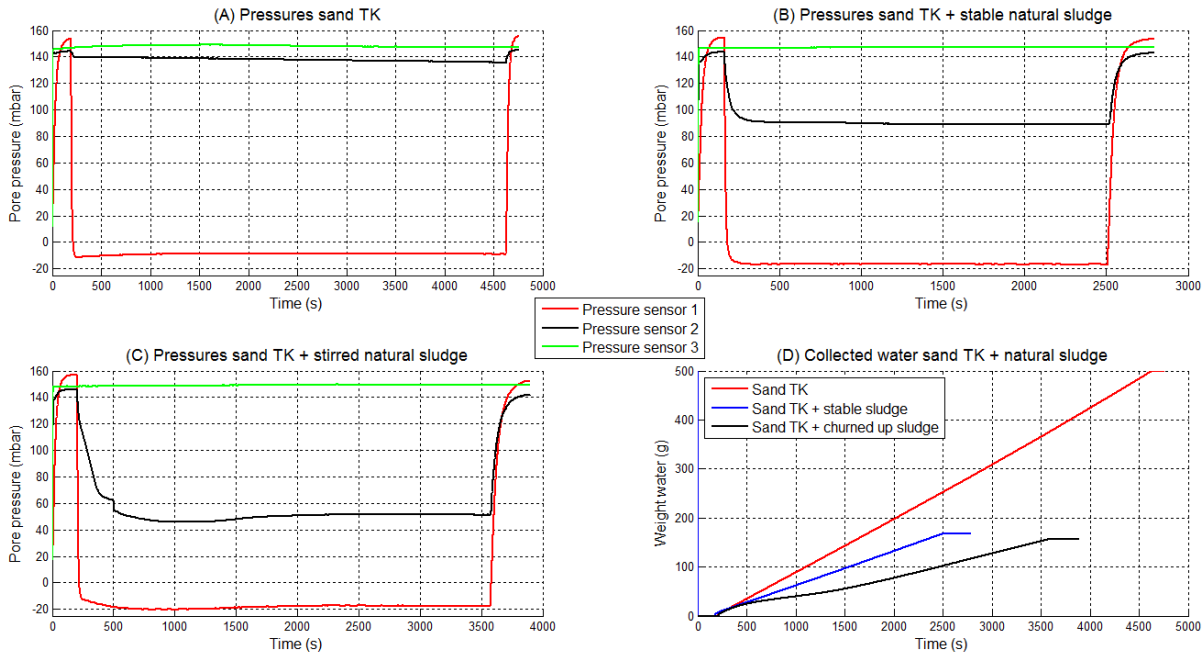


Figure 61: Complete measurement series Exp. 5, 6 and 7 for plot A, B and C respectively. Plot D presents the collected water of all three experiments.